THE EFFECTS OF SURFACE ROUGHNESS ON THE WAVE FORCES ON A CIRCULAR CYLINDRICAL PILE

By

WILLIAM J. BURTON and ROBERT M. SORENSEN

Coastal and Ocean Engineering Division

Texas Engineering Experiment Station

MARCH 1970

TAMU-SG-70-211

COE Report No. 121

TEXAS A&M UNIVERSITY SEA GRANT PROGRAM

THE EFFECTS OF SURFACE ROUGHNESS ON THE WAVE FORCES ON A CIRCULAR CYLINDRICAL PILE

by

William J. Burton and Robert M. Sorensen
Coastal and Ocean Engineering Division
Texas A&M University

Partially Supported by the National Science Foundation
Sea Grant Program
Institutional Grant GH - 59 to
Texas A&M University

Sea Grant Publication No. 211
Coastal and Ocean Engineering Division
Report No. 121 - C.O.E.

March 1970

PREFACE

In recent years there has been increasing interest in harnessing the resources of the sea to supplement and replace those being gradually depleted on the continents of the earth. The anticipated increase in effort that will be directed in the future towards the extraction of vital minerals and food from in and beneath the sea will necessitate the design of adequate structures to support these activities.

Circular cylindrical piles are frequently used as structural support members for offshore installations. In order to adequately design these structures, both for safety and economy, the contribution of the effects of pile surface roughness on the wave forces on such piles should be known. Since apparently no direct studies involving surface roughness effects on wave forces on piles have been published, it is hoped that the results of this report will help to fill a deficiency in the literature available on this timely and important subject.

ABSTRACT

Circular cylindrical piles are commonly used structural members in marine applications. When these piles endure sustained exposure to a marine environment, corrosion deposits and marine organisms accumulate on their surfaces. The subsequent increase in surface roughness would be expected to influence the friction, form and inertia drag characteristics of the pile when subjected to wave action. This influence, in turn, would be expected to have an effect on the magnitude of the force developed on the pile. Apparently, no previous attempt has been made to evaluate the effects of surface roughness on wave forces developed on piles when subjected to the nonsteady flow conditions inherent in wave motion. This report is an attempt to help fill this void in the literature so that marine structural installations may be more satisfactorily and economically designed.

In order to obtain a measure of the effects of surface roughness, a series of wave tank experiments were performed on a circular cylindrical pile whose outer surface roughness was varied by gluing sand grains of designated size ranges onto its surface. Each experiment consisted of sending a train of monochromatic

waves of a selected length and height combination past the model pile and recording measured water surface elevation, horizontal force and bending moment time histories. These records were then analyzed using the semi-empirical approach of Morison to evaluate drag and inertia coefficients. Other semi-empirical approaches were also investigated which included correlating a coefficient of resistance with an acceleration modulus and an attempt to correlate drag and inertia coefficients for different degrees of surface roughness using a period parameter. The linear wave theory was used in evaluating the water particle kinematics.

The accuracy of the semi-empirical methods was found to be insufficient to measure the effects of surface roughness. However, the measurements of average maximum wave force for each experiment indicated that surface roughness has a definite effect on the magnitude of force as would be expected. The effects of surface roughness were evaluated on the basis of comparing the ratio F'_{mr}/F_{ms} obtained for a given rough surface experiment with the value of unity applied to the corresponding smooth surface experiment as a control. Here, F'_{mr} is the average modified maximum force obtained for a given rough surface experiment and it includes a reducing correction to compensate for the increase in pile diameter due to the presence of the sand grains; F_{ms} is the average maximum force obtained from a corresponding experiment on the smooth pile. For relative roughnesses, ε/D, of 0.0075, 0.0186 and 0.0361, the indicated increases in the overall averages of

F'_{mr}/F_{ms}, compared with unity for the smooth surface, were -1, 9 and 14 percent, respectively, for the 0.73×10^4 to 5.7×10^4 range of modified Reynolds numbers studied. Here, ε is the average sand grain diameter and D is the diameter of the pile including the sand grains.

If no reduction in the pile force is made to correct for the added increment of pile diameter due to the presence of the sand grains, the overall average increases in the ratio of forces obtained from the experiments using relative roughnesses of 0.0075, 0.0186 and 0.0361 are 1, 13 and 23 percent, respectively.

ACKNOWLEDGEMENTS

This project was partially funded by the National Science Foundation Sea Grant Program Institutional Grant GH-59 made to Texas A&M University.

A special note of gratitude is extended to Prof. Edwin S. Holdredge for his advice on design of the instrumentation and in trouble-shooting the recording equipment; to Dr. Robert E. Schiller, Jr., for his painstaking effort in performing some of the photography; and to Mr. Joseph C. Brusse for his enlightening discussions on fabricating and assembling techniques of the apparatus.

Throughout the period of active research involved in this study, the writers have benefited from the assistance of several persons from time to time. The help of Miss Rosella Duke with the meticulously tedious task of reducing much of the data and preparing many of the tables and figures of this report is greatly appreciated. Special thanks go to Mr. William B. Jones for a similar job well done reducing data and helping to perform the exneriments. The efforts of Mrs. Linda M. Christiansen in the data reduction and computations to check the comouter program are gratefully acknowledged. The help of Mr. William G. Janacek in the gathering and reduction of data is also deeply appreciated, as is the help of Mr. David J. Knoll with the data reduction. The writers also extend their thanks to Mr. Stephen S. Rawe, Mr. Allan J. Henderson and Mr. Mohammed A. Rahman for their assistance in installing the experimental setup and getting it to operate satisfactorily. The typing of the manuscript by Miss Loretta Bayer is sincerely appreciated.

TABLE OF CONTENTS

TABLE OF CONTENTS (Continued)

LIST OF TABLES

LIST OF TABLES (Continued)

LIST OF FIGURES

LIST OF FIGURES (Continued)

LIST OF SYMBOLS

In the dimensions used below

F is the force dimension

L is the length dimension

T is the time dimension

Q is the charge dimension, and

Θ is the temperature dimension

Symbol	Description	Units	Dimensions
a	Acceleration	$\frac{ft}{sec^2}$	$\frac{L}{T^2}$
a_{hmax}	Maximum horizontal particle acceleration	$\frac{ft}{sec^2}$	$\frac{L}{T^2}$
a_{hrms}	Root mean square of horizontal particle acceleration over the depth span of the water	$\frac{ft}{sec^2}$	$\frac{L}{T^2}$
$a_{h\theta_2}(j)$	Horizontal particle acceleration at the jth depth-level in the water corresponding to a phase angle of θ_2	$\frac{ft}{sec^2}$	$\frac{L}{T^2}$
A	Projected area	ft^2	L^2
b	Distance between the midpoints of the upper and lower strain gage sections	in	L
c	Distance from the neutral axis to the outer fiber of the cross section	in	L

LIST OF SYMBOLS (Continued)

Symbol	Description	Units	Dimensions
C	Coefficient of resistance	-	-
C_m	Coefficient of mass or inertia	-	-
C_D	Coefficient of drag	-	-
C_{urms}	Coefficient of resistance determined on the basis of root mean square of horizontal particle velocity	-	-
d	Depth of the water	ft	L
D	Diameter of cylinder, disc, or pile with sand grains, as applicable	in	L
D_s	Diameter of smooth pile	in	L
e	Output voltage from a Wheatstone bridge	volts	$\frac{FL}{Q}$
E	Modulus of elasticity of a material	$\frac{lb_f}{in^2}$	$\frac{F}{L^2}$
E	Strain	-	-
f	Function designation in equations (2), (3), (6) and (7)	-	-
f_{pu}	Period parameter defined by equation (83)	-	-

LIST OF SYMBOLS (Continued)

Symbol	Description	Units	Dimensions
$f_{p\xi}$	Period parameter defined by equation (84)	-	-
F	Horizontal wave force	lb_f	F
$F_{hmax}(i)$	Maximum (peak) horizontal force which occurs for the ith wave	lb_f	F
$F_{h\theta_1}(i)$	Horizontal wave force corresponding to a phase angle of θ_1 for the ith wave	lb_f	F
$F_{h\theta_2}(i)$	Horizontal wave force corresponding to a phase angle of θ_2 for the ith wave	lb_f	F
$\overline{F}_{hmax}$	Average of the maximum (peak) forces for N waves	lb_f	F
$\overline{F}_{h\theta_1}$	Average of the forces corresponding to the phase angle θ_1 for N waves	lb_f	F
$\overline{F}_{h\theta_2}$	Average of the forces corresponding to the phase angle θ_2 for N waves	lb_f	F
F'_{mr}	Modified maximum force on the rough pile after being decreased to account for the increase in diameter due to the presence of the sand grains	lb_f	F
F_{ms}	Maximum force on the smooth pile	lb_f	F

LIST OF SYMBOLS (Continued)

Symbol	Description	Units	Dimensions
g	Acceleration of gravity	$\frac{ft}{sec^2}$	$\frac{L}{T^2}$
h	Height of the center of a pressure transducer above the bottom of the basin	in	L
H	Wave height	in	L
$H(i)$	Wave height of the ith wave	in	L
$\overline{H}$	Average wave height of N waves	in	L
$\overline{H}_a$	Average wave height based on all corresponding experiments which involved the same percent speed and half-stroke settings of the wave generator	in	L
i	Index	-	-
I	Iversen's modulus	-	-
i	Designates interval size	in	L
I	Moment of inertia of a cross sectional area about its centroidal axis	in^4	L^4
j	Index	-	-
k	Virtual mass coefficient	-	-
K_1'	Constant defined by equation (21)	-	-

LIST OF SYMBOLS (Continued)

Symbol	Description	Units	Dimensions
K'_2	Constant defined by equation (22)	-	-
$K'_{1\theta_1}$	Constant of the type defined by equation (21), but evaluated at phase angle θ_1 based on $\overline{S}_{s\theta_1}$ and $\overline{L}$	-	-
$K'_{2\theta_2}$	Constant of the type defined by equation (22), but evaluated at angle θ_2 based on $\overline{S}_{s\theta_2}$ and $\overline{L}$	-	-
ℓ	Length of a strain gage before being strained	in	L
ℓ_{arm}	Length of the generator stroke arm including its bearing	in	L
ℓ_G	Distance between wave gages	ft	L
ℓ_{vert}	Vertical distance from the middle of the upper transducer to the bottom of the pile	in	L
L	Wave length	ft	L
$L(i)$	Length of the ith wave	ft	L
L_{est}	Estimated wave length at the time the experiment was made	ft	L
$\overline{L}$	Average wave length of N waves	ft	L

LIST OF SYMBOLS (Continued)

Symbol	Description	Units	Dimensions
$\bar{L}_a$	Average wave length based on all corresponding experiments which involved the same percent speed and half-stroke setting of the generator	ft	L
M	Bending moment	$in\text{-}lb_f$	FL
M_1, $M_{①}$	Bending moment about the midpoint of the upper (no. 1) strain gage section	$in\text{-}lb_f$	FL
M_2, $M_{②}$	Bending moment about the midpoint of the lower (no. 2) strain gage section	$in\text{-}lb_f$	FL
N	Number of waves averaged in one experiment	-	-
N_{da}	Number of the day of the month	-	-
N_{disp}	Number of depth intervals at which the horizontal and vertical particle displacements are calculated	-	-
N_{intj}	Number of depth intervals down to the jth level	-	-
N_{kin}	Number of depth intervals at which the kinematic quantities of velocity and acceleration are calculated	-	-
N_{mo}	Number of the month of the year	-	-

LIST OF SYMBOLS (Continued)

Symbol	Description	Units	Dimensions
N_{pad}	Number designation of the wave generator paddle position setting	-	-
N_r	Experiment (run) number	-	-
N_{sp}	Percent speed setting of the wave generator variable speed motor	-	-
N_v	Number of values of an array of data which are input to the program	-	-
N_{yr}	Number of the last two digits of the year	-	-
P	Pressure intensity	$\frac{lb_f}{in^2}$	$\frac{F}{L^2}$
P_d	Dimensionless parameter given by equation (86) involving water depth	-	-
P_F	Dimensionless parameter given by equation (88) involving force	-	-
P_H	Dimensionless parameter given by equation (87) involving wave height	-	-
P_p	Dimensionless parameter given by equation (89) involving pile diameter	-	-
P_s	Dimensionless relative roughness given by equation (90)	-	-

LIST OF SYMBOLS (Continued)

Symbol	Description	Units	Dimensions
q	Total flow displacement obtained in unidirectional flow with constant acceleration	in	L
R	Reynolds number	-	-
R_{cal}	Calibrate resistor	ohm	$\frac{FLT}{Q^2}$
R_{rms}	Reynolds number based on root mean square velocity over the depth span of the water	-	-
R_w, R_x, R_y, R_z	Resistors in the w, x, y, z-arms of a Wheatstone bridge	ohm	$\frac{FLT}{Q^2}$
s	Area per unit length of the pile	in^2	L^2
δ_{half}	Half-stroke setting of the wave generator paddle stroke arm	in	L
S	Surface area	in^2	L^2
S_s	Wave surface elevation above the bottom	ft	L
$\overline{S}_{s\theta_1}$	Average wave surface elevation above the bottom corresponding to the phase angle θ_1 for N waves	ft	L
$\overline{S}_{s\theta_2}$	Average wave surface elevation above the bottom corresponding to the phase angle θ_2 for N waves	ft	L

LIST OF SYMBOLS (Continued)

Symbol	Description	Units	Dimensions
t	Time	sec	T
$t_A(i)$, $t_B(i)$, $t_{A'}(i)$	Array of time values used in equations (30) and (31) for calculating average wave length	sec	T
$t_H(i)$	Array of time values corresponding to the times at the wave crests	sec	T
T	Wave period	sec	T
$\bar{T}$	Average wave period for N waves	sec	T
$\bar{T}_a$	Average wave period based on all corresponding experiments which involved the same percent speed and half-stroke settings of the wave generator	sec	T
T_w	Temperature of the water	°F	Θ
u	Horizontal particle velocity	$\frac{ft}{sec}$	$\frac{L}{T}$
$u_{\theta_1}(j)$	Horizontal particle velocity at the jth depth-level in the water corresponding to a phase angle of θ_1	$\frac{ft}{sec}$	$\frac{L}{T}$
u_{rms}	Root mean square of horizontal particle velocity	$\frac{ft}{sec}$	$\frac{L}{T}$
U_m	Maximum (peak) horizontal particle velocity	$\frac{ft}{sec}$	$\frac{L}{T}$

LIST OF SYMBOLS (Continued)

Symbol	Description	Units	Dimensions
v	Water particle velocity in the vertical y-direction	$\frac{ft}{sec}$	$\frac{L}{T}$
V	Voltage	volts	$\frac{FL}{Q}$
V_m	Volume of a mass of fluid	in^3	L^3
$y_{\theta_1}(j)$	Vertical distance from the still water level down to a water particle situated at some depth-level, j, corresponding to a phase angle of θ_1	in	L
$y_{\theta_2}(j)$	Vertical distance from the still water level down to a water particle situated at some depth-level, j, corresponding to θ_2	in	L
$y_{0\theta_1}(j)$	Vertical distance from the still water level down to the mean vertical coordinate of a water particle whose orbit is centered at some depth-level, j, corresponding to a phase angle of θ_1	in	L
$y_{0\theta_2}(j)$	Vertical distance from the still water level down to the mean vertical coordinate of a water particle whose orbit is centered at some depth-level, j, corresponding to a phase angle of θ_2	in	L
$\bar{z}_F$	Distance between the point of application of the resultant horizontal wave force and the midpoint of the upper gage section	in	L

LIST OF SYMBOLS (Continued)

Symbol	Description	Units	Dimensions
α	Angle between the flow direction and a normal to the surface of the pile	deg	-
β	Constant defined by equation (36)	volts	$\frac{FL}{Q}$
γ	Specific weight	$\frac{lb_f}{ft^3}$	$\frac{F}{L^3}$
Δ	Small increment of	-	-
ϵ	Average diameter of the sand grains	in	L
ζ_t	Total vertical displacement of a particle as it traverses its orbit	in	L
$\zeta_{t\theta_1}(j)$	Total vertical displacement of a particle whose orbit is centered at some depth-level, j, corresponding to a phase angle of θ_1	in	L
ζ_{tmax}	Maximum total vertical particle displacement which occurs	in	L
ζ_{trms}	Root mean square of total vertical particle displacement over the depth span of the water	in	L
η	Wave surface elevation with respect to still water level	in	L

LIST OF SYMBOLS (Continued)

Symbol	Description	Units	Dimensions
$\eta_{\theta_1}(i)$	Wave surface elevation corresponding to a phase angle of θ_1 for the ith wave	in	L
$\overline{\eta}_{\theta_1}$	Average wave surface elevation for N waves corresponding to a phase angle of θ_1	in	L
$\eta_{\theta_2}(i)$	Wave surface elevation corresponding to a phase angle of θ_2 for the ith wave	in	L
$\overline{\eta}_{\theta_2}$	Average wave surface elevation for N waves corresponding to a phase angle of θ_2	in	L
θ	Phase angle equal to $\frac{2\pi t}{T}$ in equation (20)	rad	-
θ_1	Phase angle corresponding to the crest of the wave	rad	-
θ_2	Phase angle corresponding to the one-quarter period past the wave crest	rad	-
λ	Cylinder length	in	L
μ	Dynamic viscosity	$\frac{lb_f\text{-sec}}{ft^2}$	$\frac{FT}{L^2}$
ν	Kinematic viscosity	$\frac{ft^2}{sec}$	$\frac{L^2}{T}$

LIST OF SYMBOLS (Continued)

Symbol	Description	Units	Dimensions
ξ_t	Total horizontal displacement of a particle as it traverses its orbit	in	L
$\xi_{t\theta_2}(j)$	Total horizontal displacement of a particle whose orbit is centered at the depth level, j, corresponding to a phase angle of θ_2	in	L
ξ_{tmax}	Maximum total horizontal particle displacement which occurs	in	L
ξ_{trms}	Root mean square of total horizontal particle displacement over the depth span of the water	in	L
ρ	Density of the water	$\frac{lb_f\text{-}sec^2}{ft^4}$	$\frac{FT^2}{L^4}$

CHAPTER I

INTRODUCTION

Marine structures, such as piles, which undergo sustained exposure to a water environment accumulate corrosion deposits and marine organisms which increase the roughness of their surfaces. A number of papers have appeared in the literature which dwell on the subject of wave forces on piles, but only a few have considered the effects of roughened surfaces. Moreover, the investigations which considered surface roughness have been restricted to the regime of steady flow. The flow field resulting from wave action is oscillatory in nature and, therefore, unsteady. To the writers' knowledge, no account of a previous attempt to evaluate the effects of surface roughness on wave forces on piles has appeared in the literature.

The roughening of a pile surface subjected to wave action would be expected to influence the friction and form drag characteristics of the pile and, consequently, the magnitude of the force developed on the pile. The objectives of the study reported herein were to determine by experiment the nature and magnitude of the effects of surface roughness on wave forces on piles and to attempt to determine which particular parameters would best predict these effects. To this end a series of wave tank experiments were conducted on a circular cylindrical model pile whose outer surface roughness was varied by gluing sand grains of selected size ranges onto the surface. Each experiment consisted of subjecting the model pile to monochromatic waves of a designated height and length combination and recording measured water surface elevation, horizontal force and bending moment time histories. These records were then analyzed using several methods of approach in order to evaluate the effects of surface roughness.

CHAPTER II

LITERATURE SURVEY

Status of Previous Research

No published information presenting the effects of surface roughness on wave forces on marine structures has been found in the literature. However, some investigators have studied related aspects of the problem such as: experimental investigations of drag forces on rough cylinders in steady flow; special studies involving unidirectional acceleration of a fluid past a smooth cylinder; and development of various techniques of analyzing the data characteristically obtained in studies involving wave forces on structures. Some of these studies will be discussed in this chapter.

The nonsteady motion of the water particles, coupled with their oscillatory behavior in response to wave motion, has, so far, prevented any rigorous mathematical treatment of wave and pile interactions of a general nature. Furthermore, the gathering and analysis of experimental data is complicated by this unsteady aspect of the motion. As a result, it has been necessary to rely on semi-empirical, statistical and dimensional analysis methods in predicting wave forces on piles and submerged objects.

Roughened Surfaces in Steady Flow

One of the earliest accounts of an attempt to evaluate surface roughness effects was presented by Fage and Warsap [1]*. They evaluated drag coefficients, C_D, for steady flow conditions, from wind tunnel experiments using smooth and roughened cylinders. A portion of their data is shown in Fig. 1 where the drag coefficient has been plotted as a function of Reynolds number, uD/ν, for varying degrees of relative roughness, ε/D. Here u is the horizontal fluid velocity, D is the diameter of the cylinder, ν is the kinematic viscosity of the fluid, and ε is the average surface roughness height. The data show that the transition Reynolds number decreases as the cylinder surface is made rougher and also that the decrease in drag coefficient at transition is less as the roughness is increased.

A more recent study of the effects of surface roughness for conditions of steady flow has been published by Blumberg and Rigg [2]. Their investigations involved the towing of a cylinder with selected surface roughnesses in the high-speed towing tank of the Naval Ship Research and Development Center. Drag coefficients were evaluated for supercritical Reynolds numbers in the range of 1×10^6 to 6×10^6. They found that C_D remained essentially constant for a given surface roughness but increased with increasing roughness from 0.59 for a smooth cylinder to 1.02 for the same 3-ft. diameter cylinder covered with bitumastic and oyster shell with concrete fragments.

---

*Numbers in brackets designate references at the end of the report.

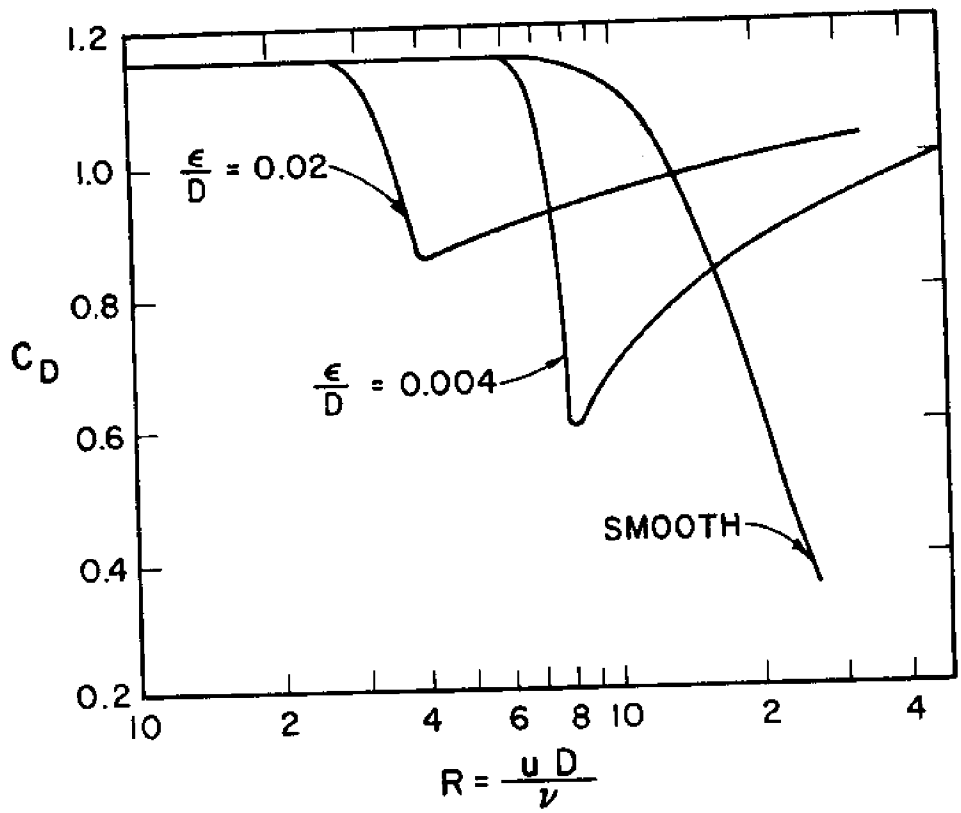

Fig. 1 C_D versus Reynolds number for steady flow around cylinders (after Fage and Warsap [1])

Studies Involving Unidirectional Acceleration

Iversen and Balent [3] performed experiments on discs accelerated vertically in still water. In analyzing their data, the velocity was taken to be linearly dependent upon acceleration and the force on the disc, F, was expressed by the relation

$$F = C\ 1/2\rho v^2 A \qquad (1)$$

where ρ is the density of the fluid, v is the vertical velocity, A is the area of the disc and C is designated the coefficient of resistance.

The coefficient of resistance was shown to be, in general, a function of geometry, Reynolds number, vD/ν, Froudes modulus, v^2/gD, and an acceleration modulus, aD/v^2; i.e.,

$$C = f_1(\text{geometry}, \frac{vD}{\nu}, \frac{v^2}{gD}, \frac{aD}{v^2}) \qquad (2)$$

where D, the diameter of the disc, is shown here as a characteristic length, g is the acceleration of gravity and a is the acceleration of the body in the fluid.

For their particular studies involving discs, Iversen and Balent obtained good correlation of C with acceleration (Iversen's) modulus.

Kiem [4] performed experiments on cylinders of various length-diameter ratios by accelerating them vertically from rest in water using constant drive forces. In this case a correlation was found to exist between the coefficient of resistance and acceleration modulus, using Reynolds number and the length-diameter ratio, λ/D, as parameters; i.e.,

$$C = f_2\left(\frac{VD}{\nu}, \frac{aD}{V^2}, \frac{\lambda}{D}\right) \tag{3}$$

Laird, Johnson and Walker [5] performed experiments to determine possible effects of acceleration and rates of change of acceleration on the forces exerted on horizontally mounted, circular cylinders immersed in water and moved horizontally normal to their long axes. The accelerations and velocities used were commensurate to those encountered in ocean waves. Both constant and variable linear accelerations and decelerations were used. In the case of a single horizontal cylinder, the drag coefficients, C_D, agreed with similar values obtained from plots of drag coefficient versus Reynolds number for conditions of uniform motion. However, when the cylinder was decelerated deviations of the drag coefficient from accepted values for uniform motion occurred. They also found that the acceleration modulus, aD/u^2, failed to correlate with the resistance coefficient, C, near boundary layer transition.

Sarpkaya and Garrison [6] have investigated the case of a circular cylinder subjected to unidirectional flow with constant acceleration. For these conditions, they found the drag coefficient, C_D, and the inertia coefficient, C_m, to be a function of the relative displacement of the fluid, q/D, where q is the total flow displacement. Their results yielded evidence that C_D and C_m are interrelated and, for the case of constant acceleration, they showed analytically that a relationship exists between C_D and C_m.

Semi-empirical Methods

The most commonly used method of treating wave forces on piles is that due to Morison, O'Brien, Johnson and Schaaf [7]. The horizontal wave force is assumed to consist of two components — one representing the drag force and proportional to the square of the horizontal particle velocity; the other representing the inertia (virtual mass) force and proportional to the horizontal particle acceleration. It is assumed that the drag and inertia components are mutually independent and can be added linearly. Expressing this mathematically for a differential force, dF, acting over a differential segment of a rigid vertical pile, dy, the equation is

$$dF = \left[C_m\left(\frac{\rho\pi D^2}{4}\right)\frac{\partial u}{\partial t} + C_D\frac{\rho D}{2}|u|u\right] dy \qquad (4)$$

where D is the diameter of the pile, u is the horizontal component of the particle velocity in the absence of the pile and t represents time.

The equation for differential moment, dM, about the bottom of the pile is

$$dM = (d + y)dF \qquad (5)$$

where d is the still water depth and y is the depth below the still water measured negatively downward.

Equations (4) and (5) and their integrated forms have been extensively used in determining values of C_D and C_m for use in the design of piles subjected to wave action. The procedure involves the use of measured values of wave profile, wave force and/or bending moment along with the analytically determined particle velocity and acceleration in the above equations. When this is done, C_D and C_m become the unknowns. Then by judiciously selecting the value of force or moment recorded when the drag and inertia contributions individually become zero, C_D and C_m may be calculated.

The above semi-empirical procedure has been employed by many investigators in handling the wave-force-pile problem. It was used by Morison, Johnson, and O'Brien [8] in analyzing the results from wave tank studies of forces on piles. Also, Wiegel, Beebe and Moon [9] used the same procedure to analyze the results of a rather extensive prototype test program. Both groups of investigators used the Airy theory for waves of low steepness to describe the particle motions in order to evaluate C_D and C_m.

The application of the Morison approach using wave theories of finite steepness to determine the separate drag and inertia contributions to total pile force has been employed by Reid and Bretschneider [10] for a range of waves in shallow, intermediate and deep water. The drag and inertia coefficients were determined on the basis of field data.

An alternate method of using equation (4) is to calculate the kinematic flow field using the stream function representation presented by Dean [11]. Dean's stream function theory is applicable to nonlinear ocean waves and, in turn, to symmetrical and unsymmetrical nonbreaking waves. Aagaard and Dean [12] employed this representation in their mathematical model for calculating ocean wave forces on offshore drilling structures.

The coefficients of drag and mass obtained by the Morison approach, using measured forces and moments in equation (4) or (5), respectively, possess a large amount of scatter when an attempt is made to correlate them with Reynolds number. This has led a number of investigators to seek alternate approaches to handling the problem of wave forces on piles.

Keulegan and Carpenter [13], retaining the basic Morison equation (4), experimentally determined time histories of wave forces on horizontal cylinders and rectangular plates located at the node of a standing wave. The average drag and mass coefficients over an entire wave length were then obtained through a Fourier analysis of the forces obtained. These coefficients showed no correlation with Reynolds number, but were found to possess definite dependencies on the so-called period parameter, $U_m T/D$, where U_m is the maximum velocity, T is the period of the oscillations, and D is the diameter of a cylinder or the breadth of a rectangular plate.

Wiegel [14] compared the empirical plots of C_D and C_m versus $U_m T/D$ obtained by Keulegan and Carpenter for cylinders with field data reported by Wiegel, Beebe and Moon [9] and Reid [15] for a circular cylindrical pile. In the case of C_D, the empirical curve of Keulegan and Carpenter was found to yield an approximate upper envelope for the field data. On the other hand, the empirical curve for C_m was found to be an approximate lower envelope for the field data.

Harleman and Shapiro [16] proposed another procedure for correlating experimental data and predicting forces on prototype piles. They retained the Morison approach, but they used the MacCamy-Fuchs [17] diffraction theory for evaluating the inertia component and obtained the drag contribution on the basis of a steady state drag coefficient. They found that the degree of correlation between experimental and theoretical results was a function of the relative contributions of drag and inertia to the total force. Generally speaking, the agreement between theory and experiment was good, although in the limited range from 50 to 75 percent drag component the experimental values averaged 24 percent less than the theoretical values.

Crooke [18] applied the Iversen approach to published and unpublished horizontal wave force data of Morison, et. al. [7, 8] for model horizontal cylinders, vertical cylinders and spheres in oscillatory flow. He obtained reasonable correlation of C with Iversen's modulus for each geometrical model except for values of Iversen's modulus below about 0.1. No attempt was made to correlate C and Iversen's modulus for the case of actual field data.

Statistical Studies of Wave Forces

A number of investigators, for example, Bretschneider [19], Pierson and Holmes [20], Borgman [21] and Brown and Borgman [22] have studied the statistical distribution of wave forces on cylindrical piles. A fairly recent paper by Jen [23] applies some of these theories to statistical analyses of wave forces resulting from the action of irregular waves on a model pile.

Since this study is concerned with monochromatic waves, statistical approaches will not be further discussed.

Dimensional Analysis Approaches

Priest [24], questioning the relevance of so much attention to C_D and C_m on the part of some investigators, proposed that a purely experimental approach be taken and that the results be presented using dimensionless parameters including physical quantities pertinent to the problem. He then collected data from wave tank experiments to determine pressure intensities on the surface of a vertical cylinder that was subjected to the action of smooth shallow-water waves and to the action of shallow-water breaking waves of the spilling type. The data for smooth waves (the only waves of interest here) were graphically presented in dimensionless form using the function:

$$f_3(\frac{h}{d}, \frac{P}{\gamma d}, \frac{H}{d}) = 0 \qquad (6)$$

where h is the height of the center of the pressure transducers above the bottom of the basin, P is the pressure intensity, γ is the specific weight of the fluid and H is the wave height. Rather well-defined plots were obtained.

Priest points out that, although there is no apparent influence of the pile diameter, D, in his results, it may be possible that had substantially smaller values of a dimensionless parameter, D/d, been attained in the tests, some influence of this parameter may have been witnessed due to separation effects.

Paape and Breusers [25] recommended the establishment of experimental relationships of certain dimensionless parameters apropos to the wave and pile conditions. They performed model experiments in a wave tank using square piles subjected to a range of wave conditions, water depths and pile dimensions. The data were plotted on the basis of

$$\frac{F_{max}}{\rho g D^2 H} = f_4\left(\frac{H}{D}, \frac{d}{gT^2}, \frac{H}{gT^2}\right) \quad (7)$$

where F_{max} is the maximum wave force in the direction of wave motion.

The data provided a fairly distinct evaluation of the effects of each parameter and indicated H/D as a good independent variable for use in wave-pile studies.

The test program included experiments on different model scales and, although some data scatter were present, there were no scale effects observed using this method.

CHAPTER III

THEORETICAL CONSIDERATIONS

The Morison Equation

The so-called Morison equation (4) which was presented in the previous chapter arises from a more fundamental form which will now be developed. The expression for the incremental horizontal force, ΔF, acting on an incremental element of a rigid cylindrical body, due to accelerated flow past the body, may be expressed as the sum of three terms as follows:

$$\Delta F = \rho(\Delta V_m) \frac{d(ku)}{dt} + \oint (P\cos\alpha)dS + 1/2\ C_D\rho(\Delta A)|u|u \quad (8)$$

where ΔV_m is the volume of fluid displaced by the incremental element of the pile; dS is an elemental surface area; P is the fluid pressure in the absence of the pile; α is the angle between the flow direction and a normal to the surface of the pile; ΔA is the projected area of the incremental pile element perpendicular to the velocity; and k is the virtual mass coefficient.

For the special case of a circular cylindrical pile, we may write the differential force acting on a differential segment of the pile, dy, as

$$dF = \left[\rho(\frac{\pi D^2}{4}) \frac{d(ku)}{dt} + \oint (P\cos\alpha)ds + 1/2\ C_D\rho D|u|u\right]dy \quad (9)$$

where ds is the incremental area per unit length of the pile. The three terms appearing on the right-hand side of the above equation constitute the added mass, pressure gradient, and viscous drag contributions to the net incremental force, respectively.

The virtual mass coefficient, k, is a time dependent factor which, when multiplied by the volume of the fluid displaced by the pile, gives the effective mass of fluid accelerated in the flow field surrounding the pile. The value of k is one for a circular cylinder in a field of potential flow. However, in the case of a real fluid flowing past a pile, the value of k will vary depending upon the prior history of the fluid motion, the fluid viscosity and the surface roughness of the pile since each of these factors influences the flow pattern at any given time.

The pressure gradient term arises due to the force exerted on the pile as a result of the fluid accelerating in the flow field to which the pile is subjected. Since the mass of fluid displaced by the pile would experience an acceleration, due to the pressure gradient, equal to that of the ambient fluid, the second term of equation (9) may be written

$$\oint P\cos\alpha\, ds = \rho\left[\frac{\pi D^2}{4}\right]\frac{du}{dt}. \tag{10}$$

If equation (10) is now substituted into equation (9) and the additional assumption is made that k is constant with time, then

$$dF = \left[(1 + k)\ \rho\ \frac{\pi D^2}{4}\ \frac{du}{dt} + \frac{C_D}{2}\ \rho D|u|u\right]dy. \tag{11}$$

Usually the quantity (1 + k) is combined to form a single constant, C_m, which is called the coefficient of mass or inertia and the resulting equation becomes the expression commonly referred to as the Morison equation; i.e.,

$$dF = \left[C_m \rho \frac{\pi D^2}{4} \frac{du}{dt} + \frac{C_D}{2} \rho D|u|u\right] dy. \tag{12}$$

The coefficient C_m thus absorbs the effects of inertia and pressure gradient as well as the u dk/dt term arising in equation (9).

As was shown in Fig. 1, the drag coefficient, C_D, for steady flow is dependent upon the geometry, Reynolds number and the relative roughness. Moreover, for conditions of steady flow, the critical Reynolds number, where the drag coefficient experiences a sharp decrease, also depends upon the relative roughness. This sharp decrease in C_D occurs when the boundary layer becomes turbulent and the separation point shifts downstream.

In the case of unsteady flow, such as occurs in the oscillatory behavior of water particles in response to wave motion, the shift in separation point and the resulting decrease in C_D may not occur. The turbulent eddies which are generated and then swept back past the pile due to wave action may result in a turbulent boundary layer at substantially lower Reynolds numbers than are typical of steady flow.

In order to apply equation (12), numerical values of the coefficients C_m and C_D are required. These coefficients are obtained by measuring wave force and wave surface time-histories experimentally and using these data in conjunction with analytical expressions for particle velocity and acceleration to solve for the coefficients. In this semi-empirical method it is assumed that the drag and inertia coefficients are constants and mutually independent. Thus, the drag coefficient, C_D, is unaffected by the magnitude, direction and rate of acceleration of the fluid. Furthermore, both C_D and C_m are assumed invariant with depth in the fluid.

Also implied in the application of equation (12), using the semi-empirical method to be described, is the Froude-Kriloff hypothesis discussed by Korvin-Kroukovsky [26] and Beckmann [27] which assumes that the wave height, length and period are not affected by the presence of the pile itself. This condition holds when the diameter of the pile is small compared with the wave length.

The procedure for applying equation (12) will now be outlined.

Evaluation of Drag and Inertia Coefficients

Fig. 2 shows a geometrical sketch of a wave train and pile along with a designation of the sign convention employed in the equations used. The origin is chosen at a point corresponding to the still water level at the crest position.

The method of evaluating C_D and C_m will be presented on the basis of using the linear wave theory for small amplitude waves. Higher order wave theories could, in principle, be applied in an analogous manner. However, the laboratory studies of Morison and Crooke [28] and Le Mehaute, Divoky and Lin [29] indicate that

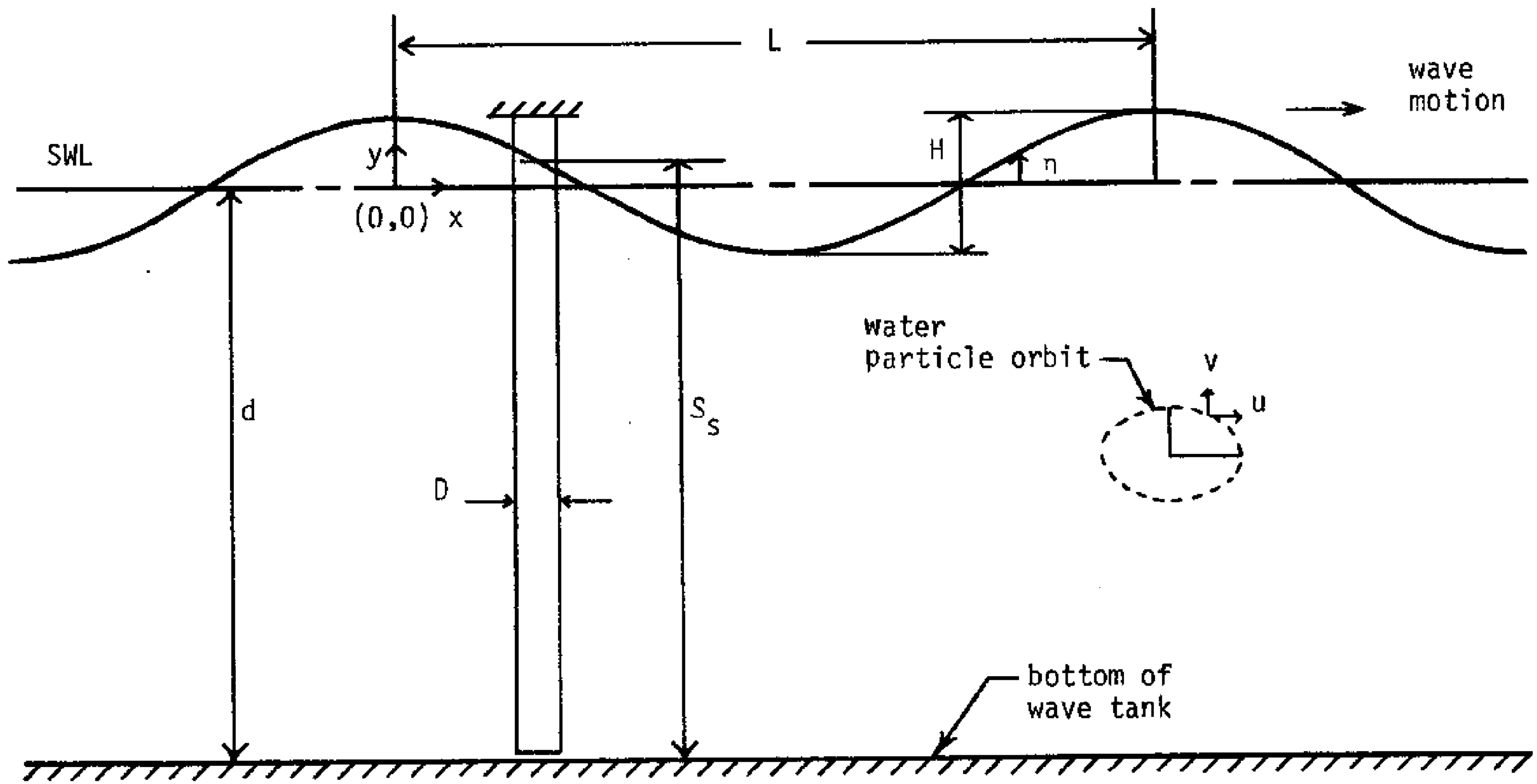

Fig. 2 Schematic of wave-pile geometry and sign convention

the more complicated representations would not predict the velocities or accelerations with much, if any, more accuracy than do the corresponding equations for the linear theory.

If the wave profile is taken as sinusoidal, then for a fixed point in the flow field, say at x = 0 for convenience, the surface elevation, η, may be expressed as a function of time, t, by

$$\eta = \frac{H}{2} \cos \frac{2\pi t}{T} . \tag{13}$$

By solving Laplace's equation,

$$\nabla^2 \phi = 0 \tag{14}$$

for potential flow and imposing the boundary conditions applicable to small amplitude, linear wave theory, the velocity potential, ϕ, may be obtained. Once an expression for ϕ is known, the particle velocities and accelerations are readily available through straightforward differentiation of the velocity potential. The detailed derivations are given by Kinsman [30] and since the solutions for the linear wave theory are well-known, the complete development will not be included here. The equations are presented in the form given by Wiegel [14] and employ the Eulerian description for conditions at a point in the fluid.

The expression for the horizontal particle velocity at a fixed point x = 0 in the flow field is

$$u = \frac{\pi H}{T} \frac{\cosh [2\pi(y + d)/L]}{\sinh 2\pi d/L} \cos \frac{2\pi t}{T} \tag{15}$$

where y is the distance measured negatively downwards from the still water level to the water particle.

The water particle total acceleration for two-dimensional flow is given by

$$\frac{du}{dt} = \frac{\partial u}{\partial t} + u \frac{\partial u}{\partial x} + v \frac{\partial u}{\partial y} \tag{16}$$

where u and v are the water particle velocities in the x and y-directions, respectively. For linear theory, the field accelerations are small compared with the local acceleration and, therefore, are neglected (see reference [14]). The water particle acceleration then becomes

$$\frac{\partial u}{\partial t} = - \frac{2\pi^2 H}{T^2} \frac{\cosh [2\pi(y + d)/L]}{\sinh 2\pi d/L} \sin \frac{2\pi t}{T} . \tag{17}$$

Two other quantities of interest in studying water particle kinematics are the total horizontal and vertical orbital displacements of the particles. Still using linear theory and choosing a convenient point x = 0 in the flow field, the expression for the total horizontal particle displacement is

$$\xi_t = H \frac{\cosh[2\pi(y_0 + d)/L]}{\sinh 2\pi d/L} \sin \frac{2\pi t}{T} \tag{18}$$

where y_0 is the mean vertical coordinate of the water particle for a given orbit.

The corresponding expression for the total vertical displacement of a particle is

$$\zeta_t = H \frac{\sinh[2\pi(y_0 + d)/L]}{\sinh 2\pi d/L} \cos \frac{2\pi t}{T} . \tag{19}$$

In order to evaluate the total force acting on a pile subjected to wave action, the expressions for u and $\partial u/\partial t$ are substituted into equation (12) and the resulting expression is integrated, assuming constant C_D and C_m, to obtain the resultant horizontal force. This integration yields

$$F = \pi\rho D \frac{H^2 L}{T^2}\left[-\frac{\pi D}{4H} C_m K_2' \sin\frac{2\pi t}{T} + C_D K_1' \left|\cos\frac{2\pi t}{T}\right|\cos\frac{2\pi t}{T}\right] \quad (20)$$

where

$$K_1' = \frac{\left(\frac{4\pi S_s}{L}\right) + \sinh\left(\frac{4\pi S_s}{L}\right)}{16\left[\sinh\left(\frac{2\pi d}{L}\right)\right]^2} \quad (21)$$

$$K_2' = \frac{\sinh\frac{2\pi S_s}{L}}{\sinh\frac{2\pi d}{L}} \quad (22)$$

$$S_s = \eta + d. \quad (23)$$

Equation (20) may now be employed to evaluate the drag and inertia coefficients. The quantity $2\pi t/T$ may be treated as a phase angle, θ, and using the coordinate system described in Fig. 2, θ is defined to be zero degrees at the crest position of the wave and 180 degrees at the trough position. Referring to equation (20) it may be observed that when $\theta = 2\pi t/T$ is zero and 180 degrees, the inertia contribution to the total force is zero. On the other hand, when θ equals 90 and 270 degrees, the drag contribution to the total force is zero. Therefore, by inserting measured values of F, H, L, T and S_s along with known values of ρ and D into equation (20) at a time corresponding to that at the crest of the wave ($\theta = 0°$), the value of C_D may be calculated.

Likewise, by making similar substitutions at a time when θ equals 90 degrees, the value of C_m may be calculated.

Relationship Between Dimensionless Parameters

Equation (12) may be rewritten in the form,

$$\frac{2\,\frac{dF}{dy}}{\rho D u^2} = C_m \frac{\pi}{2}\left[\frac{D\,\frac{du}{dt}}{u^2}\right] + C_D = C. \qquad (24)$$

The quantity in brackets may be recognized as Iversen's modulus or the acceleration modulus and C is the total resistance coefficient. Crooke's [18] studies of wave force data obtained from experiments on model cylinders showed Iversen's modulus to correlate C fairly well — at least to the extent of defining the shape of a curve.

The parameter $U_m T/D$ was found by Keulegan and Carpenter [13] to correlate values of C_D and C_m obtained as average values over an entire wave length for oscillatory flow past a cylinder. Here U_m is the maximum horizontal particle velocity.

Wilson [31] has demonstrated that Iversen's modulus and the Keulegan and Carpenter period parameter are related through the expressions for particle velocity and acceleration, equations (15) and (17). The relationship is

$$\frac{\frac{\partial u}{\partial t}D}{u^2} = \frac{2\pi}{U_m T/D} \qquad (25)$$

Furthermore, Wiegel [14] has shown that for the linear theory,

$$\frac{U_m T}{D} = \frac{\pi \xi_t}{D} \quad . \tag{26}$$

The significant aspect of the above discussion is that Iversen's modulus and the Keulegan and Carpenter parameter are different ways of expressing the same thing, namely the ratio of the relative total horizontal particle displacement to the diameter of the pile. It is also worthy of note that the investigations of Sarpkaya and Garrison [6] and those of Paape and Breusers [25] in each case revealed a ratio of particle displacement to the diameter of the immersed body as a significant parameter to use in wave force data correlations.

CHAPTER IV

EXPERIMENTAL PROCEDURE

Arrangement of Equipment

The experiments were conducted in a two-dimensional wave tank equipped with a mechanical wave generator driven by a variable speed electric motor. A sketch of the wave tank facility is shown in Fig. 3. The motor speed and paddle stroke arm length were set at a required combination of values to produce the desired wave height and length characteristics for each test run. The nominal dimensions of the wave tank are 2 ft. wide by 3 ft. deep by 120 ft. long. The wind, current and probe carriage capabilities of the wave tank were not used.

The arrangement of the laboratory equipment used is shown schematically in Fig. 4. A photograph of the actual operational system is presented in Fig. 5. The experimental apparatus consisted of a model pile which was mounted rigidly to a supporting frame and extended vertically downward into the wave tank. The lower end of the model pile cleared the bottom of the wave tank as indicated in Fig. 4. The water depth was set at 2 ft. The test pile was located 56 ft. from the wave generator and monochromatic waves of selected height and length combinations were mechanically generated at the pile.

The model pile was instrumented so that measurements of wave

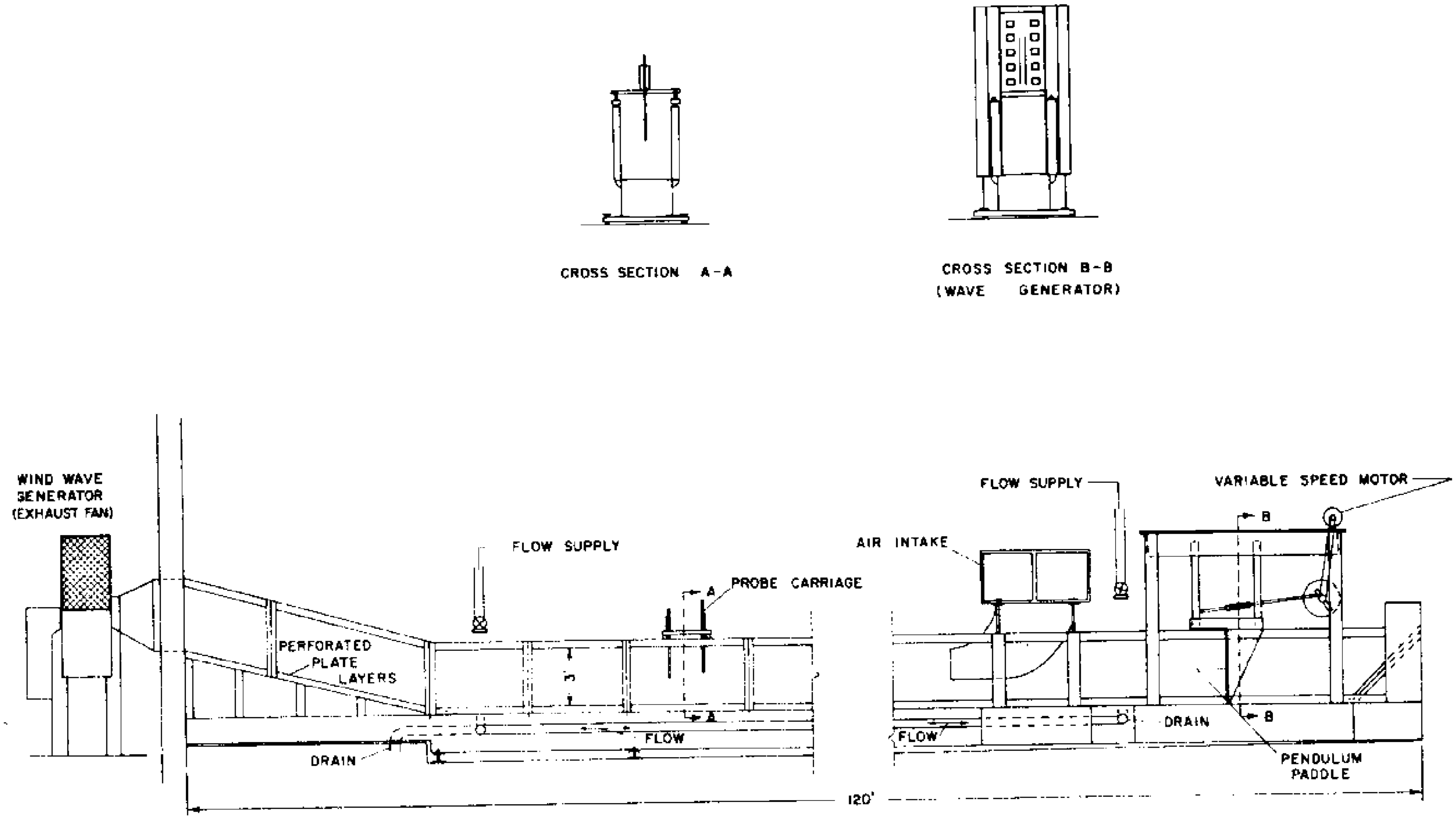

Fig. 3 The wave tank

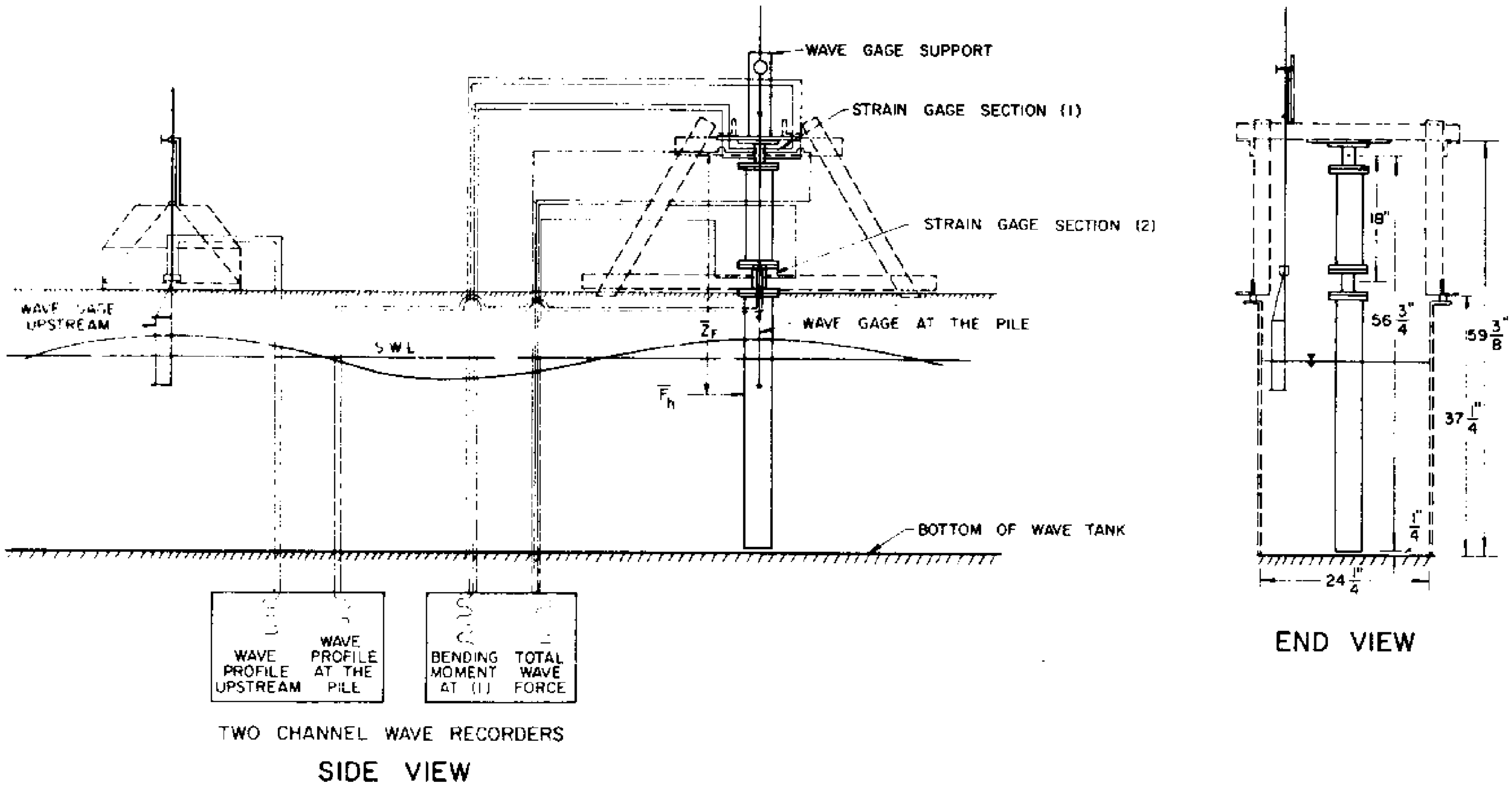

Fig. 4 Schematic of the arrangement of the experimental equipment

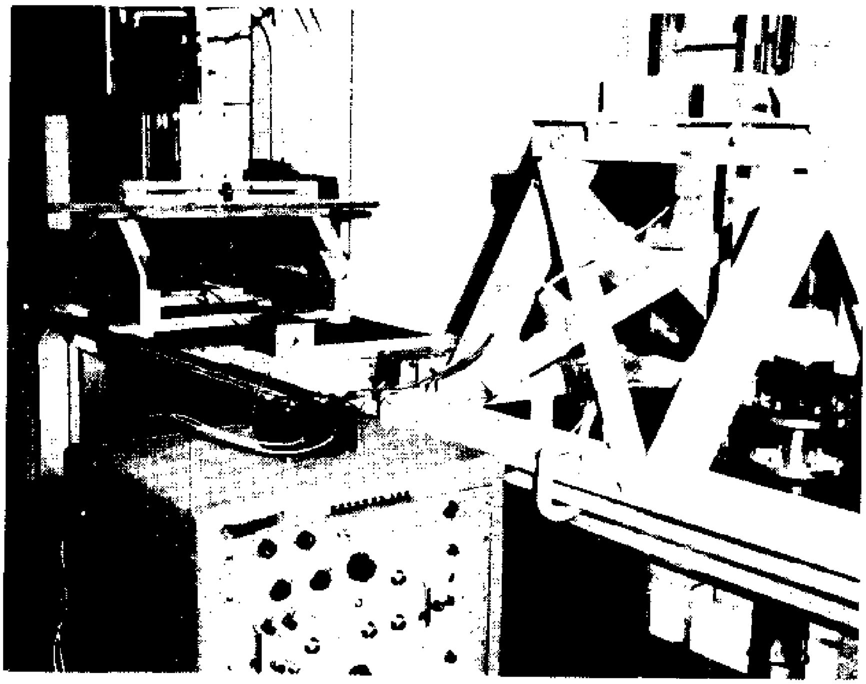

Fig. 5 Actual arrangement of the experimental equipment

force and bending moment could be accomplished by the use of strain gages mounted at selected sections of the pile. The instrumented pile consisted of essentially four sections (see Fig. 4): (1) an upper strain gage section, (2) a lower strain gage section, (3) an interconnecting portion of pile between the upper and lower strain gage sections, and (4) a lower section of pile which constituted the section on which the variations of pile surface roughness were made. The measurements of wave force and bending moment about the midpoint of the upper gage section were obtained as continuous time histories on a direct writing Sanborn 150 Dual Channel Carrier Amplifier-Recorder.

Only the lower pile section projected into the water. This particular configuration permitted all of the instrumentation to be located well above the water level and allowed the bottom pile section to be unbolted and removed. This latter feature permitted the removal of one roughness from the pile surface and the application of the next without risking damage of the instrumentation.

Two capacitance-type wave gages were employed to measure the wave surface elevation time-histories. One wave gage was located at the pile and thus recorded the wave phasing with respect to the force and moment traces. The second wave gage was situated 7 ft. upstream from the test pile and recorded the undisturbed surface time-histories of the approaching waves. The distance of 7 ft. was chosen so that there would always be less than two full waves between the wave gages, thus facilitating identification of common physical points on the two wave traces. The fixed distance between the two gages, in turn, allowed the wave length to be readily calculated since both traces were recorded with respect to a common time.

The water temperature was measured with a thermometer at the time each experiment was performed.

More complete details of the instrumentation design and data reduction techniques will be given in later portions of this paper.

Water Conditions

Sodium dichromate was added to the water in the wave tank to serve as a corrosion inhibitor.

Density comparisons of the sodium dichromate solution and distilled water were made using a pycnometer and analytical balance. It was found that the density of the sodium dichromate solution slightly exceeded that for distilled water, but the two values differed by only 0.05 percent.

Measurements of dynamic viscosity, μ, were also made of the sodium dichromate solution and distilled water using an Ostwald viscosimeter. A comparison of the viscosities obtained for the two fluids indicated that the viscosity of the sodium dichromate solution was larger than that for distilled water by about 1.8 percent.

The above changes in density and dynamic viscosity were considered inconsequential in view of other factors influencing experimental accuracy. Therefore, the values of density and kinematic viscosity, $\nu = \mu/\rho$, used in analyzing the experimental data were taken to be those readily available in tables for distilled water.

Wave Gages

The capacitance-type wave gages used in the experiments operate on the basic principle of a variable capacitor. A metal wire with a dielectric coating is mounted rigidly onto a supporting frame as indicated in Fig. 4. The metal wire inside the dielectric acts as one plate of the capacitor and the water surrounding the dielectric forms the other plate. As a wave moves past the gage, the change in water elevation along the dielectric coated wire varies the capacitance. By wiring this capacitor into the arm of a Wheatstone bridge and employing the necessary auxiliary circuitry and calibration, the wave record may be obtained on a direct writing recorder. The particular dielectric coated wire used was 8062, "No. 20 Hvy. Polythermaleze," manufactured by Belden. The recorder used was a Hewlett-Packard Model 321 Dual Channel Carrier Amplifier Recorder. The circuitry for this system is diagramed and explained in Appendix 1. Other descriptions of similar type wave gages have been presented by Killen [32], Hsu [33], and Harleman and Shapiro [16].

Wave Gage Calibration

The wave gage calibrations were obtained by adjusting the gains on the recorder amplifiers so that a known displacement of relative water level would give a convenient stylus deflection on the chart. The calibrations were checked before and after each experiment. A typical wave gage calibration for one experiment is presented in Fig. 6. The solid line represents the average of the calibration measurements made before and after an experiment was performed. Usually good agreement was obtained between the two sets of readings after correcting for a small amount of recorder drift. The gage wires were cleaned before the calibration check preceding each experiment. Also, the water was allowed to settle to a calm state prior to performing the calibration routine both before and after an experiment was executed.

The Model Pile

The detailed dimensions and assembly of the test pile are given in Fig. 7.

The interconnecting and lower pile sections were made from 6061-T6 aluminum tubing. The flanges which were welded onto these two portions of the apparatus were cut from 6061-T6 aluminum plate material. The upper and lower strain gage sections, designated No. 1 and No. 2, respectively, in Fig. 7, were machined as one piece, along with their flanges, to the required dimensions from

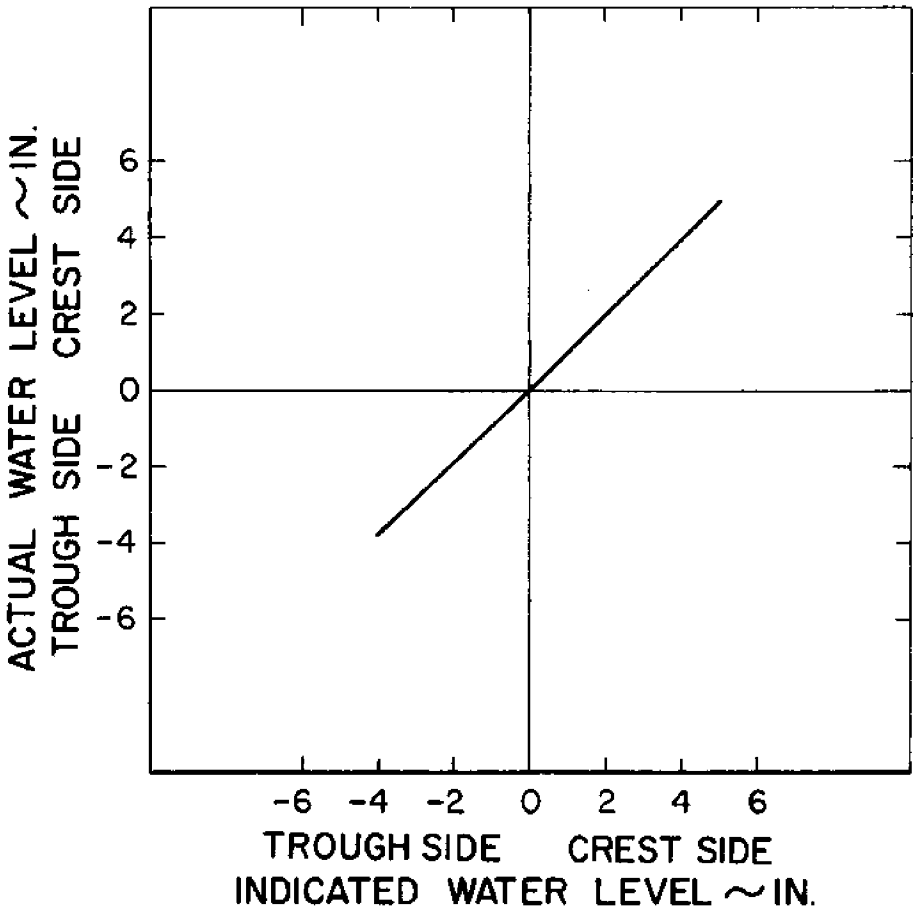

Fig. 6 Typical wave gage calibration curve

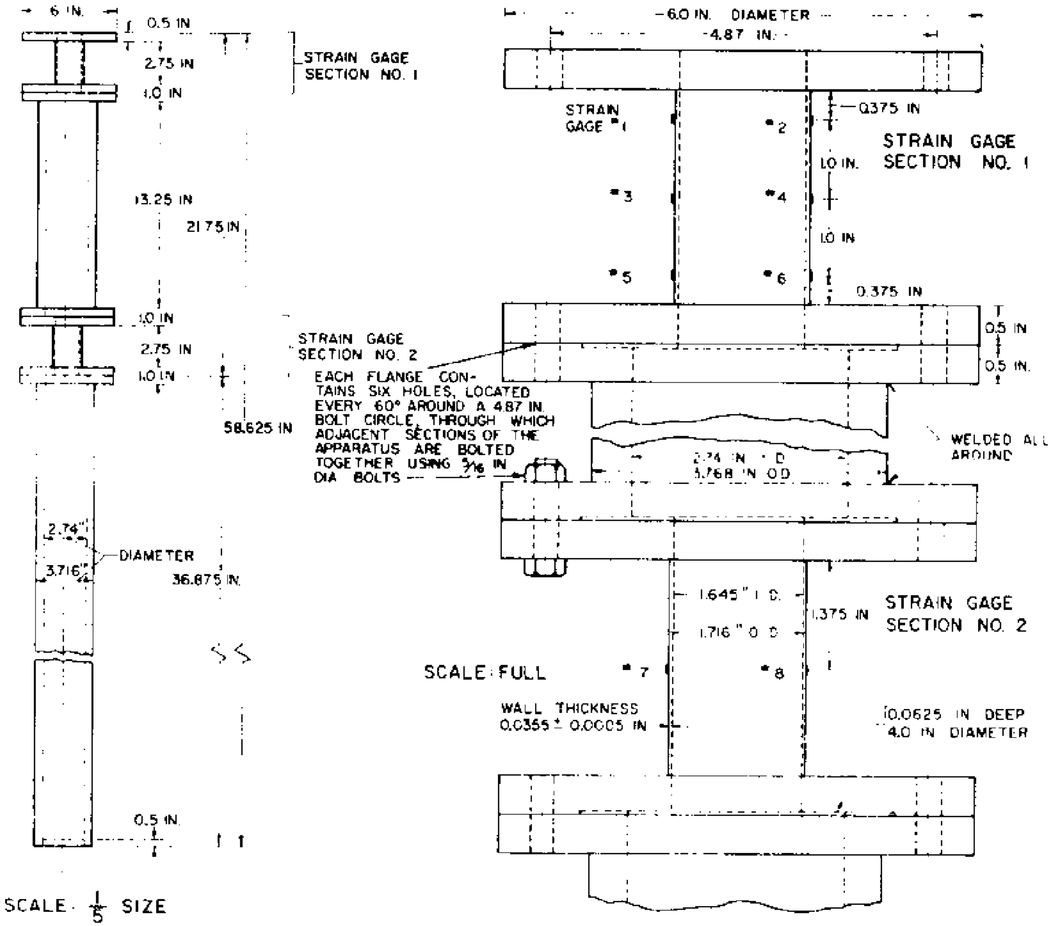

NOTES:

1 THE CYLINDRICAL MAIN PILE UPPER AND LOWER SECTIONS ARE 6061-T6 ALUMINUM TUBING OF THE SIZES INDICATED

2 THE CYLINDRICAL STRAIN GAGE SECTIONS AND THEIR FLANGES ARE MACHINED AS ONE PIECE FROM 7075-T6 BARE ALUMINUM STOCK TO THE DIMENSIONS INDICATED

3 THE PILE FLANGES ARE CUT FROM 6061-T6 ALUMINUM PLATE MATERIAL.

4 ALL JOINTS OF THE MAIN PILE AND FLANGES AND THE CAP PLATE AT THE BOTTOM ARE WELDED WATERTIGHT

5 NARROW WIDTH STRAIN GAGES ARE USED IN ORDER TO PREVENT EXCESSIVE CURVATURE OF THE GAGES WHEN THEY ARE APPLIED TO THE CURVED SURFACES 120 OHM BUDD STRAIN GAGES (C6-141-B, LOT NO A8-FBG-1) ARE USED THE ELEMENTS ARE ALIGNED PARALLEL TO THE AXIS OF THE PILE

6 STRAIN GAGES ARE MOUNTED EXACTLY DIAMETRICALLY OPPOSITE EACH OTHER. MARKINGS ARE MADE ON THE MATCHING GAGE SECTION AND ADJOINING PILE SECTION FLANGES TO ASSURE PROPER REALIGNMENT IN THE EVENT A DISASSEMBLY OF THE APPARATUS IS REQUIRED

7 THE STRAIN GAGE WIRING ON EACH GAGE IS RAN TO CONNECTORS WHICH ARE SCREWED TO THE FLANGES OF THE GAGE SECTION TO FACILITATE THE EXCHANGE OF GAGE SECTIONS STRAIN GAGES # 1, 2, 5 AND 6 COMPRISE THE FOUR ACTIVE ARMS OF A BRIDGE FOR MEASURING BENDING MOMENT STRAIN GAGES # 3, 4, 7 AND 8 COMPRISE THE FOUR ACTIVE ARMS OF A BRIDGE FOR MEASURING DIFFERENCE IN BENDING MOMENT, OR FORCE.

8 BECAUSE OF THE FLEXIBLE NATURE OF THE APPARATUS IN ITS FULL ASSEMBLY CONFIGURATION, THE BOTTOM MAIN PILE SECTION IS LEFT DETACHED DURING TRANSPORT AND INSTALLATION OPERATIONS UNTIL AFTER THE UPPER PILE SECTION WITH THE ATTACHED STRAIN GAGE SECTIONS IS MOUNTED ON THE SUPPORT RIG AT THE WAVE TANK.

9 THE APPROXIMATE WEIGHT OF THE APPARATUS ASSEMBLY IS 34 LBS

Fig. 7 Details of the test pile

7075-T6 bare aluminum stock. The mounting positions of the strain gages on the gage sections are shown in Fig. 7.

The natural frequency of the assembled pile in its installed position with 2 ft. of water in the wave tank was approximately 4.5 cps. With the tank drained of water, the natural frequency was around 5.5 cps. The frequencies of the water waves were between 0.6 and 1.24 cps; therefore conditions of sustained resonance were excluded.

The pile apparatus was equipped with alignment pins and machined indexes in order to assure that it would always be assembled in the same manner. The flange bolts were each tightened to a uniform torque of 150 in-lbs using a torque wrench so that the strain gage sections would not experience nonuniform stresses as a result of being assembled.

The lower main test section of the pile was machined so that the outer surface formed a true circular cylinder. The test section was then smoothed and highly polished in preparation for the experiments with the smooth surface. The smoothing was accomplished by starting with 320 carborundum wet or dry abrasive paper and then using progressively finer paper until the final smoothing using 500 grit was done. The pile surface was then polished with No. 39925 Hoppich Semichrome Polishing Paste. The final outside diameter of the smooth pile was 3.716 in. Fig. 8 shows a photograph of the smooth, polished pile. For the experiments involving the roughened pile surface, sand grains were glued

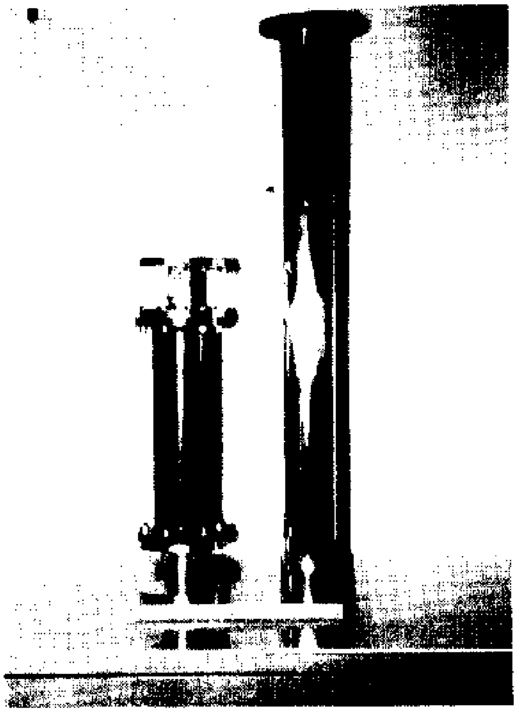

Fig. 8 The smooth pile

onto the same cylindrical pile that was used for the smooth surface experiments.

Strain Gage Section Design

The sections on which the strain gages were mounted had to be thin enough to provide measurable amounts of strain in response to the relatively small applied wave forces. At the same time, the gage sections had to be stiff enough to restrict the pile deflections to small values so that the pile accelerations could be neglected in analyzing the data. In order to satisfy these requirements, the cross section should have as large a radius of gyration as possible. A thin-walled circular cylinder was selected for the gage section geometry since its cross section has a relatively large radius of gyration and it can readily be machined with precision.

Preliminary calculations indicated that the wave forces which would be acting on the smooth pile should not exceed a magnitude of 5 lbs. The effects of pile roughness were unknown, but a design force of 7 lbs. was believed to be a conservative estimate of the maximum force which the pile would have to sustain in the experiments.

Imposing the requirement that the pile deflection be restricted to a small value, the gage sections were designed so that a 7-lb. applied load would not deflect the bottom of the pile more than 0.1 in. This deflection criterion was somewhat arbitrary;

Harleman and Shapiro [16] used a similar value with apparent success in their studies. The results indicated that a wall thickness of 0.0355 in. would experience 215 micro-strains. This was considered adequate and the gage sections were machined to the dimensions shown in Fig. 7.

Strain Gage Installations

The locations of the strain gages are shown in Fig. 7. Type C6-141-B, 120 ohms, Budd strain gages were used. These gages have a gage factor of 2.05 ± 1/2%.

Strain gages 1, 2, 5 and 6 comprise a Wheatstone bridge of four active arms wired so that its output is proportional to the bending moment about the midpoint of the upper strain gage section. Referring to Fig. 4, this moment, M_1, may be expressed analytically as

$$M_1 = \bar{z}_F F \tag{27}$$

where $\bar{z}_F$ is the vertical distance between the point of application of the resultant horizontal wave force and the midpoint of the upper strain gage section. (The $\overline{F}_h$ notation shown in Fig. 4 complies with that obtained by an averaging technique described in the next chapter.)

Strain gages 3, 4, 7 and 8 comprise a Wheatstone bridge of four active arms wired so that its output is proportional to the difference in the bending moment about the midpoint of the upper strain gage section, M_1, and the bending moment about the midpoint of the lower strain gage section, M_2. This allows direct measurement of wave force, through a calibration, since, referring to Fig. 4 and letting b equal the vertical distance between the midpoints of the upper and lower strain gage sections,

$$F\bar{z}_F - F(\bar{z}_F - b) = M_1 - M_2 \tag{28}$$

and, therefore,

$$F = \frac{M_1 - M_2}{b} \tag{29}$$

where the subscripts 1 and 2 refer to the upper and lower gage sections, respectively.

The use of four active arms provides maximum output signal and also provides automatic temperature compensation.

The circuit diagrams, along with an explanation of their principles of operation, are presented in Appendix 1.

Calibration for Wave Force and Bending Moment

The calibrating system is pictured in the upper right-hand portion of the photograph in Fig. 9.

The instrumented pile was calibrated by applying dead weights to a cord which transmitted the load through a system of pulleys so that the force was applied to the pile in a longitudinal direction parallel to the wave tank. The gains on the recorder amplifiers were then adjusted to give a convenient reading on the chart per unit of force and bending moment. Loads of varying magnitude were

Fig. 9 Pile calibration system

applied at different lengths of moment arm in order to check the linearity with force and with moment arm. The calibration was checked at the beginning and end of each day's running and spot-checks were made each time the paper was changed in the recorder. The calibrations were linear over a large portion of the range of interest and only slight changes in the calibration occurred as the test program progressed. Without exception, the calibration for a particular day remained the same. The deviations in linearity were accounted for, where applicable, in reducing the data. A typical wave force calibration curve is shown in Fig. 10.

Sand Grains

A range of prepared surfaces from smooth to very rough was studied. The initial set of experiments was performed on the smooth, polished pile surface. The data obtained using the smooth surface served as a control for comparison of the results obtained from a similar set of experiments ran on each of the roughened surfaces.

Roughening of the pile surface was accomplished by gluing sand grains of a designated size onto the surface of the pile with lacquer. Good adherence of the grains to the pile was achieved with only random dislodging of some grains due to the wave action. The weight comparisons of the test section of the pile before and after each set of experiments are shown in Table 1.

The sand grain size for a selected roughness was controlled

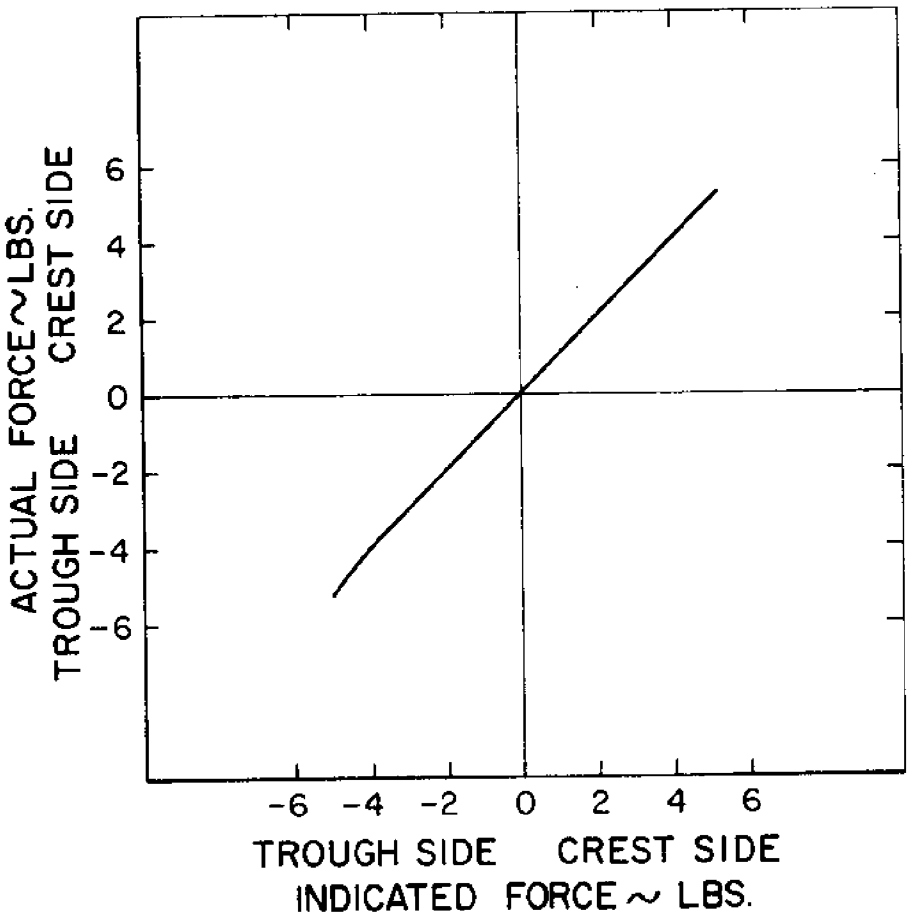

Fig. 10 Typical wave force calibration curve

Table 1 Comparison of weights of the bottom pile section before and after testing

Surface type	Pile test-section weight		
	Before testing	After testing	Difference
Smooth	18 lbs, 12.5 oz	18 lbs, 12.5 oz	—
Roughness No. 1	19 lbs, 6.0 oz	19 lbs, 5.8 oz	0.2 oz
Roughness No. 2	20 lbs, 4.5 oz	20 lbs, 3.8 oz	0.7 oz
Roughness No. 3	21 lbs, 11.8 oz	21 lbs, 10.8 oz	1.0 oz

on the basis of preferred screening utilizing sieve openings defined by the U.S. Bureau of Standards [34]. The sand size ranges studied were:

Roughness No. 1, 0.0232 - 0.0331 in.,

Roughness No. 2, 0.065 - 0.0787 in., and

Roughness No. 3, 0.132 - 0.157 in.

Using average particle diameters, the relative roughnesses, ε/D, of the three roughened surfaces were 0.0075, 0.0186 and 0.0361.

Photographs of the three roughnesses are presented in Figs. 11, 12 and 13. The levels of roughness may be judged by considering roughness no. 3 to correspond approximately to that exhibited by marine growth of 1.73 in. diameter on a 4-ft. diameter pile.

Wave Characteristics

The wave characteristics used in this study covered a range of combinations of wave height, length and period. A set of experiments on a particular pile surface consisted of 22 combinations. By using a fairly wide range of wave characteristics, varying degrees of drag and inertia contributions to the total wave force could be obtained.

A summary of the wave characteristics, including the $d/\bar{L}_a$ and $\bar{H}_a/\bar{L}_a$ ratios, is presented in Table 2. Here $\bar{H}_a$, $\bar{L}_a$ and $\bar{T}_a$ are the average values obtained for wave height, length and period, respectively, over the four sets of experiments. The corresponding averages for a wave of a particular set may show some deviation

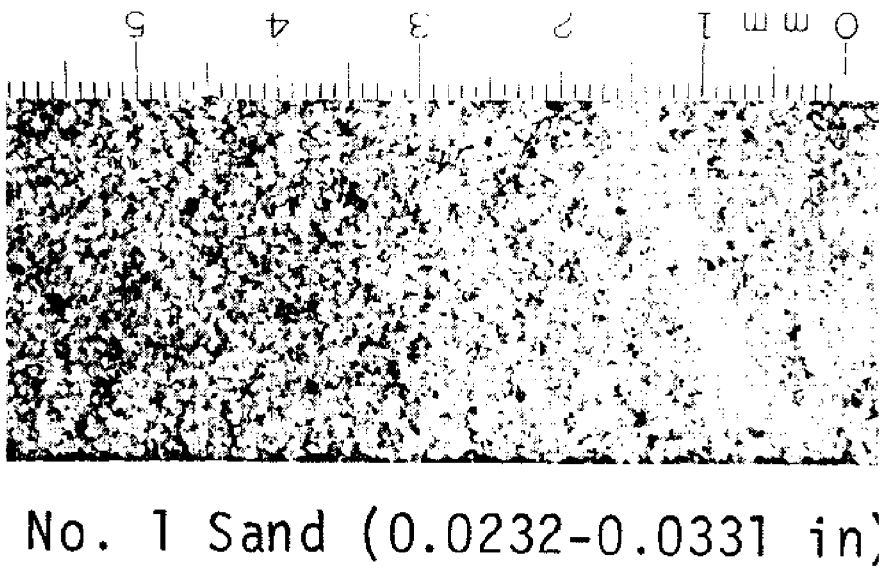

Fig. 11 Surface roughness no. 1

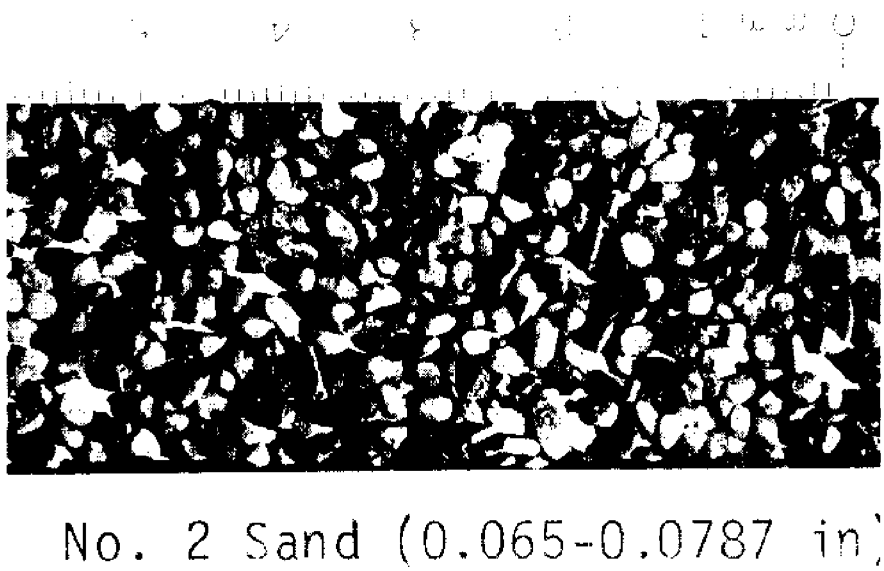

Fig. 12 Surface roughness no. 2

No. 3 Sand (0.132-0.157 in)

Fig. 13 Surface roughness no. 3

Table 2 Summary of average wave characteristics

Wave	$\overline{H}_a$ (in)	$\overline{L}_a$ (ft)	$\overline{T}_a$ (sec)	$d/\overline{L}_a$	$\overline{H}_a/\overline{L}_a$
1	1.88	5.08	0.84	0.542	0.042
2	4.17	3.66	0.82	0.547	0.095
3	4.79	3.90	0.84	0.512	0.102
4	2.06	5.50	1.04	0.363	0.031
5	4.02	5.49	1.03	0.364	0.061
6	5.97	5.53	1.04	0.362	0.090
7	6.26	5.18	1.02	0.386	0.101
8	1.83	7.85	1.27	0.255	0.019
9	3.78	7.85	1.28	0.255	0.040
10	5.66	8.00	1.30	0.250	0.059
11	8.29	7.27	1.25	0.275	0.094
12	8.68	7.19	1.20	0.278	0.101
13	2.14	10.00	1.52	0.201	0.018
14	3.94	10.04	1.52	0.199	0.033
15	6.96	9.51	1.48	0.210	0.061
16	7.46	9.38	1.48	0.213	0.066
17	8.64	8.62	1.35	0.232	0.084
18	2.22	11.72	1.66	0.170	0.016
19	4.28	11.20	1.64	0.178	0.032
20	6.27	11.27	1.67	0.177	0.046
21	8.03	11.52	1.65	0.174	0.058
22	9.78	10.65	1.56	0.188	0.077

from that presented in Table 2. The waves were duplicated as nearly as possible for the set of experiments involving each selected surface roughness, but the duplication was not exact.

CHAPTER V

DATA REDUCTION

Data Records

Fig. 14 shows a typical set of data traces obtained from the direct writing recorders. The traces are continuous plots in time of the variations of wave profile at the pile, wave profile seven feet upstream from the pile, net horizontal wave force acting on the pile and the bending moment about the midpoint of the upper strain gage section due to the applied wave force. Analysis of the data presented in this report is based upon the two wave profile traces and the wave force trace. The moment trace would have provided an alternate measurement by which to analyze the data had the force instrumentation failed. Also, the moment measurement could have been used in conjunction with the force measurement to determine the point of application of the net force should this information have been needed.

As mentioned previously, the wave profile at the pile provided the proper phasing of the wave and force traces. In order to make the data consistent with the sign convention for which the equations were written, each wave was considered to begin with a phase angle of zero degrees at the crest. Each wave was divided into four equal parts and the phase angles of 0, 90, 180, 270 and 360 degrees were assigned successively to the end points of the equal segments

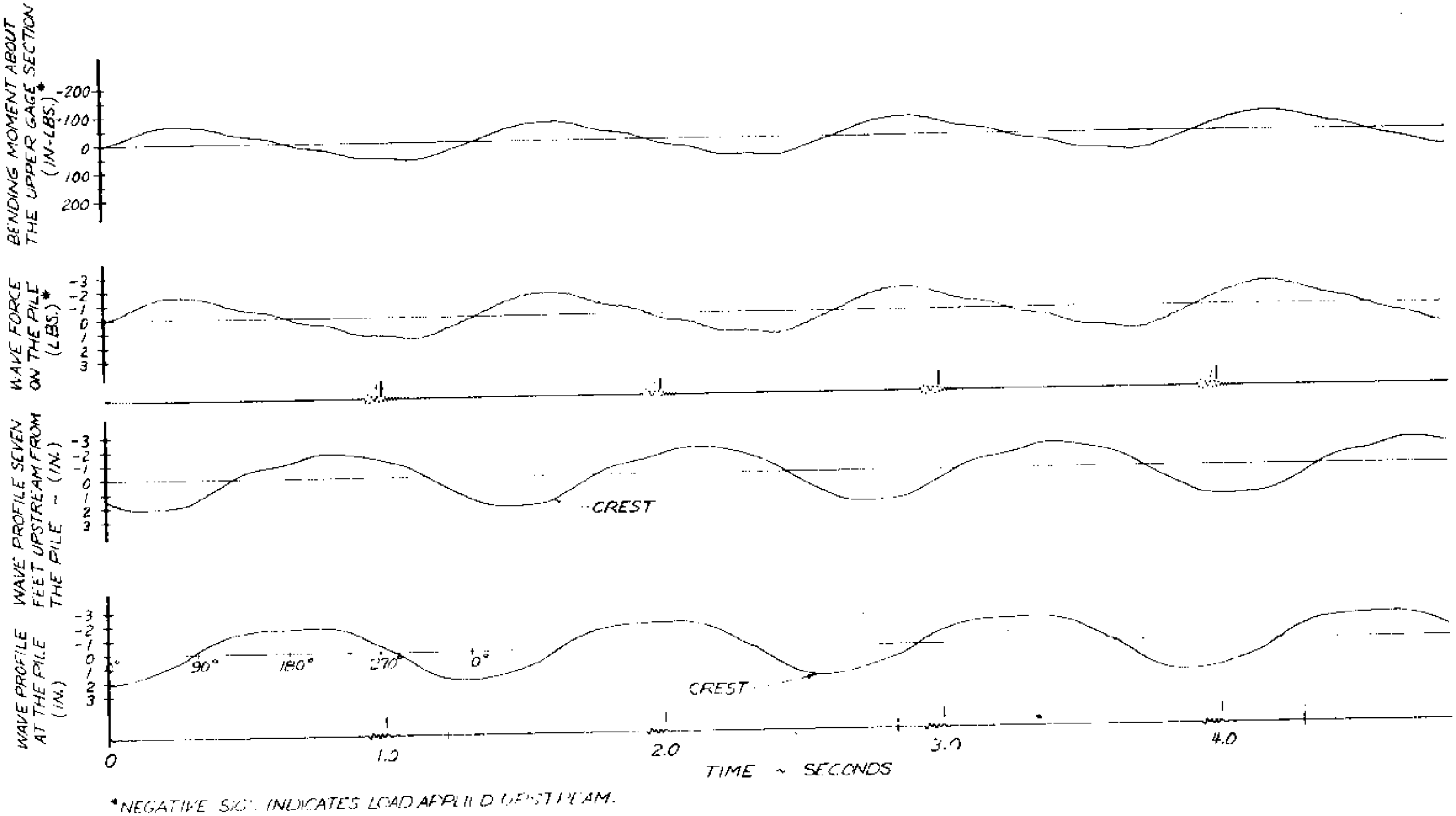

Fig. 14 Typical portion of a data record

as indicated in Fig. 14. These phase angles were used in selecting simultaneous values of force and surface elevation which were, in turn, substituted into the equations for calculating C_D and C_m.

Evaluation of Wave Characteristics and Forces

The wave height, length and period for each experiment were evaluated for each individual wave and then the average value of each quantity was determined by averaging the results obtained for a specified number of waves, N. The number of waves averaged was established by determining the number required to make the average wave height and maximum wave force approach a constant mean value within 1 percent for all of the experiments. Twenty waves satisfied this criterion in almost all cases; occasionally 21 waves were required for an experiment. The average wave height and period were determined from the wave record recorded 7 ft. upstream from the pile, whereas the evaluation of the average wave length required the use of the records obtained from both the upstream and the pile position wave gages. The procedure for evaluating the wave length will now be further explained.

Referring to Fig. 15, the common physical points at times $t_A(1)$ and $t_{A'}(1)$ of the two wave profiles recorded a distance, ℓ_G, apart were determined by inspection. Knowledge of the distance between the wave gages and the approximate length of the wave recorded were needed to make this determination. The time $t_B(1)$ corresponding to one wave period earlier than $t_A(1)$ was located

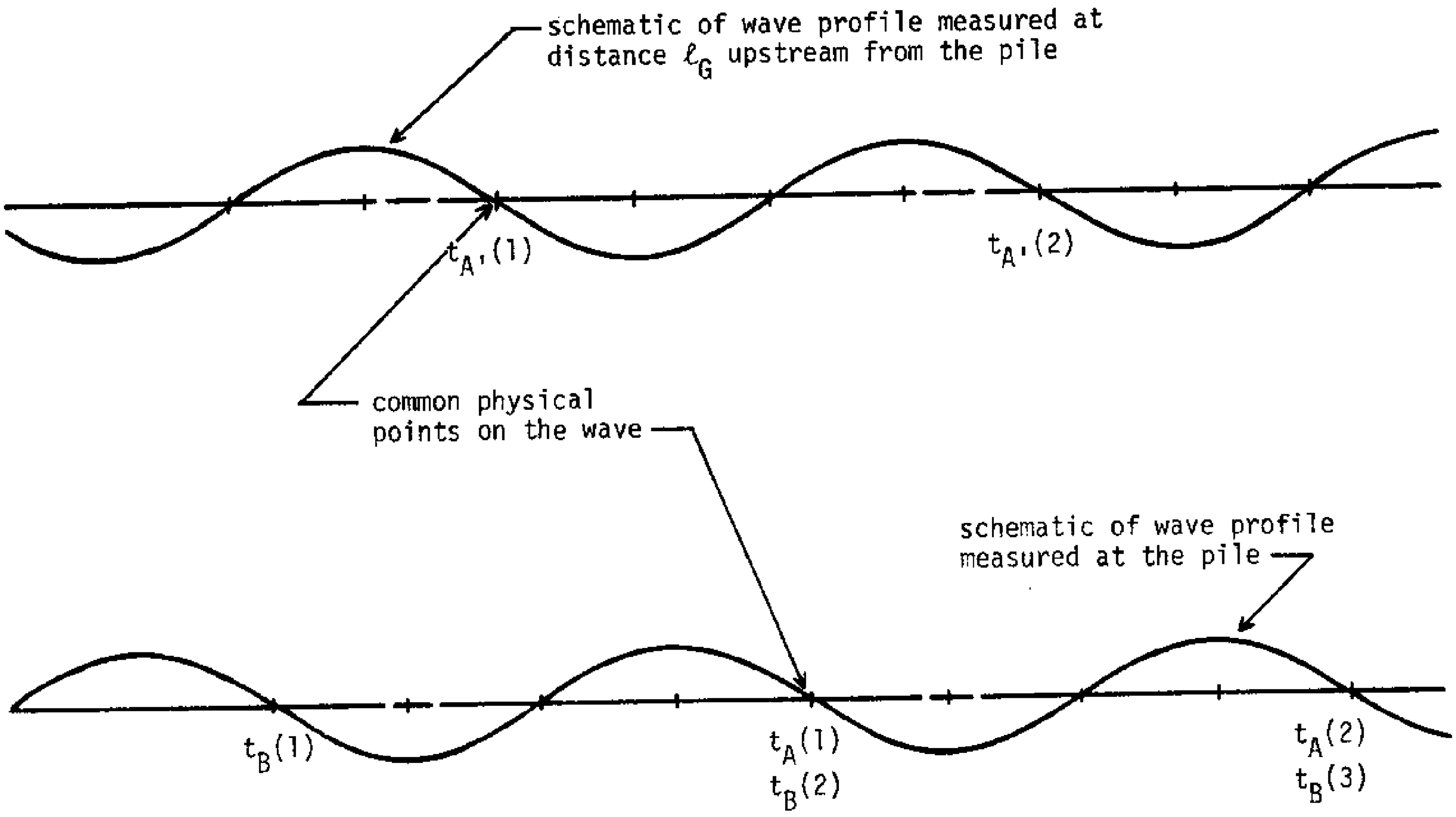

Fig. 15 Schematic showing common physical points on wave records taken at two different locations

as shown in Fig. 15. Once the initial time values were selected, the remaining values of $t_A(i)$, $t_{A'}(i)$ and $t_B(i)$ were marked as indicated in Fig. 15. Since the records were made a fixed distance, ℓ_G, apart and were recorded on the same time scale, the following proportionality holds,

$$L(i) = \frac{t_A(i) - t_B(i)}{t_A(i) - t_{A'}(i)} \ell_G \tag{30}$$

and the average for N waves is

$$\overline{L} = \frac{\sum_{i=1}^{N} L(i)}{N} . \tag{31}$$

The values of wave surface elevation, η, and wave force, F, occurring simultaneously for a given phase angle, θ, were also averaged over N waves before being substituted into equations (20), (21), (22) and (23) for evaluation of C_D and C_m. The values of η were read from the upstream wave record after transposing the phase angles, established on the basis of the wave record at the pile, to account for the distance between the wave gages.

Calculation of Correlation Parameters

The correlating parameters, such as Reynolds number, Iversen's modulus and the Keulegan and Carpenter parameter, involve such quantities as particle displacement, velocity and acceleration. Since the waves in each set of experiments spanned a range of wave characteristics, the distributions of displacement, velocity and acceleration with depth would also cover a range of possibilities. Therefore, it seemed that root mean square values of these kinematic quantities would be a reasonable representation.

The root mean square of horizontal particle velocity, u_{rms}, and acceleration, a_{hrms}, at a given phase angle position were obtained on the basis of dividing the distance between the surface elevation and the bottom of the wave tank into 13 equal intervals and evaluating the horizontal particle velocity or acceleration at each of the resulting 14 levels. The choice of interval size is to some extent arbitrary, but it was felt that an interval size of around two inches would be a reasonable choice if one attempted to obtain experimental data for evaluation of particle velocity or acceleration.

For evaluation of the root mean square of the total horizontal particle displacement, ξ_{trms}, and the total vertical particle displacement, ζ_{trms}, a slightly different breakdown of the depth was used in order to more conveniently apply equations (18) and (19). Here 12 intervals were taken, two inches apart, beginning at the still water level and progressing to the bottom of the wave tank.

The pile diameter (including the sand grains) was used in evaluating the numerical values of the correlating parameters which involved D as a characteristic length.

A computer program was written to perform the calculations necessary in obtaining numerical values of the dimensionless parameters, as well as the drag and mass coefficients, needed for analyzing the data. A step-by-step description of the computation procedure and a listing of the program appear in Appendix 2.

Adaption of the Data to Theory

Some compromise was necessary in adapting the experimentally obtained data to the theory used. First of all, the waves obtained experimentally were not pure sinusoids and this resulted in the wave profile trace having some finite magnitude at the phase angles where a sinusoidal profile would have had zero surface elevation with respect to the still water level. These finite values of surface elevation were small and constituted only a minor change when their values were added to or subtracted from the water depth in the force equation (20).

A second adjustment of the experimental data arose in connection with the wave forces. For the experiments involving the larger wave heights, the model pile vibrated at its natural frequency and these oscillations were superimposed on the force traces. These oscillations were filtered out by dividing the peak to peak distance of the pile oscillation in two and then fairing a line through these midpoints to obtain the actual force trace. This fairing procedure was done by the same person for all of the data and this fact, coupled with the averaging of at least twenty values of force for calculation of any parameter involving force, should, in the final analysis, essentially remove any subjective element involved in comparing the differences between the results obtained for each set of data.

Another problem arose due to development of long period waves in the wave tank upon which the generated waves became superimposed as an experiment progressed. The use of average values of the wave characteristics obtained from a fairly large number of waves, hopefully minimizes the effect of this source of error.

Consistency was maintained in all procedures involved in the gathering and reduction of the data. This aspect, in conjunction with the ultimate aim of evaluating the differences in the results obtained as the pile surface was progressively roughened, should render the influence of experimental deficiencies on the final results small in magnitude.

CHAPTER VI

DISCUSSION OF RESULTS

A plot of drag coefficient, C_D, versus Reynolds number, $u_{rms}\,D/\nu$, obtained for the smooth and roughened surfaces is presented in Fig. 16. The Reynolds number is based on the overall pile diameter and the root mean square velocity obtained over the depth span of the water. As mentioned in Chapter V, page 53, the root mean square values were used for representing the velocity and other particle kinematics since this provided a convenient means of incorporating the range of possible depth variations of these quantities into the final results. The values of C_D in Fig. 16 were obtained by using the Morison approach described in Chapter III. The scatter exhibited by these data is typical of that obtained by other investigators using this approach (see Reference [14]). No particular trends or groupings of the data with respect to pile surface roughness appear for the four surfaces represented. This observation would indicate that surface roughness has no effect on C_D — as obtained using the Morison approach.

The presently recommended value of C_D for design is in the range of 1.0 to 1.2 (see References [12] and [35]). The averages of the data of Fig. 16 comply generally with these values, yielding an overall average C_D less than design values for Reynolds numbers above 2×10^4 while below Reynolds numbers of 2×10^4, an apparent increase in the overall average of C_D to values above those recom-

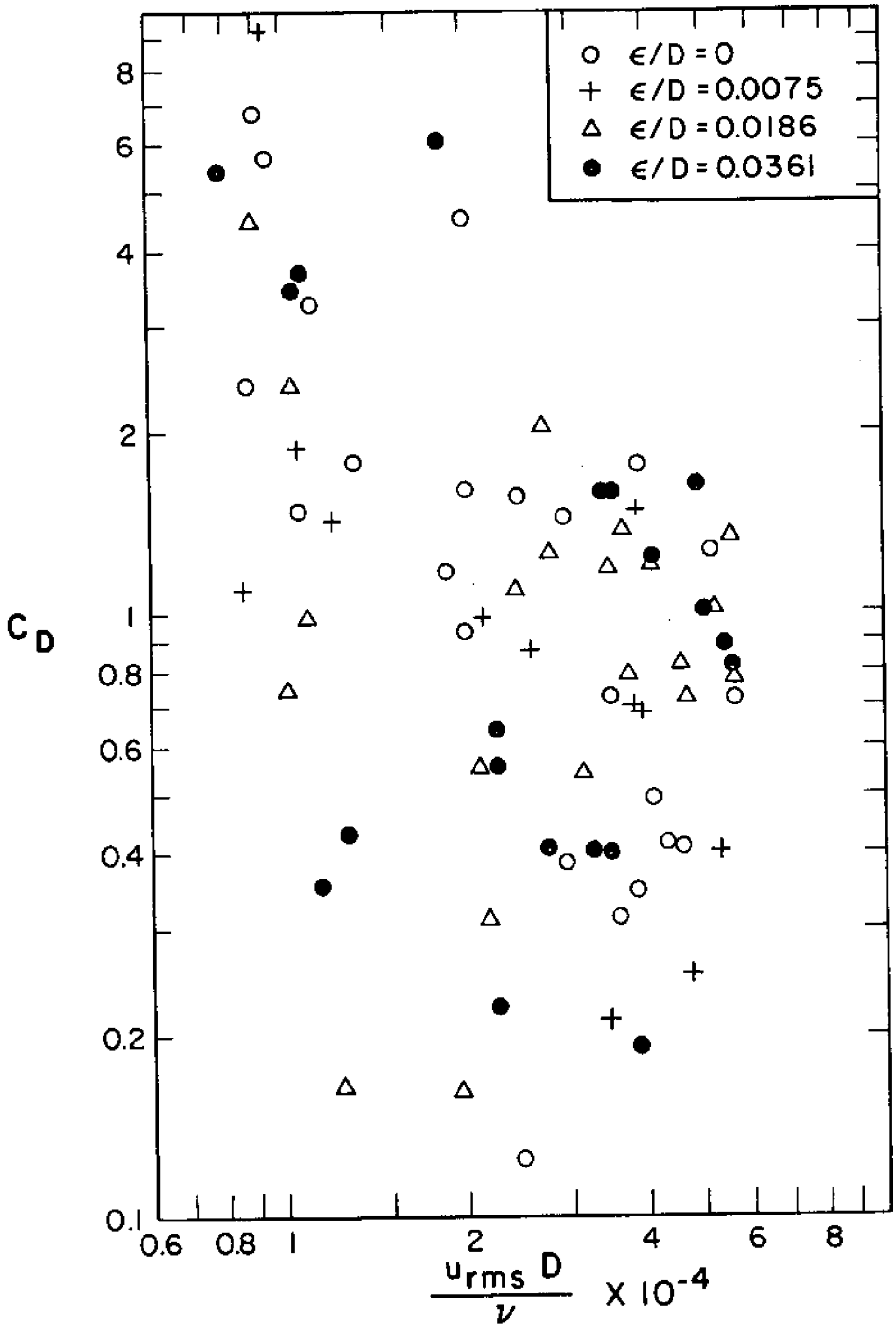

Fig. 16 Drag coefficient versus Reynolds number

mended for design occurs for both the smooth and rough surface conditions. These relatively high values of C_D tend to occur when the conditions of small wave steepness and, thus, small particle velocities prevail. This tendency is consistent with that for laminar flow past a cylinder in steady flow [36].

The inadequacy of the semi-empirical method employed with these data is evident from the fact that in some cases the attempt to use the experimental data in conjunction with the analytical expressions based on idealized assumptions resulted in negative values of C_D. These negative C_D's, as well as the pronounced scatter present in the results, apparently resulted from the, so far, intractable aspect of adequately describing theoretically the wave and force interactions with the pile. The wave profiles obtained experimentally are not pure sinusoids as assumed in the theory and this in turn yields a force response different to that which would be obtained were the wave sinusoidal. This results in a negative value of force occurring for a wave phase angle of θ_1 in some cases. These negative forces, in turn, yield negative values of C_D when used in the Morison equation (20). The values of C_D were considered as absolute values for plotting purposes in Fig. 16. The wave records were obtained at 100 mm/sec paper speed on the recorders and the matching of the wave and force records in time were considered accurate enough to preclude any pronounced misreading of the wave and force records with respect to phase angle.

Fig. 17 shows a plot of inertia coefficient, C_m, versus

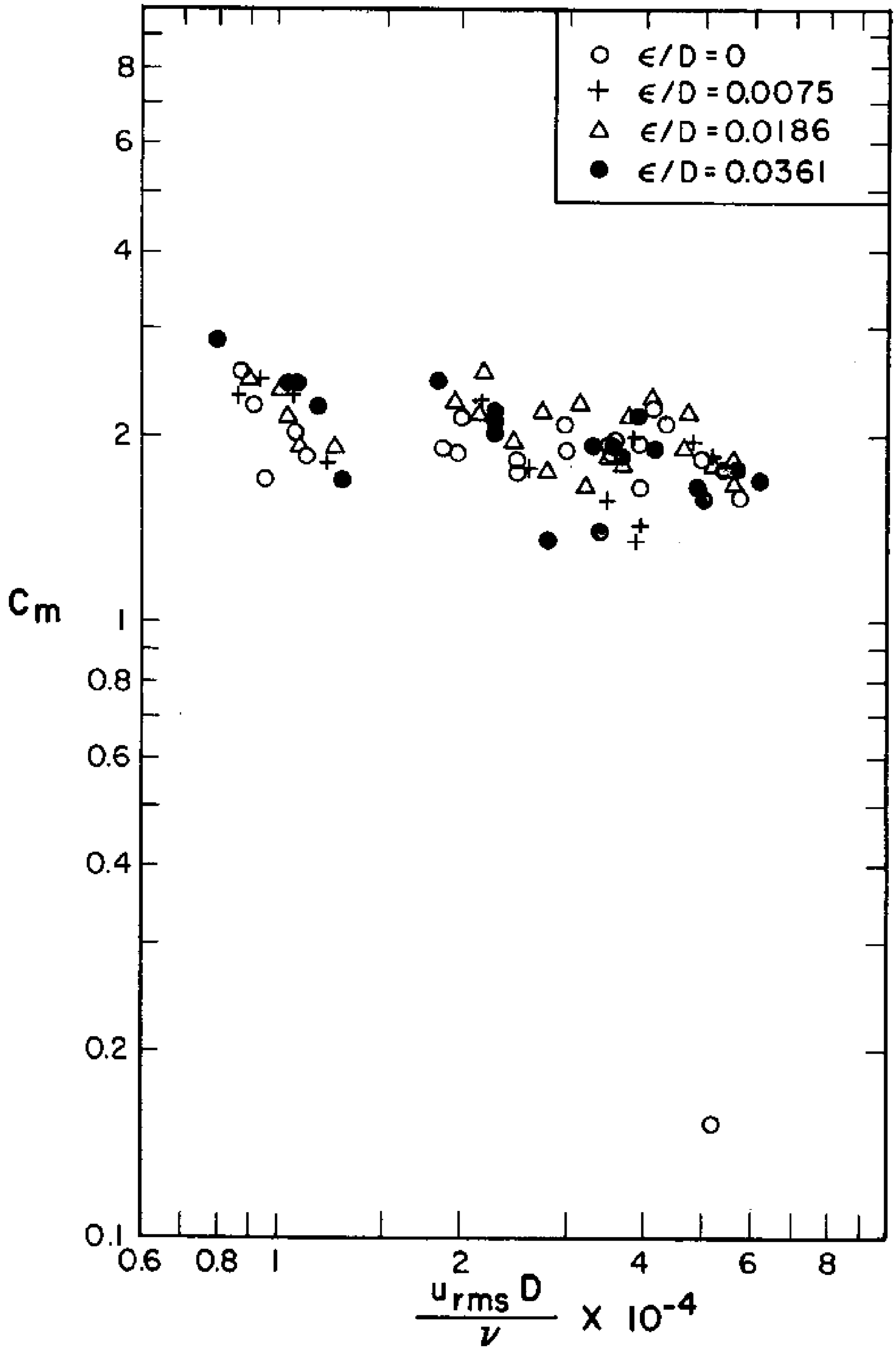

Fig. 17 Inertia coefficient versus Reynolds number

Reynolds number. These results were obtained using the Morison approach and here, as in the case of C_D, there is no apparent effect of surface roughness. The presently recommended value of C_m is 1.5 (see References [12] and [35]). The values of C_m are congregated around a value of 2.0 which is the theoretical value for a circular cylinder in steady flow. This value is high when compared with the accepted design value; however, the C_m's appear to be approaching the value of 1.5 as the Reynolds number increases.

Fig. 18 presents a plot of all of the force data corresponding to the wave phase angles θ_1 and θ_2 at which the drag and inertia coefficients, respectively, were evaluated. The data fall predominantly in the region where the inertia forces are larger than the drag forces. This representation of $\overline{F}_{h\theta_1}$ and $\overline{F}_{h\theta_2}$ based on experimental readings also yields no particular grouping of the data with respect to degrees of surface roughness.

Plots of C_D and C_m using a procedure analogous to that employed by Keulegan and Carpenter [13] appear in Fig. 19. In this figure, the values of C_D and C_m were obtained using the Morison equation (20). The procedure for evaluating the period parameter, u_{rms} T/D, was modified from that used by Keulegan and Carpenter [13]. The period parameters in Fig. 19 were evaluated on the basis of root mean square of velocity over the depth span of the water, whereas the studies of Keulegan and Carpenter involved standing waves and they used the maximum velocities in evaluating the period parameters. Fig. 19 shows a general overlap of the data obtained from the

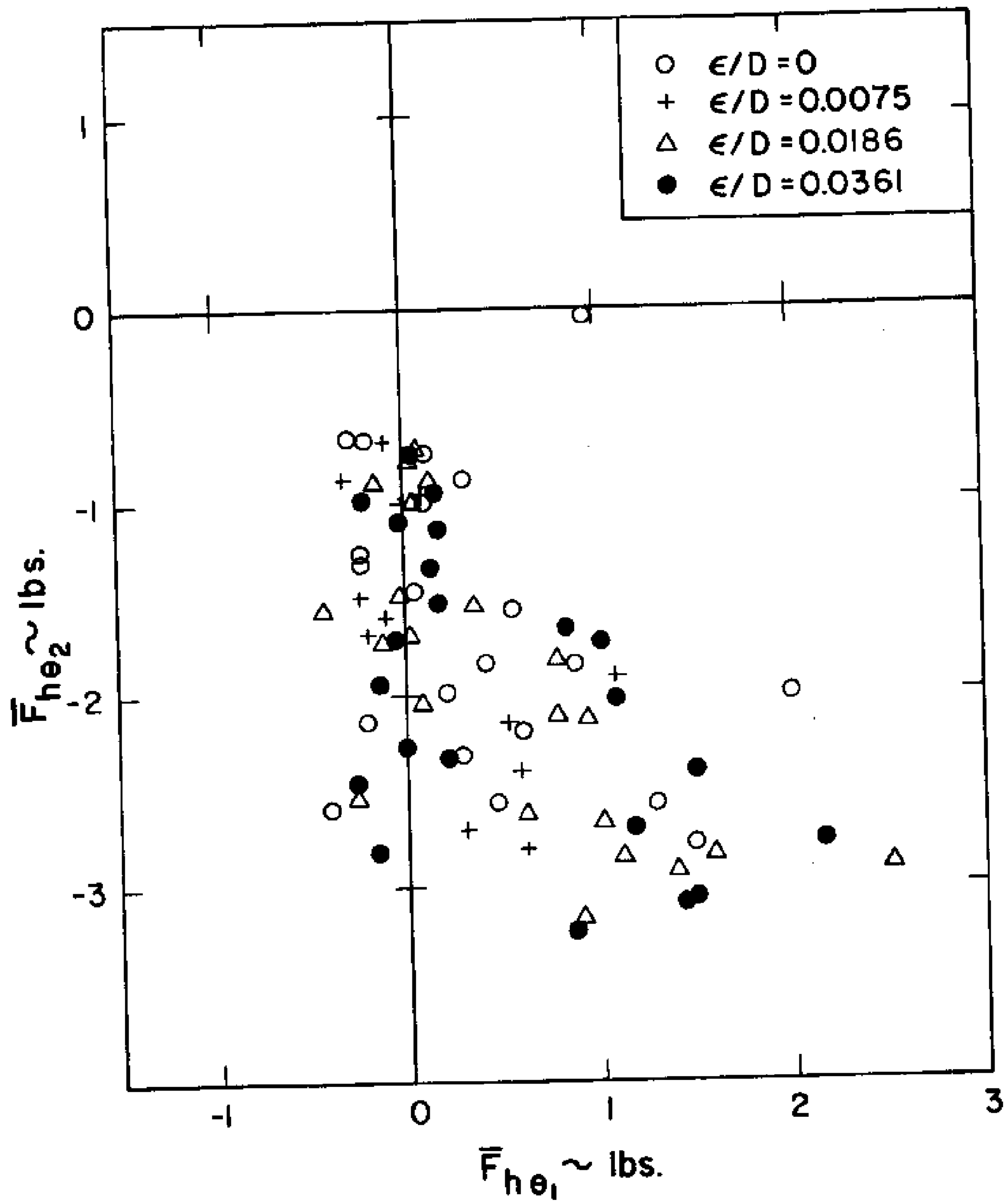

Fig. 18 Average force at θ_2 versus average force at θ_1

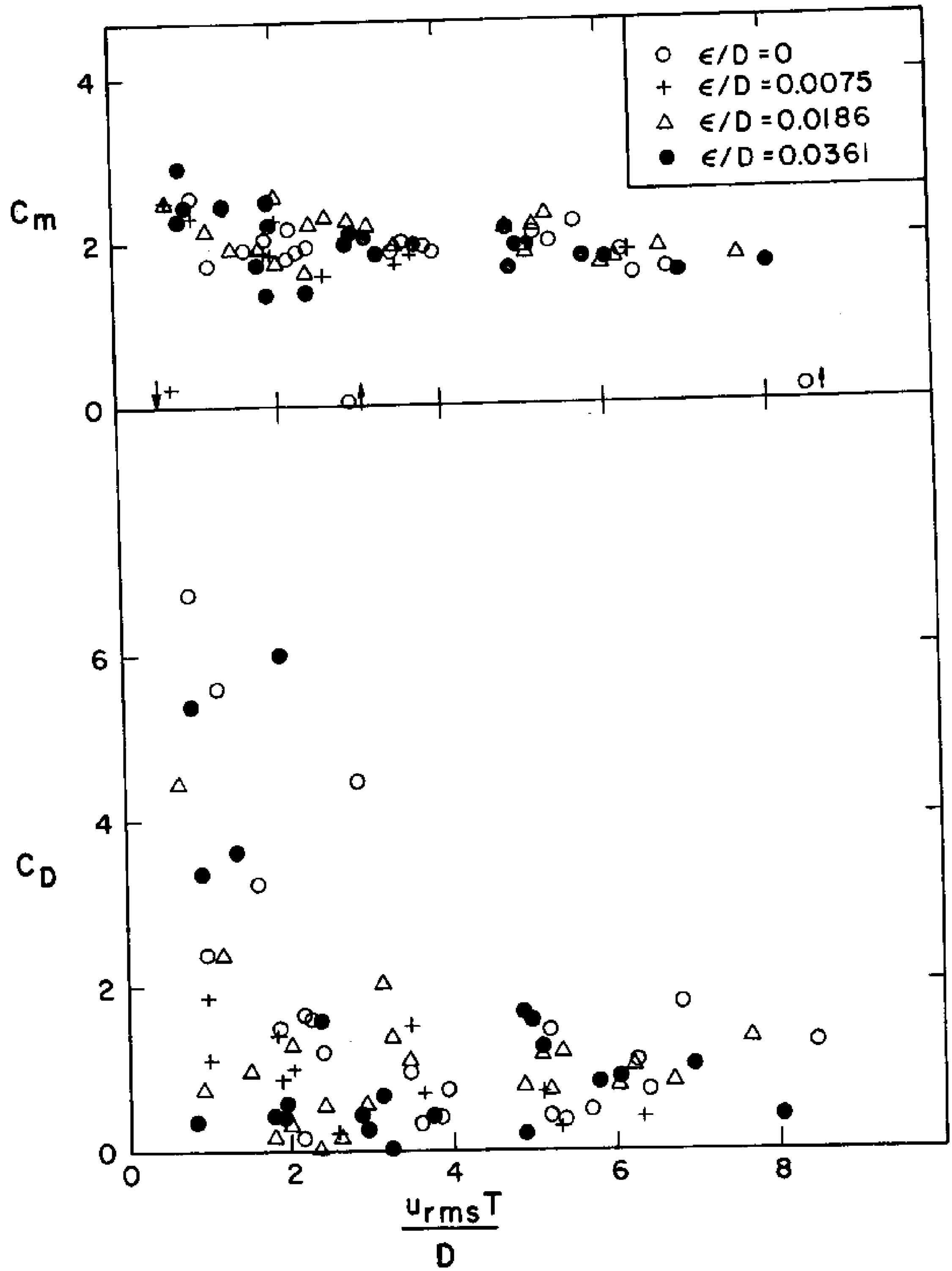

Fig. 19 C_D and C_m versus modified period parameter experiments involving the various degrees of surface roughness with the result that roughness appears to have no influence on the correlations of C_D and C_m with u_{rms} T/D. The apparent narrower scatter band for C_D in Fig. 19 compared with that in Fig. 16 is deceptive since the scale is linear in Fig. 19 and logarithmic in Fig. 16.

An attempt to establish the effects of surface roughness using an acceleration modulus is shown in Fig. 20. Here an acceleration modulus,

$$\frac{a_{hrms} D}{u_{rms}^2}$$

has been calculated for each experiment based on the root mean square of horizontal particle velocity, u_{rms}, and acceleration, a_{hrms}, evaluated at phase angles θ_1 and θ_2, respectively.

The ordinate of Fig. 20 is a resistance coefficient, C_{urms}, calculated on the basis of equations (24) and (91). This choice of parameters provides a fairly good correlation of the data, but, as in the previous cases discussed, it fails to predict any measure of the effects of surface roughness.

All of the figures discussed so far in this chapter have resulted from some attempt to use theoretical expressions in conjunction with certain experimentally measured quantities to establish a suitable set of parameters for predicting the effects of pile surface roughness on wave forces on piles. Since none of the previous methods yielded a fruitful means of accomplishing this,

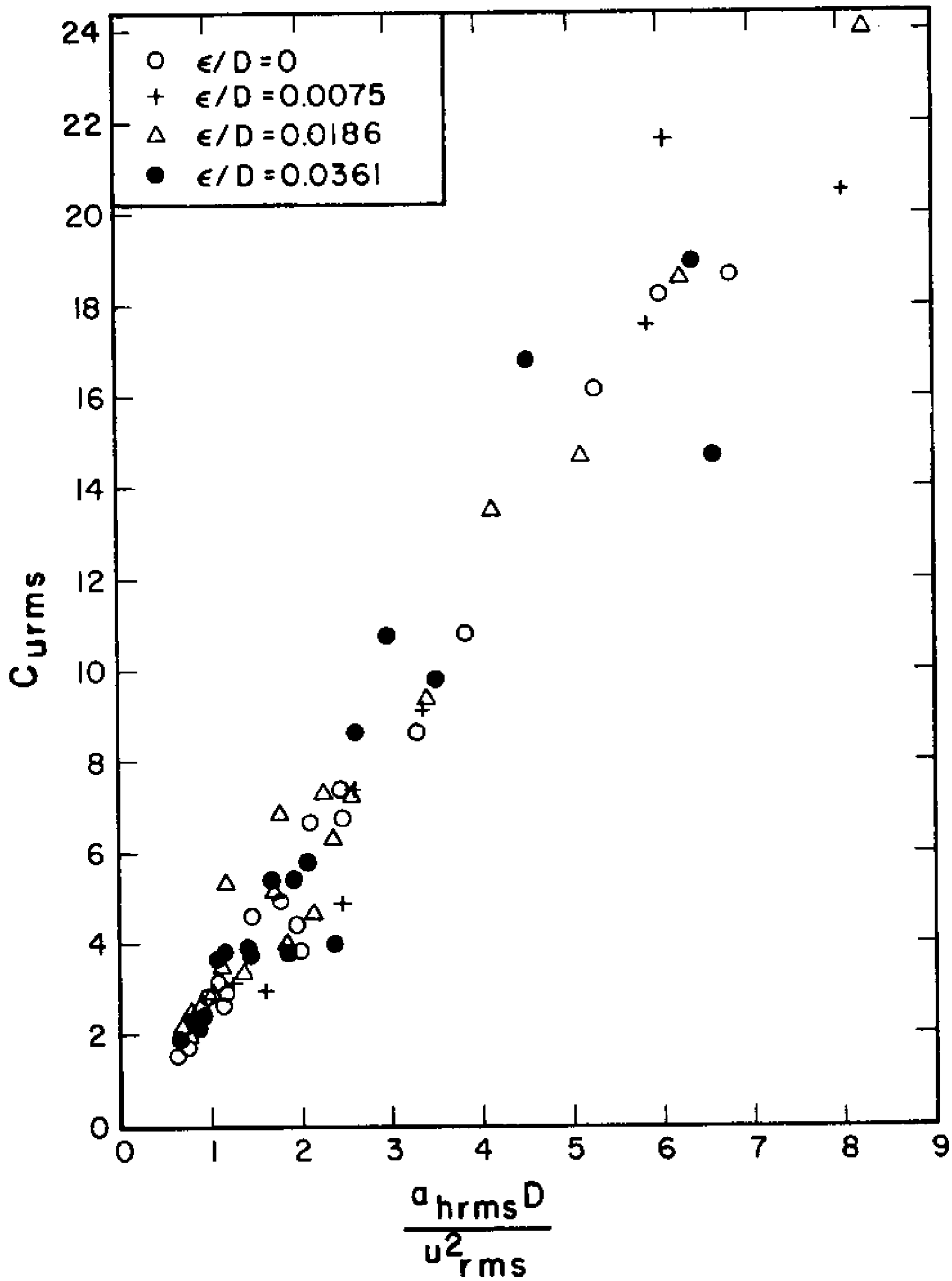

Fig. 20 Coefficient of resistance versus acceleration modulus

an attempt was made to establish some relations using a purely dimensional analysis approach as recommended by Paape and Breusers [25]. It turned out that considerable additional data involving other water depths and pile diameters are needed before anything conclusive can be established from using this method.

Despite the failures of the usual correlating methods to predict an effect of surface roughness on wave forces on piles, the degree of roughness was found to influence the magnitude of the resultant maximum force. For each experiment which involved both the smooth and rough surfaces, the average maximum force occurring for N waves was evaluated. Since the pile diameters of the roughened surfaces were slightly larger than that for the smooth surface pile, the average maximum force and the Reynolds number obtained for each experiment with a rough surface were reduced by the ratio of the rough to smooth diameters; i.e., by the ratio $(D_s + 2\varepsilon)/D_s$. The modified maximum force on the pile was designated as F'_{mr} and the modified Reynolds number by $(u_{rms} D/\nu)'$. The ratio of F'_{mr} to the average maximum force for the smooth pile, F_{ms}, was evaluated for each experiment and the result was plotted versus the corresponding modified Reynolds number for each experiment as shown in Fig. 21. Here it may be seen, qualitatively, that as the degree of surface roughness is increased, the ratio F'_{mr}/F_{ms} increases. A possible exception to this may occur at the lower Reynolds numbers, especially in the case of small relative roughness. For these latter conditions, it appears that a small degree of roughness

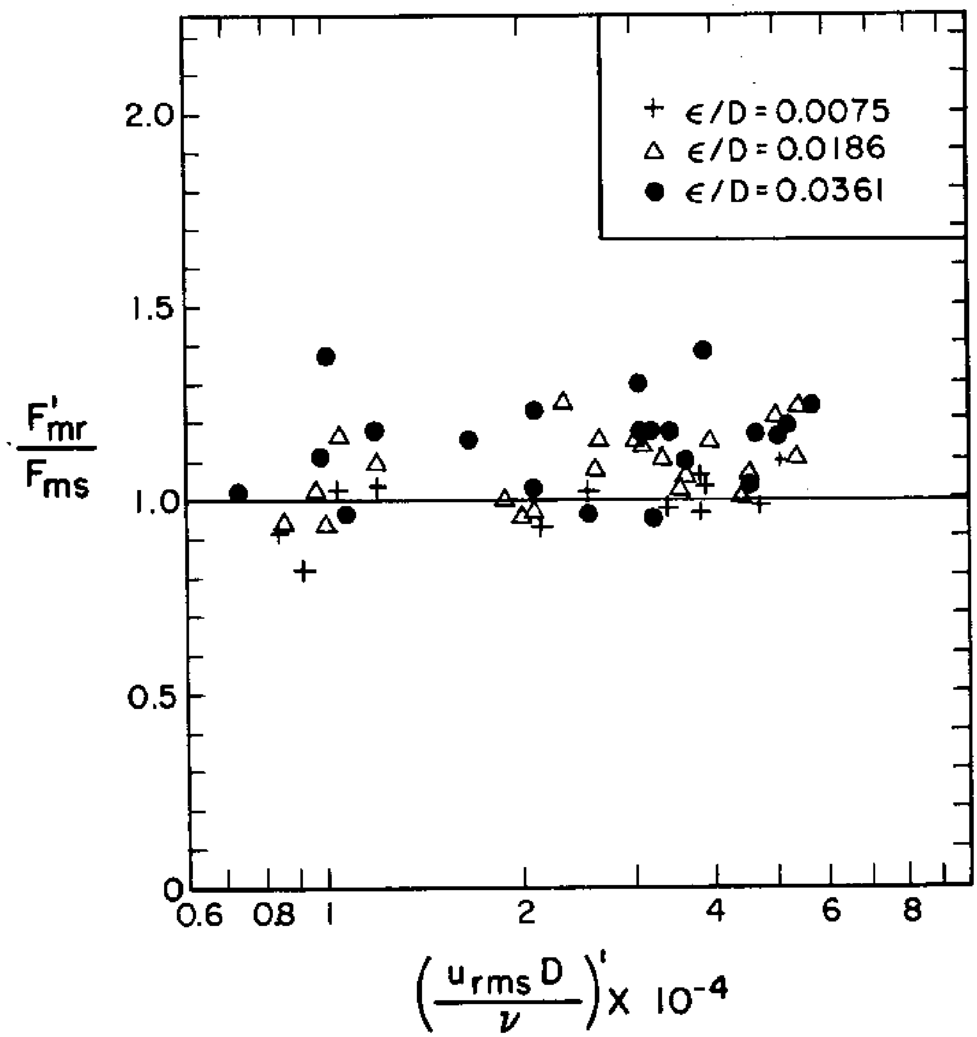

Fig. 21 Ratio of modified rough to smooth maximum force versus modified Reynolds number

results in the pile experiencing a smaller load than would be the case if the pile were smooth. However, there appears to be a point of diminishing return since the ratio F'_{mr}/F_{ms} in general tends to increase with surface roughness.

A more quantitative measure of the effects of surface roughness is shown in Fig. 22. In this figure the average value of F'_{mr}/F_{ms} has been determined for the data of each roughness which fell in each Reynolds number interval of 1×10^4. The averages were then plotted and the curves fitted through these points as indicated in Fig. 22. Some of the scatter of the data in both Figs. 21 and 22 result from the wave characteristics not being exactly duplicated for the experiments conducted on each roughened surface. The overall average increases in the modified force ratio for roughnesses 1, 2 and 3 are -1, 9 and 14 percent, respectively.

If no allowance is made for the increase in diameter due to the presence of the sand grains, the overall average increases in the force ratio for roughnesses 1, 2 and 3 are 1, 13 and 23 percent, respectively. The condition just described would be the likely situation if a clean structural member were erected at an offshore installation and then marine growth accumulated with time. Thus, in view of the somewhat idealized conditions under which the above evaluations of surface roughness were obtained and also on the basis of the work of Blumberg and Rigg [2], it is probable that the percentage increases in maximum forces which a

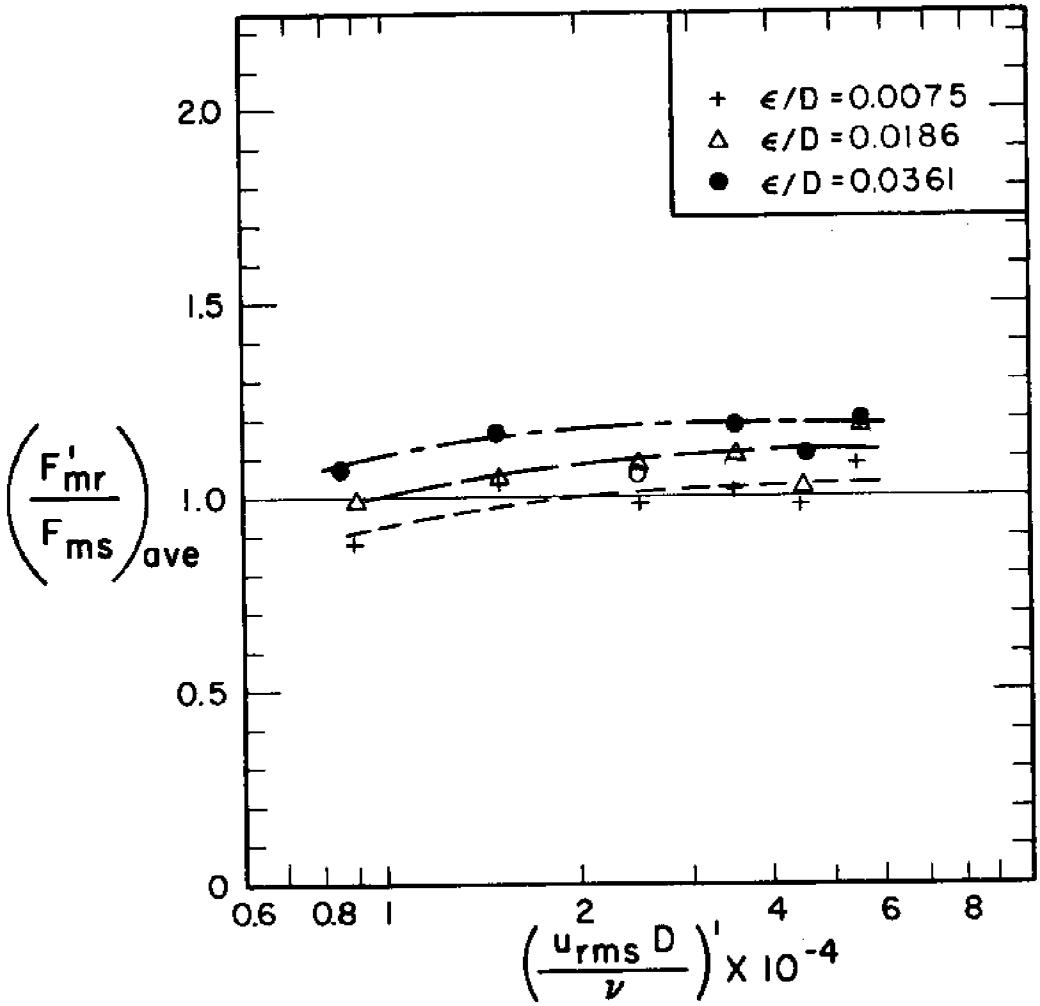

Fig. 22 Average value of the ratio of modified rough to smooth maximum force versus modified Reynolds number

prototype pile would have to sustain under field conditions would likely be in excess of those given above.

It may be noted from the above discussion that no effects of surface roughness were evidenced in the values of C_D and C_m obtained and yet a definite increase in the maximum force which the pile had to withstand occurred as the roughness was increased. This provides another example disclosing the limitations of the semi-empirical methods and perhaps adds support to the arguments of Priest [24] and Paape and Breusers [25] that more emphasis be placed on dimensional analysis techniques as a means of predicting wave forces on piles.

The data from which the figures shown in this chapter were derived are summarized in tabular form in Appendix 3. The trends of the data were rather well established after analyzing the data for the two roughest surfaces (nos. 2 and 3). Therefore it was not necessary to reduce all of the roughness no. 1 data in order to establish the effects of this level of roughness on the wave forces on the pile.

CHAPTER VII

CONCLUSIONS AND RECOMMENDATIONS

Conclusions

The following conclusions may be drawn from this investigation of the effects of surface roughness on the wave forces on a circular cylindrical pile:

1. The maximum force which the pile must sustain in response to wave action is dependent upon the degree of surface roughness. The results indicate that for relative roughnesses, ε/D, of 0.0075, 0.0186 and 0.0361, the average increases in the ratio of average maximum force on the rough pile to the average maximum force on the smooth pile are -1, 9 and 14 percent, respectively, for the range of Reynolds numbers studied. These percentages include a reducing correction to compensate for the added diameter due to the presence of the sand grains.

   If the diameter including the sand grains is used in evaluating the increases in maximum force due to roughness, the overall average increases in the ratio of average maximum force on the rough pile to the corresponding average maximum force on the smooth pile are 1, 13 and 23 percent for relative roughnesses of 0.0075, 0.0186 and 0.0361, respectively. This condition would be the more realistic situation in practice, since the pile would more than likely be relatively smooth at the time of installation and would accumulate a marine growth on its surface with the passage of time.

2. At Reynolds numbers below, say, 2×10^4 there is an indication that a small degree of relative roughness results in a decrease of the maximum force which the pile must sustain. However, there appears to be a point of diminishing return, since, in general, the maximum force increases as the surface roughness is increased.
3. The accuracy of the semi-empirical methods used is not sufficient to measure the effects of pile surface roughness on wave forces. The simplifying assumptions used in attempting to combine theory and experiment to obtain the necessary coefficients for predicting wave forces on piles results in an apparent sacrifice of accuracy beyond that which permits the contribution due to surface roughness to be evaluated.

Recommendations

A number of possibilities offer themselves as alternate avenues of approach in investigating further the effects of surface roughness and perhaps at the same time offering further insight into the complications of the wave-force-pile problem. The following three are suggested for consideration:

1. An attempt should be made to evaluate the particle

velocities and accelerations experimentally for use in the Morison equation (12) and the correlating parameters which depend upon these kinematic quantities. One approach could be to obtain these quantities through measurements of velocity using a hot-film anemometer or, perhaps, through photographic studies of the motions of polystyrene beads suspended in the water as the wave action takes place. This latter technique would also provide direct measurements of horizontal and vertical particle displacements of the particles in their orbit trajectories. The same wave generator settings should be used for these studies as were used for obtaining the force data presented in this paper. This would provide a measure of compatibility of all of the data even though the studies were made at different times. By obtaining actual measurements of velocity and, in turn, acceleration for use in the Morison equation, the values of C_D and C_m would then be obtained on the basis of experimental data and the dependence upon calculated velocities and accelerations would be eliminated.

2. Another possibility which would maybe improve the results obtained using semi-empirical methods would be to evaluate the particle kinematics using Dean's [11] stream function theory. Since this method may be applied to nonlinear waves which have either symmetrical or unsymmetrical

profiles with steepness up to breaking, it seems that this method would have the potential of allowing for the nonlinearities which were unaccounted for using the linear wave theory. Hopefully, this refinement would give a better rendition of the flow description and in turn provide quantitative evaluation of the effects of surface roughness.

3. Additional data are needed involving other water depths and pile diameters (i.e. larger Reynolds numbers) in order to adequately determine the effects of surface roughness using a purely dimensional analysis approach. A rather extensive addition of experiments would be required. However, the data reduction time would be substantially reduced since the need for reading wave force and profile data with respect to appropriate phase angles would be eliminated.

REFERENCES

1 A. Fage and J. H. Warsap, "The Effects of Turbulence and Surface Roughness on the Drag of Circular Cylinders," Report 1283, Aeronautical Research Council, London, 1930.

2 R. Blumberg and A. M. Rigg, "Hydrodynamic Drag at Supercritical Reynolds Numbers," paper presented at Petroleum Session, ASME meeting, June 14, 1961, Los Angeles, California.

3 H. W. Iversen and R. Balent, "A Correlating Modulus for Fluid Resistance in Accelerated Motion," Journal of Applied Physics, Vol. 22, 1951, pp. 324-328.

4 S. R. Keim, "Fluid Resistance to Cylinders in Accelerated Motion," Journal of the Hydraulics Division, Proc. ASCE, Vol. 82, No. HY 6, December, 1956, Paper No. 1113, pp. 1-14.

5 A. D. K. Laird, C. A. Johnson and R. W. Walker, "Water Forces on Accelerated Cylinders," Journal of the Waterways and Harbors Division, Proc. ASCE, Vol. 85, No. WW1, March, 1959, pp. 99-119.

6 T. Sarpkaya and C. J. Garrison, "Vortex Formation and Resistance in Unsteady Flow," Journal of Applied Mechanics, Vol. 30, Trans. ASME, Series E, March 1963, pp. 16-24.

7 J. R. Morison, M. P. O'Brien, J. W. Johnson and S. A. Schaaf, "The Force Exerted by Surface Waves on Piles," Petroleum Transactions, AIME, Vol. 189, 1950, No. TP 2846, pp. 149-154.

8 J. R. Morison, J. W. Johnson and M. P. O'Brien, "Experimental Studies of Forces on Piles," Proceedings of the Fourth Conference on Coastal Engineering, 1953, pp. 340-370.

9 R. L. Wiegel, K. E. Beebe and J. Moon, "Ocean Wave Forces on Circular Cylindrical Piles," Journal of the Hydraulics Division, Proc. ASCE, Vol. 83, No. HY 2, April, 1957, Paper No. 1199, pp. 1-36.

10 R. O. Reid and C. L. Bretschneider, "Surface Waves and Offshore Structures: The Design Wave in Deep or Shallow Water, Storm Tide, and Forces on Vertical Piles and Large Submerged Objects," Technical Report, Department of Oceanography, Agricultural and Mechanical College of Texas, October, 1953.

11 R. G. Dean, "Stream Function Representation of Nonlinear Ocean Waves," Journal of Geophysical Research, Vol. 70 (18), September, 1965, pp. 4561-4572.

12 P. M. Aagaard and R. G. Dean, "Wave Forces: Data Analysis and Engineering Calculation Method," Preprints of the First Annual Offshore Technology Conference, May, 1969, Houston, Tex., Vol. I, Paper No. 1008, pp. 95-106.

13 G. H. Keulegan and L. H. Carpenter, "Forces on Cylinders and Plates in an Oscillating Fluid," Journal of Research of the National Bureau of Standards, Vol. 60, No. 5, May 1958, pp. 423-440.

14 R. L. Wiegel, "Oceanographical Engineering," Prentice-Hall, Inc., Englewood Cliffs, N. J., 1965, pp. 17, 259, 262.

15 R. O. Reid, "Analysis of Wave Force Experiments at Caplan, Texas," Technical Report No. 38-4, Department of Oceanography, Agricultural and Mechanical College of Texas, January, 1956.

16 D. R. F. Harleman and W. C. Shapiro, "Experimental and Analytical Studies of Wave Forces on Offshore Structures," Part I, Technical Report No. 19, Hydrodynamics Laboratory, Massachusetts Institute of Technology, May, 1955.

17 R. C. MacCamy and R. A. Fuchs, "Wave Forces on Piles: A Diffraction Theory," Beach Erosion Board Technical Memorandum No. 69, U. S. Army Corps of Engineers, December, 1954.

18 C. R. Crooke, "Re-analysis of Existing Wave Force Data on Model Piles," Beach Erosion Board Technical Memorandum No. 71, U. S. Army Corps of Engineers, April, 1955.

19 C. L. Bretschneider, "On the Probability Distribution of Wave Force and on Introduction to the Correlation Drag Coefficient and the Correlation Inertial Coefficient," Santa Barbara Specialty Conference, Coastal Engineering, October, 1965, Santa Barbara, Calif., pp. 183-217.

20 W. J. Pierson Jr. and P. Holmes, "Irregular Wave Forces on a Pile," Journal of the Waterways and Harbors Division, Proc. ASCE, Vol. 91, No. WW4, November, 1965, Paper No. 4528, pp. 1-10.

21 L. E. Borgman, "The Statistical Distribution of Ocean Wave Forces on Vertical Piling," Technical Report HEL-9-3, Institute of Engineering Research, University of California, Berkeley, Calif.

22 L. J. Brown and L. E. Borgman, "Tables of the Statistical Distribution of Ocean Wave Forces and Methods for the Estimation of C_D and C_m," Wave Research Report HEL-9-7, Hydraulic Engineering Laboratory, University of California, Berkeley, Calif., 1966.

23 Y. Jen, "Laboratory Study of Inertia Forces on a Pile," Journal of the Waterways and Harbors Division, Proc. ASCE, Vol. 94, No. WW1, February, 1968, pp. 59-76.

24 M. S. Priest, "Shallow-Water Wave Action on a Vertical Cylinder," Journal of the Waterways and Harbors Division, Proc. ASCE, Vol. 88, No. WW2, May, 1962, Paper No. 3112, pp. 1-9.

25 A. Paape and H. N. C. Breusers, "The Influence of Pile Dimension on Forces Exerted by Waves," Proceedings of the Tenth Conference on Coastal Engineering, Vol. II, 1966, pp. 840-849.

26 B. V. Korvin-Kroukovsky, "Theory of Seakeeping," Society of Naval Architects and Marine Engineers, New York, 1961.

27 H. Beckmann, "Secondary Inertia Forces on Columns in Ocean Waves," ASCE Annual Meeting and National Meeting on Water Resources Engineering, February, 1969, New Orleans, La., Paper No. 831, pp. 1-18.

28 J. R. Morison and R. C. Crooke, "The Mechanics of Deep Water, Shallow Water and Breaking Waves," Beach Erosion Board Technical Memorandum No. 40, U. S. Army Corps of Engineers, March, 1953.

29 B. Le Mehaute, D. Divoky and A. Lin, "Shallow Water Waves: A Comparison of Theories and Experiments," Proceedings of the Eleventh Conference on Coastal Engineering, 1968, London, Chapter 7.

30 B. Kinsman, "Wind Waves," Prentice-Hall, Inc., Englewood Cliffs, N. J., 1965, Chapter 3.

31 B. W. Wilson, "Analysis of Wave Forces on a 30-inch Diameter Pile Under Confused Sea Conditions," Coastal Engineering Research Center Technical Memorandum No. 15, U. S. Army Corps of Engineers, October, 1965, p. 53.

32 J. M. Killen, "A Capacitive Wave Profile Recorder," Technical Paper No. 11, Series B, St. Anthony Falls Hydraulic Laboratory, University of Minnesota, October, 1952.

33 E. Y. Hsu, "A Wind, Water-Wave Research Facility," Technical Report No. 57, Department of Civil Engineering, Stanford University, October, 1965.

34 T. W. Lambe, "Soil Testing for Engineers," John Wiley and Sons, Inc., New York, N. Y., 1951, p. 31.

35 A. T. Ippen, "Estuary and Coastline Hydrodynamics," McGraw-Hill Book Company, Inc., New York, N. Y., 1966, p. 361.

36 H. Schlichting, "Boundary-Layer Theory," 6th Ed., McGraw-Hill Book Company, Inc., New York, N. Y., 1968, p. 17.

37 A. Miller, Personal Communication, April, 1968.

38 W. M. Murray and P. K. Stein, "Lectures and Laboratory Exercises on Strain Gage Techniques," Department of Engineering, University of California at Los Angeles, 1960, pp. 162, 360.

39 C. C. Perry and H. R. Lissner, "The Strain Gage Primer," 2nd. Ed., McGraw-Hill Book Co., New York, N. Y., 1962, p. 18.

40 H. Rouse, "Engineering Hydraulics," John Wiley and Sons, Inc., New York, N. Y., 1950, p. 1011.

APPENDIX 1

ELECTRICAL CIRCUITS

Capacitance Wave Gages

The circuitry used for each capacitance gage is shown in Fig. 23. This circuitry was designed so that the signal induced by the variation in capacitance as a wave passed the gage could be recorded as a measure of water elevation by using a Hewlett-Packard Model 321 Dual Channel Carrier Amplifier Recorder. The circuit was designed by Miller [37], and an excerpt of his description of its operation is as follows:

> The two transformers, the two .01 mfd capacitors and the 1000 ohm resistor are mounted together close to the capacitance probe itself. The transformers take care of isolation and impedance matching functions. The 0-12 transformer provides a floating center tapped excitation source for the bridge. (The secondary of this transformer constitutes one half of the bridge.) Because of the high impedance of the bridge, it is possible to use this transformer as a step up device to deliver a higher voltage to the bridge than is available at terminals B and D of the connector.
>
> The bridge output appears across points a and b as a voltage in series with a capacitance of 0.02 mfd. After transformation by the step down transformer, this signal appears at points x and y as a smaller voltage in series with a capacitance of 0.6 mfd if the 0-9 transformer is used, and 0.4 mfd if the 0-27 transformer is used. At the bridge excitation frequency of 2400 Hertz, this corresponds to a capacitance reactance of 100-150 ohms. For proper operation of the balancing controls, the Model 321 carrier amplifier normally expects to look back into a substantially resistive source. For this reason the 1000 ohm resistor has been

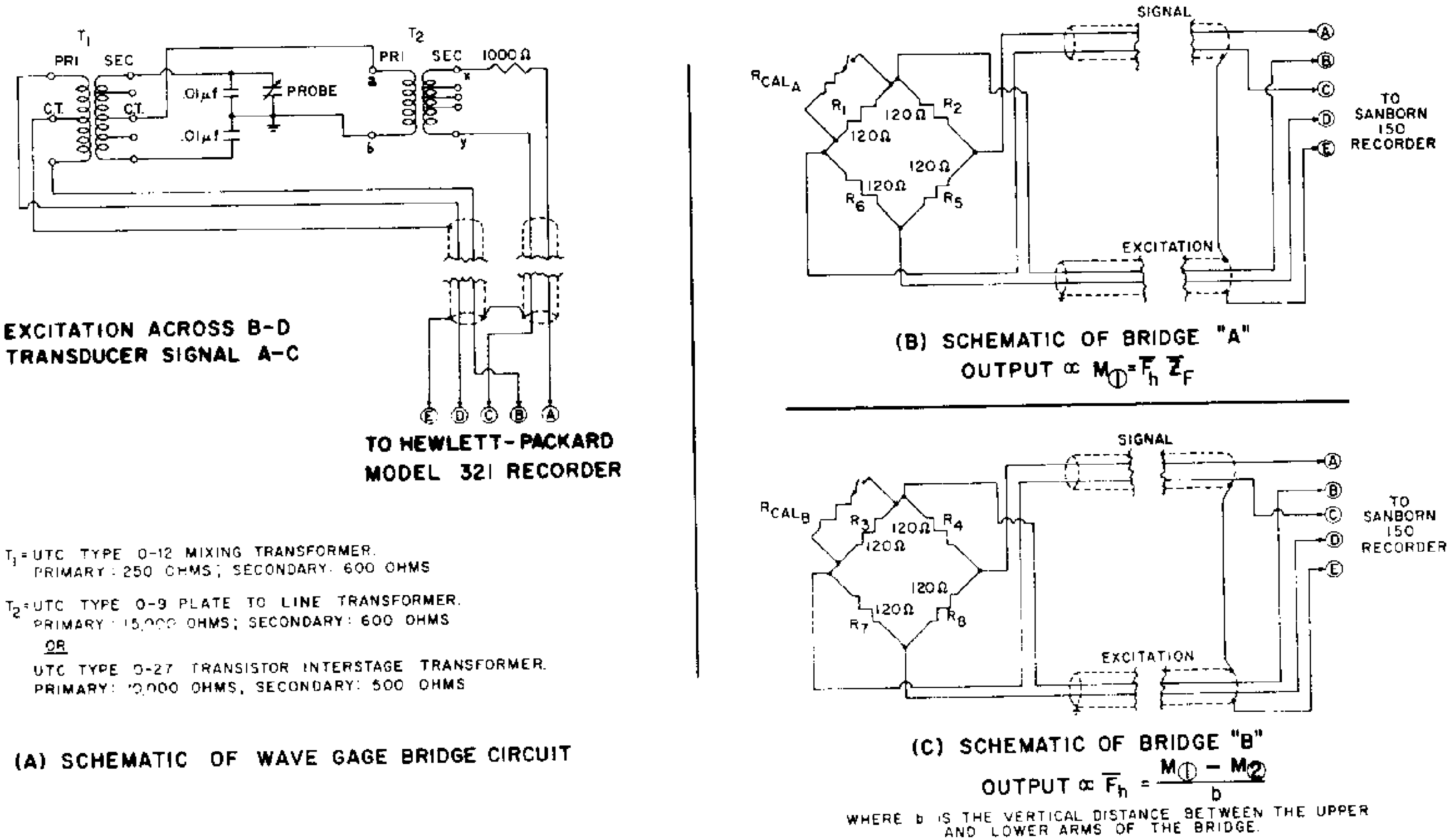

Fig. 23 Schematic of electrical circuits

added to swamp out the 100 ohm reactive impedance of the bridge.

The pair of .01 mfd capacitors should be matched within about one percent. The smaller one can then be connected across the wire probe.

The dielectric constant of Teflon is 2.1, and assuming that you use #20 wire with the standard insulation thickness of .01 inches, the capacitance change of the probe will be about 7.3 picofarads per inch of immersion. After making allowance for the transformer ratios and loading effects of the amplifier on the bridge, I would estimate a signal of about 200 microvolts at the amplifier input for each inch of immersion. This is enough to produce at least two centimeters of deflection on the chart. You would then be able to resolve water level changes as small as one tenth of an inch.

Strain Gage Bridges

In strain gage circuits, use is made of the Wheatstone bridge where one or more of the arms consist of a resistance strain gage. If the assumption is made that such a bridge is initially balanced and the changes in resistance of one or more of the arms are small, then the change in output voltage, Δe, is given very closely by (see Reference [38])

$$\Delta e = V \frac{R_x R_z}{(R_x + R_y)(R_z + R_w)} \left[\frac{\Delta R_x}{R_x} - \frac{\Delta R_y}{R_y} + \frac{\Delta R_z}{R_z} - \frac{\Delta R_w}{R_w} \right] \quad (32)$$

where the notation is as defined in Fig. 24.

By definition, the gage factor is given by (see References [38] and [39])

$$\text{Gage Factor, G.F.} = \frac{\Delta R/R}{\Delta \ell/\ell} \quad (33)$$

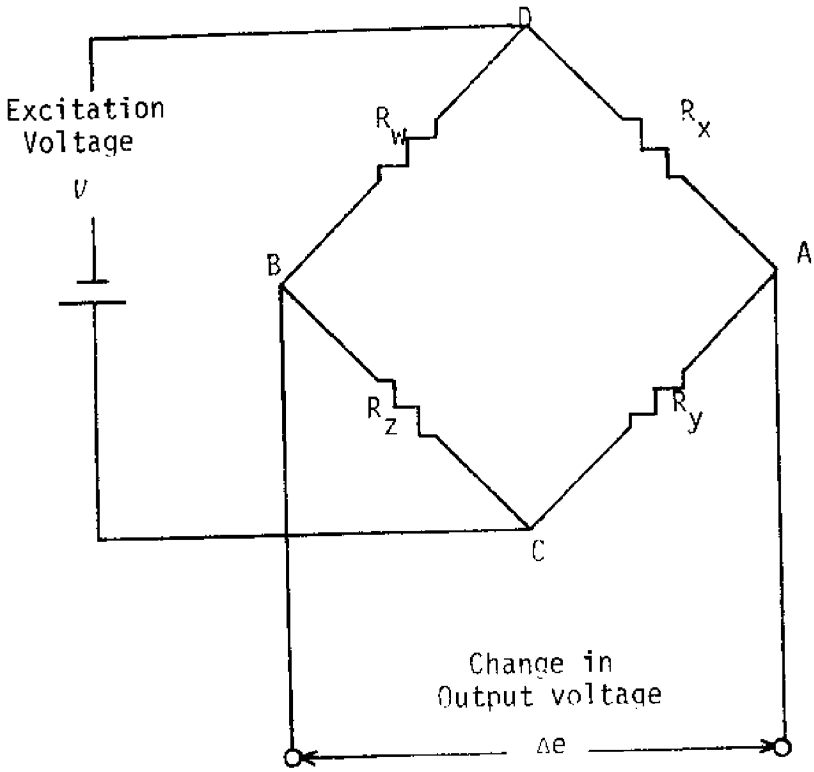

Fig. 24 Schematic and notation for a Wheatstone bridge

where ℓ is the length of the strain gage before being strained and $\Delta\ell$ represents the change in length of the gage due to the induced strain.

The denominator of equation (33) may be recognized as the definition of strain, E. Therefore equation (33) may be re-written in the form

$$\frac{\Delta R}{R} = (G.F.)E. \tag{34}$$

Making use of the general equation (34) in equation (32), results in

$$\Delta e = V \frac{R_x R_z}{(R_x + R_y)(R_z + R_w)} (G.F.)[E_x - E_y + E_z - E_w] \tag{35}$$

Letting $$\beta = V \frac{R_x R_z}{(R_x + R_y)(R_z + R_w)} (G.F.) \tag{36}$$

equation (35) becomes

$$\Delta e = \beta[E_x - E_y + E_z - E_w]. \tag{37}$$

The application of equation (37) to the bridges shown schematically in Figs. 23b and 23c will now be demonstrated. The resistors R_{cal_A} and R_{cal_B} shown in Fig. 23 were used to simulate known applied loads to the pile. These resistors were switched into the circuit before performing an experiment to establish whether or not the bridge was functioning properly and still maintained its calibration. These calibration resistors are assumed to be switched off during the remainder of this discussion.

Considering the bridge for measuring bending moment, assume the force is applied to the pile as shown in Fig. 4 and that the orientation of the strain gage positions conforms with that in Fig. 7. The strains for such a loading would be as shown in Fig. 25 where the plus and minus signs indicate tension and compression of the gage elements, respectively.

Applying equation (37) to the conditions implied in Fig. 25 gives

$$\Delta e = \beta[+(-\varepsilon_2) - (+\varepsilon_5) + (-\varepsilon_6) - (+\varepsilon_1)]. \tag{38}$$

Since gages 1 and 2 are diametrically opposite one another, and likewise gages 5 and 6, the following relationships pertain to the magnitudes of strain

$$|\varepsilon_1| = |\varepsilon_2| \tag{39}$$

$$|\varepsilon_5| = |\varepsilon_6| \tag{40}$$

If a cross section through gages 1 and 2 is designated A' and a similar section through gages 5 and 6 is designated A" as shown in Fig. 25, then, using equations (39) and (40), equation (38) may be written as

$$\Delta e = \beta[-2\varepsilon_{A'} - 2\varepsilon_{A''}]. \tag{41}$$

Applying the well-known relations for stress and strain equation (41) becomes

$$\Delta e = -2\beta\left[\frac{M_{A'}c}{EI} + \frac{M_{A''}c}{EI}\right] \tag{42}$$

where M_A' and $M_{A''}$ are the bending moments about sections A' and A"

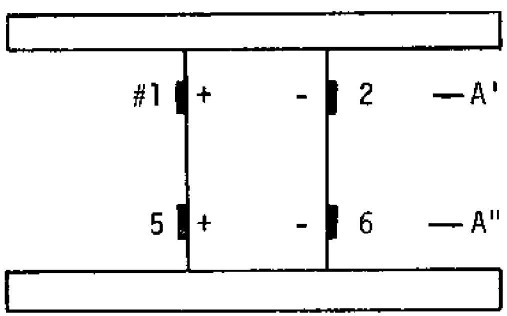

(a) Strain gages used for the moment transducer

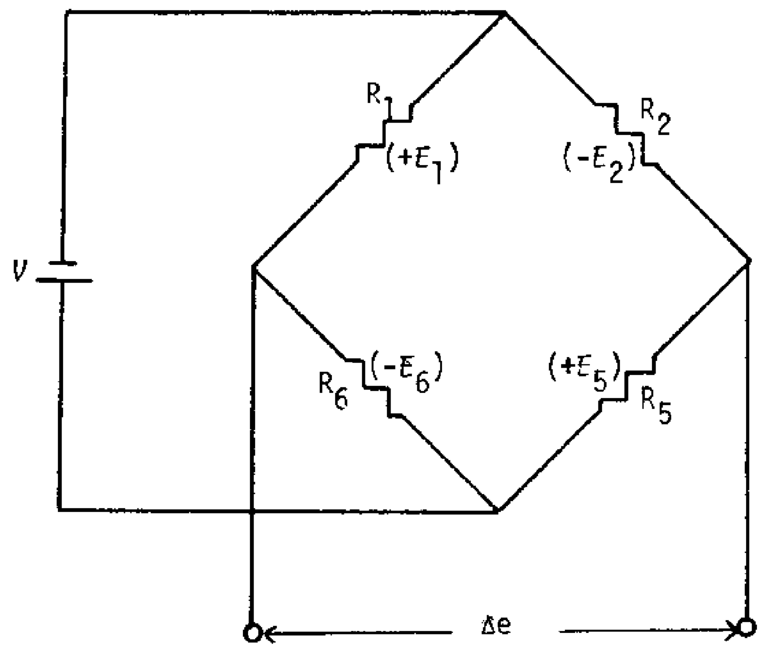

(b) Bridge showing the algebriac signs of the strains

Fig. 25 Strains induced in the bridge for measuring bending moment shown in Fig. 25, E is the modulus of elasticity of the material, I is the moment of inertia of the cross section about a line through its center of gravity and c is the distance from the neutral axis to the outer fiber of the cross section.

Equation(42) may be expressed as

$$\Delta e \; \alpha \; (M_{A'} + M_{A''}). \tag{43}$$

The moment bridge, in effect, measures the bending moment at points an equal distance above and below the midline of the gage section and then averages the two values of moment to obtain the average moment about the midline of the gage section.

The bridge employed as a force transducer will now be described. Again, assume the same load application and orientation as shown in Figs. 4 and 7. The strains for such a loading would be as shown in Fig. 26.

Applying equation (37) to the conditions implied in Fig. 26 gives

$$\Delta e = \beta[+(-E_4) - (-E_8) + (+E_7) - (+E_3)]. \tag{44}$$

By an argument which parallels that presented in regard to equations (38), (39) and (40), and designating the cross sections at the gages as ① and ② as shown in Fig. 26a, equation (44) may be written

$$\Delta e = \beta[-2\bar{E}_{①} + 2\bar{E}_{②}]. \tag{45}$$

Rewriting $\bar{E}_{①}$ and $\bar{E}_{②}$ using the well-known expressions for stress and strain, equation (45) becomes

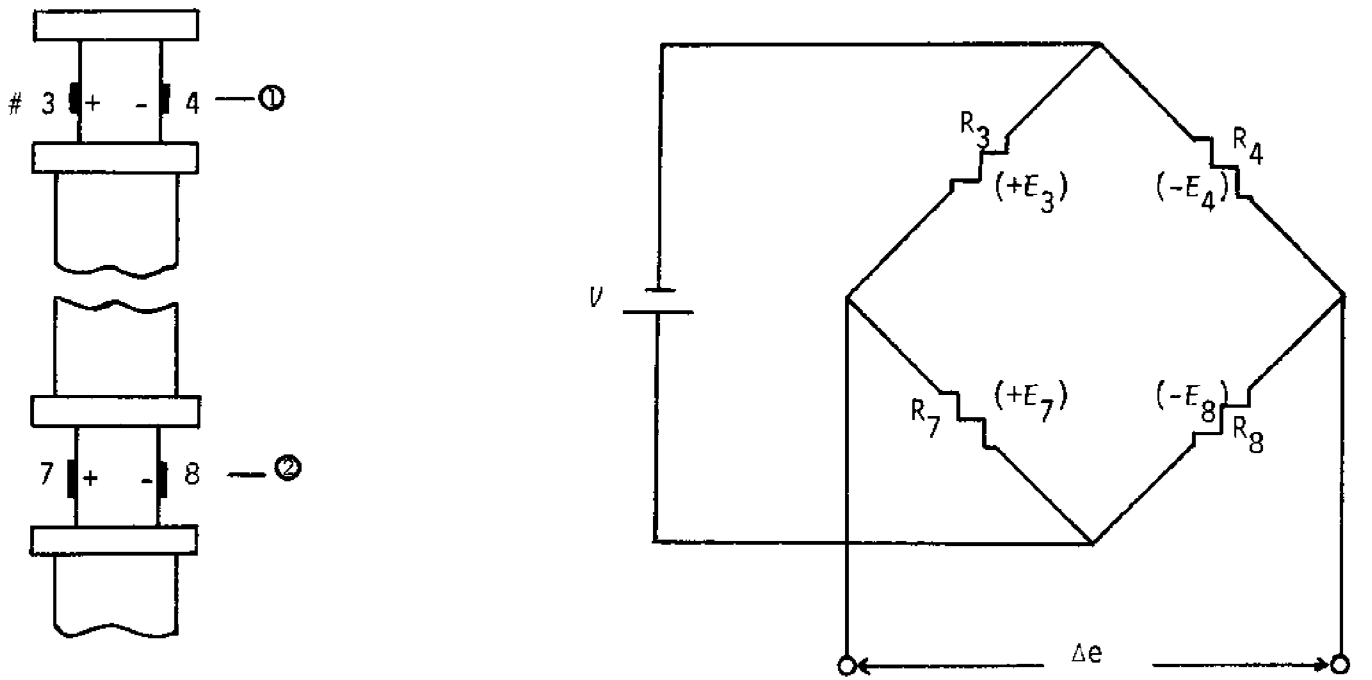

(a) Strain gages used in the force transducer

(b) Bridge showing the algebriac signs of the strains

Fig. 26 Strains induced in the bridge for measuring force

$$\Delta e = -2\beta\left[\frac{M_{①}c}{EI} - \frac{M_{②}c}{EI}\right] \qquad (46)$$

Therefore the output of the bridge in Fig. 23c is proportional to the difference in bending moment at the section ① and ②, i.e.,

$$\Delta e \; \alpha \; (M_{①} - M_{②}). \qquad (47)$$

APPENDIX 2

DATA REDUCTION PROGRAM

The program was written to perform the necessary calculations for obtaining drag and mass coefficients along with the dimensionless parameters needed for analyzing the data. The theory behind the equations used and the general procedures involved in its application to experimental data were discussed in Chapters III and V. However, a number of intermediate steps involved in the calculations were not discussed in detail. The purpose of this appendix is to show these details in a step-by-step sequence as they are programmed for the computer. The steps are listed numerically as follows:

1. The following data are read, in the order shown, as single values pertaining to a given experiment:

   N_r, N_{mo}, N_{da}, N_{yr}, N_{kin}, N_{disp}, N_{pad}, N_v

   N_{sp}, Δ_{half}, θ_1, θ_2, L_{est}, ℓ_{arm}, ε, ℓ_{vert},

   D_s, d, ℓ_G, g, T_w, ρ, and ν.

2. Some additional data are input as arrays for purposes of calculating averages. Each array consists of N_v values. For some arrays, the data from the records are read with respect to certain phase angle designations. The phase angle at the crest is called θ_1; the phase angle one-fourth of a period after θ_1 is called θ_2. The following

arrays are input in the order listed:

$$H(i),\ F_{hmax}(i),\ F_{h\theta_1}(i),\ F_{h\theta_2}(i),\ \eta_{\theta_1}(i)$$

$$\eta_{\theta_2}(i),\ t_H(i),\ t_A(i),\ t_B(i),\ \text{and}\ t_{A'}(i)$$

3. Preliminary calculations are made to calculate θ_1 and θ_2 in terms of degrees for listing purposes and to calculate the diameter of the pile including the sand grains, D; i.e.,

$$\theta_{deg} = \frac{180}{\pi}\,\theta_{rad},\ \text{and} \tag{48}$$

$$D = D_s + 2\varepsilon. \tag{49}$$

4. Twenty wave heights, $H(i)$, are averaged and a check is made to ascertain that the change in the average wave height, $\overline{H}$, due to the addition of more values remains less than one percent. If additional values are needed to comply with this criterion, they are added one at a time until the criterion is met. The average is obtained from the following relationship:

$$\overline{H} = \frac{\sum_{i=1}^{20} H(i)}{20}. \tag{50}$$

5. Twenty maximum (peak) wave forces, $F_{hmax}(i)$, are averaged and a check is made to ascertain that the change in the average wave force, $\overline{F}_{hmax}$, due to the addition of more values remains less than one percent. If additional values are needed to comply with this criterion, they are added one at a time until the criterion is met.

The average is obtained from the relationship:

$$\overline{F}_{hmax} = \frac{\sum_{i=1}^{20} F_{hmax}(i)}{20} . \tag{51}$$

Occasionally an additional value of $H(i)$ or $F_{hmax}(i)$ was needed to meet the criteria specified for $\overline{H}$ and $\overline{F}_{hmax}$, but this was never more than one additional value for these experiments.

6. Letting N equal the number of waves to be averaged, the average wave period based on the time span from when the first wave height is measured, $t_H(1)$, to the time when the last wave height is measured, $t_H(N + 1)$, is calculated; i.e.,

$$\overline{T} = \frac{t_H(N+1) - t_H(1)}{N} . \tag{52}$$

7. The average wave length, $\overline{L}$, for the N waves is determined from the following relation developed in chapter V, page 52:

$$\overline{L} = \frac{\sum_{i=1}^{N} \frac{t_A(i) - t_B(i)}{t_A(i) - t_{A'}(i)} \ell_G}{N} . \tag{53}$$

8. The average horizontal wave force which occurs at a phase angle of θ_1, $\overline{F}_{h\theta_1}$, is calculated from

$$\overline{F}_{h\theta_1} = \frac{\sum_{i=1}^{N} F_{h\theta_1}(i)}{N} . \tag{54}$$

9. The average wave surface elevation above the bottom at a phase angle of θ_1, $\overline{S}_{s\theta_1}$, is calculated from (see Fig. 2, page 18)

$$\overline{S}_{s\theta_1} = \frac{\sum_{i=1}^{N} [\eta_{\theta_1}(i) + d]}{N} . \tag{55}$$

10. For a phase angle of θ_1, the constant $K'_{1\theta_1}$ based on the values of $\overline{L}$ and $\overline{S}_{s\theta_1}$ obtained from steps 7 and 9, respectively, is calculated. The following relation applies (see equation (21), page 21):

$$K'_{1\theta_1} = \frac{\left(\frac{4\pi\overline{S}_{s\theta_1}}{\overline{L}}\right) + \sinh\left(\frac{4\pi\overline{S}_{s\theta_1}}{\overline{L}}\right)}{16\left[\sinh\left(\frac{2\pi d}{\overline{L}}\right)\right]^2} . \tag{56}$$

11. The drag coefficient, C_D, based on the average quantities obtained in the previous steps is calculated. The following relationship applies for a value of $\theta_1 = 0°$ (see equation (20), page 21):

$$C_D = \left[\frac{\overline{T}^2}{\pi\rho D\, \overline{H}^2\overline{L}}\right] \frac{\overline{F}_{h\theta_1}}{[K'_{1\theta_1}|\cos\theta_1|\cos\theta_1]} . \tag{57}$$

12. The average horizontal wave force which occurs at a phase angle of θ_2, $\overline{F}_{h\theta_2}$, is calculated from

$$\overline{F}_{h\theta_2} = \frac{\sum_{i=1}^{N} F_{h\theta_2}(i)}{N} . \tag{58}$$

13. The average wave surface elevation above the bottom at a phase angle of θ_2, $\overline{S}_{s\theta_2}$, is calculated from (see Fig. 2, page 18)

$$\overline{S}_{s\theta_2} = \frac{\sum_{i=1}^{N} [\eta_{\theta_2}(i) + d]}{N} . \tag{59}$$

14. For a phase angle of θ_2, the constant $K'_{2\theta_2}$ based on the values of $\overline{L}$ and $\overline{S}_{s\theta_2}$ obtained from steps 7 and 13, respectively, is calculated. The following relation applies (see equation (22), page 21):

$$K'_{2\theta_2} = \frac{\sinh\left(\frac{2\pi\ \overline{S}_{s\theta_2}}{\overline{L}}\right)}{\sinh\ (2\pi d/\overline{L})} . \tag{60}$$

15. The mass coefficient, C_m, based on the average force and wave characteristics obtained in the previous steps is calculated. The following relationship applies for a value of θ_2 = 90° (see equation (20), page 21):

$$C_m = -\left[\frac{\overline{T}^2}{\pi\rho D\overline{H}^2\overline{L}}\right]\left(\frac{4\overline{H}\ \overline{F}_{h\theta_2}}{\pi D\ K'_{2\theta_2}\sin\theta_2}\right) . \tag{61}$$

16. The average wave surface elevation with respect to the still water level at a phase angle of θ_1 is calculated. This quantity, $\overline{\eta}_{\theta_1}$, is given by

$$\overline{\eta}_{\theta_1} = \frac{\sum_{i=1}^{N} \eta_{\theta_1}(i)}{N} . \tag{62}$$

This quantity is shown geometrically in Fig. 27a which also geometrically describes some other quantities which will arise in some of the later steps.

17. The interval size to be used in evaluating the values of velocity at different depth-levels in the fluid is calculated. Referring to Fig. 27a, this quantity, Δi_v, is given by

$$\Delta i_v = \frac{(d + \overline{\eta}_{\theta_1})}{N_{kin}} . \qquad (63)$$

18. The total number of values of velocity to be calculated over the depth span of the water is designated by M = $(N_{kin} + 1)$. Then, at the phase angle θ_1, each of the distances, $y_{\theta_1}(j)$, from the still water level down to a water particle situated at each depth-level, j, is calculated from

$$y_{\theta_1}(j) = \left[\overline{\eta}_{\theta_1} - (N_{intj})(\Delta i_v)\right] \qquad (64)$$

where N_{intj} is the number of intervals (start with zero) down to the jth level. There will be M values of $y_{\theta_1}(j)$.

19. After calculating the array of values of $y_{\theta_1}(j)$, the array of velocities, $u_{\theta_1}(j)$, for the j-levels in the fluid may be calculated. These are obtained from (see equation (15), page 19)

$$u_{\theta_1}(j) = \frac{\pi\overline{H}}{\overline{T}} \; \frac{\cosh\left[\dfrac{2\pi(y_{\theta_1}(j) + d)}{\overline{L}}\right]}{\sinh 2\pi d/\overline{L}} \cos \theta_1 \qquad (65)$$

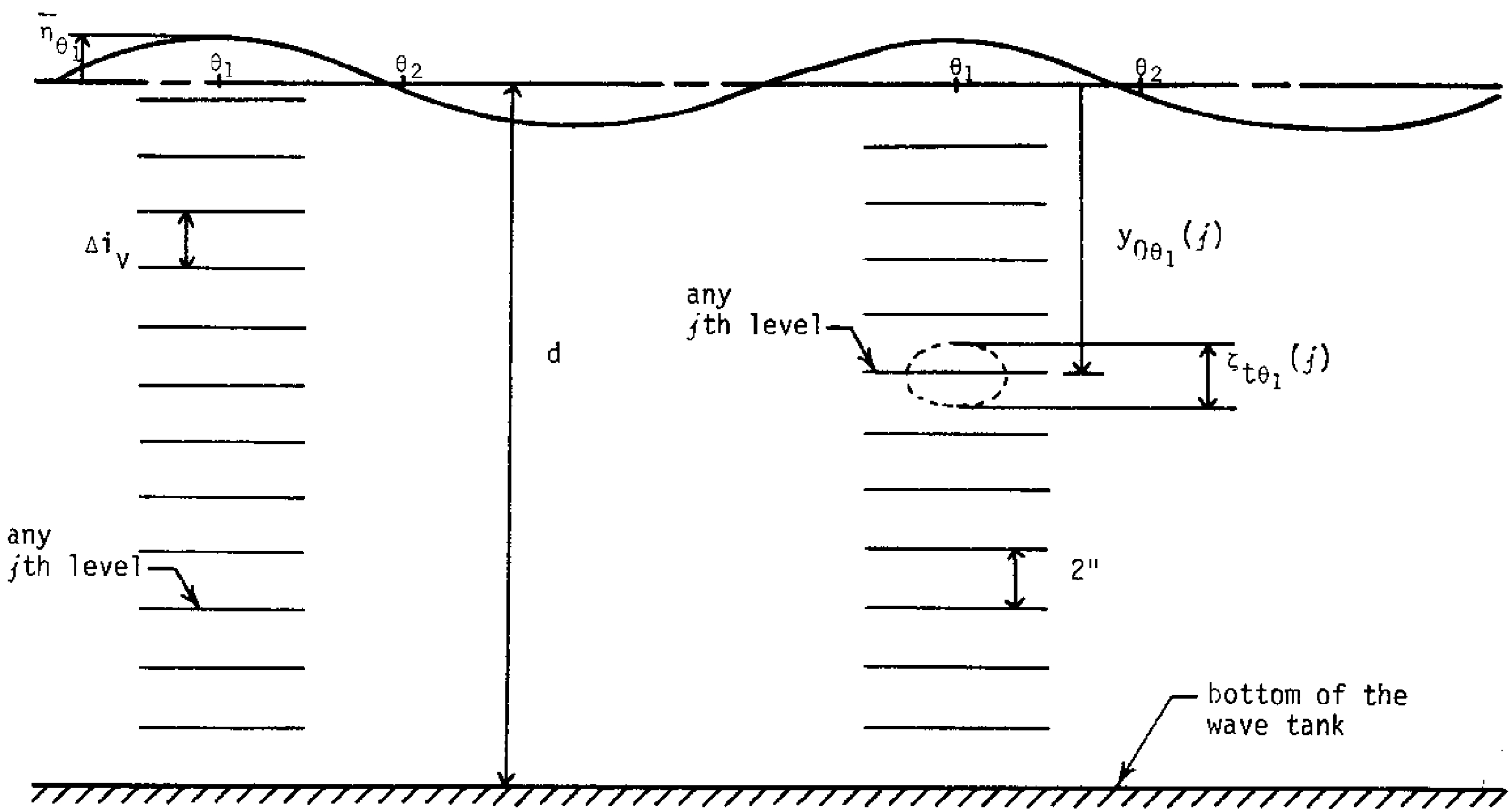

(a) For horizontal velocities (b) For vertical displacements

Fig. 27 Description of geometric divisions for computations of horizontal particle velocity and total vertical particle displacement at different depths where the values of $\overline{H}$, $\overline{T}$ and $\overline{L}$ are those obtained from steps 4, 6 and 7, respectively.

20. The root mean square of the horizontal particle velocity, u_{rms}, is calculated from

$$u_{rms} = \sqrt{\frac{\sum_{j=1}^{M} [u_{\theta_1}(j)]^2}{M}}. \qquad (66)$$

21. The total number of values of total vertical particle displacement, ζ_t, to be calculated over the depth span of the water is designated as $K = (N_{disp} + 1)$. Then, for the phase angle θ_1, each of the distances, $y_{0\theta_1}(j)$, from the still water level down to the mean vertical coordinate of a water particle whose orbit is centered at each depth-level, j, is calculated (see Fig. 27b); i.e.,

$$y_{0\theta_1}(j) = - \ [2(N_{intj})] \qquad (67)$$

where the length of each interval is 2 inches, and, again, N_{intj} is the number of intervals (start with zero) down to the jth level. There will be K values of $y_{0\theta_1}(j)$.

22. After calculating the array of values of $y_{0\theta_1}(j)$, the array of total vertical particle displacements, $\zeta_{t\theta_1}(j)$, for the j-levels in the fluid may be calculated (see Fig. 27b). These are obtained from (see equation (19), page 20)

$$\zeta_{t\theta_1}(j) = \overline{H}\ \frac{\sinh\left[\dfrac{2\pi(y_{0\theta_1}(j) + d)}{\overline{L}}\right]}{\sinh 2\pi d/\overline{L}} \cos \theta_1 \tag{68}$$

where the values of $\overline{H}$ and $\overline{L}$ are those obtained from steps 4 and 7, respectively.

23. The root mean square of the total vertical particle displacement, ζ_{trms}, is calculated from

$$\zeta_{trms} = \sqrt{\frac{\sum_{j=1}^{K} [\zeta_{t\theta_1}(j)]^2}{K}} \ . \tag{69}$$

24. The average wave surface elevation with respect to the still water level at a phase angle θ_2 is calculated. This quantity, $\overline{\eta}_{\theta_2}$, is given by

$$\overline{\eta}_{\theta_2} = \frac{\sum_{i=1}^{N} \eta_{\theta_2}(i)}{N} \ . \tag{70}$$

This quantity is shown geometrically in Fig. 28a which also geometrically describes some other quantities which will arise in some of the later steps.

25. The interval size to be used in evaluating the values of acceleration at different levels in the fluid is calculated. Referring to Fig. 28a, this quantity, Δi_a, is given by

$$\Delta i_a = \frac{(d + \overline{\eta}_{\theta_2})}{N_{kin}} \ . \tag{71}$$

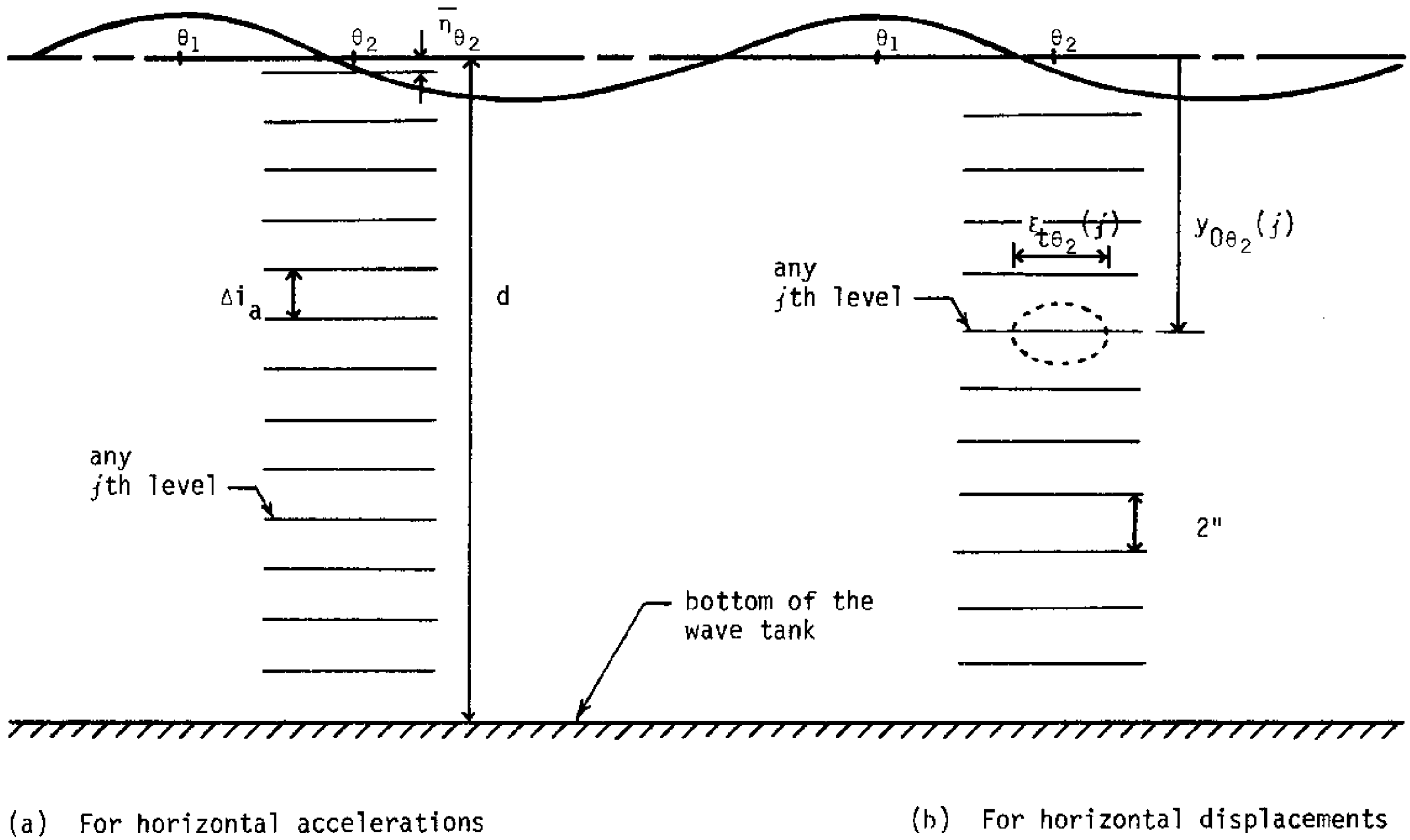

Fig. 28 Description of geometric divisions for computations of horizontal particle acceleration and total horizontal particle displacement at different depths

26. The total number of values of acceleration to be calculated over the depth span of the fluid is designated as $M = (N_{kin} + 1)$. Then, at the phase angle θ_2, each of the distances, $y_{\theta_2}(j)$, from the still water level down to a water particle situated at each depth-level j is calculated; i.e.,

$$y_{\theta_2}(j) = [\overline{\eta}_{\theta_2} - (N_{int\,j})(\Delta i_a)] \qquad (72)$$

where, again, $N_{int\,j}$ is the number of intervals (start with zero) down to the jth level. There will be M values of $y_{\theta_2}(j)$.

27. After calculating the array of values of $y_{\theta_2}(j)$, the array of horizontal accelerations, $a_{h\theta_2}(j)$, for the j-levels in the fluid may be calculated. These are obtained from (see equation (17), page 20)

$$a_{h\theta_2}(j) = -\frac{2\pi^2\overline{H}}{\overline{T}^2}\,\frac{\cosh\left[\dfrac{2\pi(y_{\theta_2}(j) + d)}{\overline{L}}\right]}{\sinh 2\pi d/\overline{L}}\sin\theta_2 \qquad (73)$$

where the values of $\overline{H}$, $\overline{T}$ and $\overline{L}$ are those obtained from steps 4, 6 and 7, respectively.

28. The root mean square of the horizontal particle acceleration, a_{hrms}, is calculated from

$$a_{hrms} = \sqrt{\frac{\sum_{j=1}^{M}[a_{h\theta_2}(j)]^2}{M}}\,. \qquad (74)$$

29. The total number of values of total horizontal particle displacement, ξ_t, to be calculated over the depth span of the water is designated as $K = (N_{disp} + 1)$. Then, for the phase angle θ_2, each of the distances, $y_{0\theta_2}(j)$, from the still water level down to the mean vertical coordinate of a water particle whose orbit is centered at each depth-level, j, is calculated (see Fig. 28b); i.e.,

$$y_{0\theta_2}(j) = -[2(N_{int j})] \tag{75}$$

where the length of each interval is 2 inches and, as before, $N_{int j}$ is the number of intervals (start with zero) down to the jth level. There will be K values of $y_{0\theta_2}(j)$.

30. After calculating the array of values of $y_{0\theta_2}(j)$, the array of total horizontal particle displacements, $\xi_{t\theta_2}(j)$, for the j-levels in the fluid may be calculated (see Fig. 28b). These are obtained from (see equation (18), page 20)

$$\xi_{t\theta_2}(j) = \overline{H} \frac{\cosh\left[\frac{(2\pi y_{0\theta_2}(j) + d)}{\overline{L}}\right]}{\sinh 2\pi d/\overline{L}} \sin\theta_2. \tag{76}$$

31. The root mean square of the total horizontal particle displacement, ξ_{trms}, is calculated from

$$\xi_{trms} = \sqrt{\frac{\sum_{j=1}^{K} [\xi_{t\theta_2}(j)]^2}{K}}. \tag{77}$$

$$I = \frac{a_{hrms} D}{u^2_{rms}} \tag{85}$$

$$P_d = \frac{d}{g\overline{T}^2} \tag{86}$$

$$P_H = \frac{\overline{H}}{g\overline{T}^2} \tag{87}$$

$$P_F = \frac{\overline{F}_{hmax}}{\rho g D^2 \overline{H}} \tag{88}$$

$$P_p = \frac{\overline{H}}{D} \tag{89}$$

$$P_s = \frac{\varepsilon}{D} \tag{90}$$

$$C_{urms} = \frac{2 \overline{F}_{hmax}}{(d + \overline{H}/2) \rho D u^2_{rms}} \tag{91}$$

34. The program prints the following quantities as output:

N_r, N_{mo}, N_{da}, N_{yr}, ℓ_{arm}, δ_{half}, N_{sp}, N_{pad},

D_s, ε, D, P_s, d, ℓ_{vert}, ℓ_G, g, T_w, ρ, ν,

L_{est}, N, θ_1, θ_2, $\overline{H}$, $\overline{F}_{hmax}$, $\overline{T}$, $\overline{L}$, $\overline{F}_{h\theta_1}$,

$\overline{F}_{h\theta_2}$, C_D, C_m, u_{rms}, a_{hrms}, U_m, a_{hmax},

ξ_{trms}, ζ_{trms}, ξ_{tmax}, ζ_{tmax}, R_{rms}, f_{pu},

$f_{p\xi}$, I, C_{urms}, P_d, P_H, P_F, P_p

35. The program is written to accept the data for the next experiment and repeat the same computations starting with step no. 1.

The symbols employed in coding the equations discussed in this appendix are identified in Table 3 along with a specification of the units required. A listing of the program follows Table 3.

Table 3 Variables for FORTRAN computer program

FORTRAN Symbol	Equation Notation	Units used in the program
AHMAX	a_{hmax}	$\frac{ft}{sec^2}$
AHRMS	a_{hrms}	$\frac{ft}{sec^2}$
AHT2(I)	$a_{h\theta_2}(i)$	$\frac{ft}{sec^2}$
CSUBD	C_D	-
CSUBM	C_m	-
CIRMU	C_{urms}	-
DBPIL	D_s	in
DTHET1	$(\frac{180}{\pi})\theta_1$	Deg
DTHET2	$(\frac{180}{\pi})\theta_2$	Deg
DPILE	D	in
DWAT	d	ft
ESTL	L_{est}	ft
ETA1(I)	$\eta_{\theta_1}(i)$	in
ETA2(I)	$\eta_{\theta_2}(i)$	in

Table 3 (Continued)

FORTRAN Symbol	Equation Notation	Units used in the program
ETAB1	$\bar{\eta}_{\theta_1}$	in
ETAB2	$\bar{\eta}_{\theta_2}$	in
ETMAX	ξ_{tmax}	in
ETT2(I)	$\xi_{t\theta_2}(j)$	in
ET2RMS	ξ_{trms}	in
FBTHT1	$\bar{F}_{h\theta_1}$	lb_f
FBTHT2	$\bar{F}_{h\theta_2}$	lb_f
FBWAVE	$\bar{F}_{hmax}$	lb_f
FSUBPE	$f_{p\varepsilon}$	-
FSUBPV	f_{pu}	-
FTHET1(I)	$F_{h\theta_1}(i)$	lb_f
FTHET2(I)	$F_{h\theta_2}(i)$	lb_f
FWAVE(I)	$F_{hmax}(i)$	lb_f
G	g	$\frac{ft}{sec^2}$

Table 3 (Continued)

FORTRAN Symbol	Equation Notation	Units used in the program
HBWAVE	$\overline{H}$	in
HSTR	δ_{half}	in
HWAVE(I)	$H(i)$	in
IA	I	-
INT1	Δi_v	in
INT2	Δi_a	in
KP11	$K'_{1\theta_1}$	-
KP22	$K'_{2\theta_2}$	-
LBAR	$\overline{L}$	ft
LGAGE	ℓ_G	ft
LVERT	ℓ_{vert}	in
NDA	N_{da}	-
NMO	N_{mo}	-
NOID	N_{disp}	-

Table 3 (Continued)

FORTRAN Symbol	Equation Notation	Units used in the program
NOIK	N_{kin}	-
NPAD	N_{pad}	-
NRUN	N_r	-
NV	N_v	-
NWAVE	N	-
NYR	N_{yr}	-
PERS	N_{sp}	%
PSUBD	P_d	-
PSUBF	P_F	-
PSUBH	P_H	-
PSUBP	P_P	-
RERMS	R_{rms}	-
RHO	ρ	$\frac{slugs}{ft^3}$
SAND	ϵ	in

Table 3 (Continued)

FORTRAN Symbol	Equation Notation	Units used in the program
SAPBL	ℓ_{arm}	in
SPAR	P_s	-
SUBS1	$\bar{S}_{s\theta_1}$	ft
SUBS2	$\bar{S}_{s\theta_2}$	ft
TBAR	$\bar{T}$	sec
THETA1	θ_1	rad
THETA2	θ_2	rad
TSUBA(I)	$t_A(i)$	sec
TSUBAP(I)	$t_{A'}(i)$	sec
TSUBB(I)	$t_B(i)$	sec
TSUBH(I)	$t_H(i)$	sec
TWAT	T_w	°F
UHMAX	U_m	$\frac{ft}{sec}$
UHRMS	u_{rms}	$\frac{ft}{sec}$

Table 3 (Continued)

FORTRAN Symbol	Equation Notation	Units used in the program
UT1(I)	$u_{\theta_1}(j)$	$\frac{ft}{sec}$
VISC	ν	$\frac{ft^2}{sec}$
WAVE	N	-
YT1(I)	$y_{\theta_1}(j)$	in
YT2(I)	$y_{\theta_2}(j)$	in
YOT1(I)	$y_{0\theta_1}(j)$	in
YOT2(I)	$y_{0\theta_2}(j)$	in
ZTAMAX	ζ_{tmax}	in
ZTAMS1	ζ_{trms}	in
ZTATT1(I)	$\zeta_{t\theta_1}(j)$	in

```
C
C      THIS PROGRAM COMPUTES DRAG AND INERTIA COEFFICIENTS AND A NUMBER
C      OF DIMENSIONLESS PARAMETERS BASED ON EXPERIMENTAL MEASUREMENTS OF
C      WAVE CHARACTERISTICS AND FORCES.
C      *    *    *    *    *    *    *    *    *    *    *
C      STATEMENT NUMBER 8005 MUST BE WRITTEN TO PROVIDE APPROPRIATE
C      IDENTIFICATION OF A GIVEN SET OF COMPUTATIONS.
C      ******************************************************************
C
       REAL LVERT, LGAGE, HBAR, LBAR, IA, LTOT, KP11, KP22,INT1, INT2
       DIMENSION ETA1(50), YT1(50), UT1(50), ZTATT1(50), YOT1(50),
      *     FTHET2(50), HWAVE(50), TSUBA(50),TSUBB(50),
      *TSUBAP(50), YT2(50), AHT2(50), YOT2(50), ETT2(50), TSUBH(50), FTHE
      *T1(50), ETA2(50), TOT(50), FWAVE(50)
 1000  READ (5,8003,END=1001) NRUN,NMO,NDA,NYR,NOIK,NOID,NPAD,NV,PERS,HST
      *R,THETA1,THETA2,ESTL,SAPBL,SAND
 8003  FORMAT(8I2,7F8.4)
       READ(5,8004)LVERT,DBPIL,DWAT,LGAGE,G,TWAT,RHO,VISC
 8004  FORMAT (7F10.4,E10.4)
       PI = 3.14159265
       READ (5,8001) (HWAVE(I), I = 1,NV)
       READ (5,8001) (FWAVE(I), I = 1,NV)
       READ (5,8001) (FTHET1 (I), I = 1,NV)
       READ (5,8001) (FTHET2 (I), I = 1,NV)
       READ (5,8001)  (ETA1  (I), I = 1,NV)
       READ (5,8001)  (ETA2  (I), I = 1,NV)
       READ (5,8002) (TSUBH(I),I = 1,NV)
       READ (5,8002) (TSUBA(I), I = 1,NV)
       READ (5,8002) (TSUBB(I), I = 1,NV)
       READ (5,8002) (TSUBAP(I), I = 1,NV)
```

```
 8001 FORMAT (11F7.1)
 8002 FORMAT (10F8.2)
C
C     PRELIMINARY CALCULATIONS
      DTHET1 = THETA1*(180./PI)
      DTHET2 = THETA2*(180./PI)
      DPILE = DRPIL + 2.0*SAND
C
C     CALCULATE AVERAGE WAVE HEIGHT
       I = 1
      TOT(1) = HWAVE(1)
      IH = 20
      DO 0022 I = 2,IH
      TOT(I) = TOT(I-1) + HWAVE(I)
 0022 CONTINUE
      I = IH
      RI = I
      HBWAVE = TOT(I)/RI
      IF (ABS(TOT(I-1)/(RI-1.)-TOT(I)/RI)-.009*TOT(I)/RI) 7760,7760,0001
 0001 I = I + 1
      IF (I.GT.NV) GO TO 1003
      TOT(I) = TOT(I-1) + HWAVE(I)
      RI = I
      HBWAVE = TOT(I)/RI
      IF (ABS(TOT(I-1)/(RI-1.)-TOT(I)/RI)-.009*TOT(I)/RI) 7760,7760,0001
C
C     CALCULATE AVERAGE PEAK WAVE FORCE
 7760 TOT(1) = FWAVE(1)
      DO 0003 J = 2,I
 0003 TOT(J) = TOT(J-1) + FWAVE(J)
      J = I
```

```
      RJ = J
      FBWAVE = TOT(J)/RJ
 0006 IF (ABS(TOT(J-1)/(RJ-1.)-TOT(J)/RJ)-.009*TOT(J)/RJ) 0004,0004,0002
 0002 J = J+1
      IF (J.GT.NV) GO TO 1005
      TOT(J) = TOT(J-1) + FWAVE(J)
      RJ = J
      FBWAVE = TOT(J)/RJ
      GO TO 0006
C
C     CALCULATE AVERAGE WAVE PERIOD
 0004 K = J
      NWAVE = K
 7753 WAVE = NWAVE
      TBAR = (TSUBH(NWAVE + 1) - TSUBH(1))/WAVE
C
C     CALCULATE AVERAGE WAVE LENGTH
      LTOT = 0.
      DO 9999 I = 1,NWAVE
 9999 LTOT = LTOT + ((TSUBA(I) - TSUBB(I))/(TSUBA(I) -TSUBAP(I))*LGAGE)
      LBAR = LTOT/WAVE
C
C     CALCULATE AVERAGE FORCE AT THETA1
      FTTOT = 0.
      DO 0009 I = 1,NWAVE
 0009 FTTOT = FTTOT + FTHET1(I)
      FBTHT1 = FTTOT/WAVE
C
C     CALCULATE AVERAGE WAVE ELEVATION ABOVE BOTTOM AT THETA1
      STOT = 0.
      DO 0010 I = 1,NWAVE
```

```
 0010 STOT = STOT + ETA1(I)/12. +DWAT
      SSUBS1 = STOT/WAVE
C
C     CALCULATE THE CONSTANT KP11
      KP11 = ((4.*PI*SSUBS1/LBAR)+SINH(4.*PI*SSUBS1/LBAR))/(16.*(SINH(2.
     **PI*DWAT/LBAR))**2)
C
C     CALCULATE DRAG COEFFICIENT
      CSUBD = TBAR**2/(PI*RHO*(DPILE/12.)*(HBWAVE/12.)**2*LBAR)*FBTHT1/(
     *KP11*ABS(COS(THETA1))*COS(THETA1))
C
C     CALCULATE AVERAGE WAVE FORCE AT THETA2
      F2TOT = 0.
      DO 0011 I = 1, NWAVE
 0011 F2TOT = F2TOT + FTHET2(I)
      FBTHT2 = F2TOT/WAVE
C
C     CALCULATE AVERAGE WAVE ELEVATION ABOVE BOTTOM AT THETA2
      ETOT2 = 0.
      DO 9011 I = 1,NWAVE
 9011 ETOT2 =          ETOT2 + ETA2(I)/12. + DWAT
      SSUBS2 = ETOT2/WAVE
C
C     CALCULATE THE CONSTANT KP22
      KP22 = SINH(2.*PI*SSUBS2/LBAR)/SINH(2.*PI*DWAT/LBAR)
C
C     CALCULATE MASS COEFFICIENT
      CSUBM = -TBAR**2/(PI*RHO*(DPILE/12.)*(HBWAVE/12.)**2*LBAR)*4.*
     *(HBWAVE/12.)*FBTHT2/(PI*(DPILE/12.)*KP22*SIN(THETA2))
C
```

```
C      CALCULATE AVERAGE WAVE ELEVATION WITH RESPECT TO SWL AT THETA1
       ETOT = O.
       DO 0012 I = 1,NWAVE
 0012  ETOT = ETOT + ETA1(I)
       ETAB1 = ETOT/WAVE
C
C      CALCULATE INTERVAL SIZE FOR DEPTH SPAN UNDER CREST
       RNOIK = NOIK
       INT1 = (DWAT*12.+ETAB1)/RNOIK
C
C      CALCULATE DEPTHS AT INTERVALS OF INT1
       M = NOIK + 1
       DO 0013 I = 1, M
       NOIJ = I-1
       RNOIJ = NOIJ
       YT1(I)     = ETAB1 -RNOIJ*INT1
C
C      CALCULATE HORIZONTAL VELOCITIES AT INTERVALS OF INT1
 0013  UT1(I) = PI*(HBWAVE/12.)/TBAR*COSH(2.*PI*(YT1(I)/12.+DWAT)/LBAR)*
      *COS(THETA1)/SINH(2.*PI*DWAT/LBAR)
C
C      CALCULATE ROOT MEAN SQUARE OF HORIZONTAL VELOCITY AT THETA1
       UTOT = 0.
       DO 0014 I = 1,M
 0014  UTOT = UTOT + UT1(I)**2
       RM = M
       UHRMS = SQRT (UTOT/RM)
C
C      CALCULATE DEPTHS AT 2 IN INTERVALS AT THETA1
       K = NOID + 1
       DO 15 I = 1,K
```

```
      NOIJ = I-1
      RNOIJ = NOIJ
      YOT1(I) = -(RNOIJ*2.)
C
C     CALCULATE TOTAL VERTICAL PARTICLE DISPLACEMENTS AT 2 IN INTERVALS
 0015 ZTATT1(I)=HBWAVE*SINH(2.*PI*(YOT1(I)/12.+DWAT)/LBAR)*COS(THETA1)
     */SINH(2.*PI*DWAT/LBAR)
C
C     CALCULATE RMS OF TOTAL VERTICAL PARTICLE DISPLACEMENT AT THETA1
      XOT = 0.
      DO 0016 I = 1,K
 0016 XOT = XOT + ZTATT1(I)**2
      PK=K
      ZTAMS1 = SQRT(XOT/PK)
C
C     CALCULATE AVERAGE WAVE ELEVATION WITH RESPECT TO SWL AT THETA2
      XOT = 0.
      DO CC17 I = 1,NWAVE
 0017 XOT = XOT + ETA2(I)
      ETAB2 = XOT/WAVE
C
C     CALCULATE INTERVAL SIZE FOR DEPTH SPAN AT THETA2
      INT2 = (DWAT*12. + ETAB2)/NOIK
C
C     CALCULATE DEPTHS AT INTERVALS OF INT2
      M = NOIK + 1
      DO 18 I = 1,M
      NOIJ = I - 1
      RNOIJ = NOIJ
      YT2(I) = ETAB2 -RNOIJ*INT2
```

```
C
C     CALCULATE HORIZONTAL ACCELERATIONS AT INTERVALS OF INT2
   18 AHT2(I)=-2.*PI**2*HBWAVE/12./TBAR**2*COSH(2.*PI*(YT2(I)/12.+DWAT)/
     *LBAR)*SIN(THETA2)/SINH(2.*PI*DWAT/LBAR)
C
C     CALCULATE ROOT MEAN SQUARE OF HORIZONTAL ACCELERATION AT THETA2
      XOT = 0.
      DO 19 I = 1,M
 0019 XOT = XOT+AHT2(I)**2
      RM = M
      AHRMS = SQRT(XOT/RM)
C
C     CALCULATE DEPTHS AT 2 IN INTERVALS AT THETA2
      K = NOID+1
      DO 20 I = 1,K
      NOIJ = I-1
      RNOIJ = NOIJ
      YOT2(I) = -RNOIJ*2.
C
C     CALCULATE TOTAL HOR. PARTICLE DISPLACEMENTS AT 2 IN INTERVALS
   20 ETT2(I) = HBWAVE*COSH(2.*PI*(YOT2(I)/12. + DWAT)/LBAR)*SIN(THETA2)
     */SINH(2.*PI*DWAT/LBAR)
C
C     CALCULATE RMS OF TOTAL HORIZONTAL PARTICLE DISPLACEMENT AT THETA2
      XOT = 0.
      DO 21 I = 1,K
   21 XOT = XOT + ETT2(I)**2
      RK = K
      ET2RMS = SQRT(XOT/RK)
C
```

```
C     CALCULATE MAXIMUM VALUES
      UHMAX = PI*(HBWAVE/12.)/TBAR*COSH(2.*PI*(ETAB1/12. + DWAT)/LBAR)*
     *COS(THETA1)/SINH(2.*PI*DWAT/LBAR)
      ETMAX = HBWAVE*COSH(2.*PI*(YOT2(1)/12. + DWAT)/LBAR)
     */(SINH(2.*PI*DWAT/LBAR))*SIN(THETA2)
      ZTAMAX = HBWAVE*SINH(2.*PI*(YOT1(1)/12. + DWAT)/LBAR)*COS(THETA1)/
     *SINH(2.*PI*DWAT/LBAR)
      AHMAX=-2.*PI**2*(HBWAVE/12.)/TBAR**2*COSH(2.*PI*(ETAB2/12.+DWAT)/L
     *BAR)*SIN(THETA2)/SINH(2.*PI*DWAT/LBAR)
C
C     CALCULATE PARAMETERS
      RERMS= UHRMS * (DPILE/12.)/VISC
      FSUBPV = UHRMS*TBAR/(DPILE/12.)
      FSUBPE = PI*ET2RMS/DPILE
      IA = AHRMS*(DPILE/12.)/UHRMS**2
      PSUBD = DWAT/(G*TBAR**2)
      PSUBH = HBWAVE/(12.*G*TBAR**2)
      PSUBF = 12.**3*FBWAVE/(RHO*G*DPILE**2*HBWAVE)
      PSUBP = HBWAVE/DPILE
      SPAR = SAND/DPILE
      CIRMU=2.0*FBWAVE/((DWAT + HBWAVE/(2.0*12.))*(RHO*(DPILE/12.0)*UHRM
     *S**2))
      WRITE(6,8005) NRUN,NMO,NDA,NYR
 8005 FORMAT(1H1,7(/),T26,'RUN NO. ',I2,'    DATE (MONTH DAY YEAR). ',I2,
     *'  ',I2,'  ',I2//T24'ROUGHNESS NO. 3.  A STUDY OF THE EFFECT OF SU
     *RFACE'/T21'ROUGHNESS ON WAVE FORCES ON A CIRCULAR CYLINDRICAL PILE
     *'///)
      WRITE(6,8048) SAPBL
 8048 FORMAT(T20,'OVERALL LENGTH OF STROKE ARM'/T20'PLUS ITS BEARING ='T
     *50,F15.3,' INCHES'/)
      WRITE (6,8007) HSTR
```

```
8007 FORMAT(T20,'HALF STROKE ='T50,F15.3,' INCHES'/)
     WRITE (6,8006) PERS
8006 FORMAT(T20,'PERCENT SPEED = 'T50,F15.3,' PERCENT'/)
     WRITE (6,8008) NPAD
8008 FORMAT (T20,'PADDLE POSITION =' T50,I15,' (NO DIM.)'/)
     WRITE(6,8050) DBPIL
8050 FORMAT(T20,'DIAMETER OF THE BARE PILE ='T50,F15.3,' INCHES'/)
     WRITE(6,8049) SAND
8049 FORMAT(T20,'AVERAGE SAND DIAMETER ='T50,F15.3,' INCHES'/)
     WRITE (6,8013) DPILE
8013 FORMAT(T20,'PILE DIAMETER INCLUDING'/T20'THE SAND GRAINS ='T50,F15
    *.3,' INCHES'/)
     WRITE (6,8051) SPAR
8051 FORMAT(T20,'RELATIVE SAND GRAIN SIZE'/T20'WITH RESPECT TO THE OVER
    *ALL'/T20'PILE DIAMETER, SAND/DPILE ='T50,F15.3,' (NO DIM.)'/)
     WRITE (6,8014) DWAT
8014 FORMAT (T20,'STILL WATER DEPTH AT PILE ='T50,F15.3,' FEET'/)
     WRITE (6,8016) LVERT
8016 FORMAT(T20,'VERTICAL DISTANCE FROM THE'/T20'MIDDLE OF THE UPPER TR
    *ANSDUCER'/T20'TO THE BOTTOM OF THE PILE ='T50,F15.3,' INCHES'/)
     WRITE(6,8045) LGAGE
8045 FORMAT(T20,'HORIZONTAL DISTANCE BETWEEN'/T20'WAVE GAGES ='T50,F15.
    *3,' FEET'/)
     WRITE(6,8046) G
8046 FORMAT(T20,'ACCELERATION OF GRAVITY AT'/T20'COLLEGE STATION, TEXAS
    * ='T50,F15.3,' FT/SEC**2'/)
     WRITE (6,8015) TWAT
8015 FORMAT (T20,'WATER TEMPERATURE ='T50,F15.3,' DEG. F.'/)
     WRITE(6,8047) RHO
8047 FORMAT(T20,'DENSITY OF WATER AT TWAT ='T50,F15.3,' SLUGS/FT**3'/)
     WRITE (6,8017) VISC
```

```
8017 FORMAT(T20,'KINEMATIC VISCOSITY OF WATER ='T50,E15.8,' FT**2/SEC'/
    *)
     WRITE (6,8009) ESTL
8009 FORMAT (T20,'ESTIMATED WAVE LENGTH ='T50,F15.3,' FEET'/)
     WRITE (6,8010) NWAVE
8010 FORMAT (T20,'NUMBER OF WAVES ='T50,I15,' (NO DIM.)'/)
     WRITE (6,8011) DTHET1
8011 FORMAT(1H1,7(/),T20,'THETA1 ='T50,F15.3,' DEGREES'/)
     WRITE (6,8012) DTHET2
8012 FORMAT (T20,'THETA2 ='T50,F15.3,' DEGREES'/)
     WRITE (6,8018) HBWAVE
8018 FORMAT(T20,'AVERAGE WAVE HEIGHT ='T50,F15.3,' INCHES'/)
     WRITE (6,8020) FBWAVE
8020 FORMAT(T20,'AVERAGE PEAK WAVE FORCE ='T50,F15.3,' LBS.'/)
     WRITE (6,8022) TBAR
8022 FORMAT(T20,'AVERAGE WAVE PERIOD ='T50,F15.3,' SECONDS'/)
     WRITE (6,8023) LBAR
8023 FORMAT(T20,'AVERAGE WAVE LENGTH ='T50,F15.3,' FEET'/)
     WRITE (6,8025) FBTHT1
8025 FORMAT(T20,'AVERAGE HORIZONTAL'/T20'FORCE AT THETA1 ='T50,F15.3,'
    *LBS.'/)
     WRITE (6,8026) FBTHT2
8026 FORMAT(T20,'AVERAGE HORIZONTAL'/T20'FORCE AT THETA2 ='T50,F15.3,'
    *LBS.'/)
     WRITE (6,8027) CSUBD
8027 FORMAT(T20,'DRAG COEFFICIENT ='T50,F15.3,' (NO DIM)'/)
     WRITE (6,8028) CSUBM
8028 FORMAT(T20,'MASS COEFFICIENT ='T50,F15.3,' (NO DIM)'/)
     WRITE (6,8029) UHRMS
8029 FORMAT(T20,'ROOT MEAN SQUARE AVERAGE OF'/T20'HORIZONTAL PARTICLE V
```

```
     *ELOCITY ='T50,F15.3,' FT./SEC.'/)
      WRITE (6,8030) AHRMS
8030 FORMAT(T20,'ROOT MEAN SQUARE AVERAGE OF'/T20'HORIZONTAL PARTICLE'/
     *T20'ACCELERATION ='T50,F15.3,' FT/SEC**2'/)
      WRITE (6,8031) UHMAX
8031 FORMAT(T20,'ARITH. AVERAGE OF PEAK'/T20'HORIZONTAL PARTICLE VELOCI
     *TY ='T50,F15.3,' FT./SEC.'/)
      WRITE(6,8032) AHMAX
8032 FORMAT(T20,'ARITH. AVERAGE OF PEAK'/T20'HORIZONTAL PARTICLE'/T20'A
     *CCELERATION ='T50,F15.3,' FT/SEC**2'/)
      WRITE(6,8033) ET2RMS
8033 FORMAT(T20,'RMS AVERAGE OF TOTAL HORI-'/T20'ZONTAL PARTICLE DISPLA
     *CEMENT'/T20'AT THETA2 ='T50,F15.3,' INCHES'/)
      WRITE(6,8034) ZTAMS1
8034 FORMAT(T20,'RMS AVERAGE OF TOTAL VERTICAL'/T20'PARTICLE DISPLACEME
     *NT'/T20'AT THETA1 ='T50,F15.3,' INCHES'/)
      WRITE (6,8035) ETMAX
8035 FORMAT(T20,'AVERAGE MAXIMUM TOTAL HORI-'/T20'ZONTAL PARTICLE DISPL
     *ACEMENT ='T50,F15.3,' INCHES'/)
      WRITE(6,8036) ZTAMAX
8036 FORMAT(T20,'AVERAGE MAXIMUM TOTAL VERTICAL'/T20'PARTICLE DISPLACEM
     *ENT ='T50,F15.3,' INCHES'/)
      WRITE(6,8037) RERMS
8037 FORMAT(1H1,7(/),T20,'REYNOLDS NUMBER BASED ON RMS'/T20'HORIZONTAL
     *PARTICLE VELOCITY ='T50,F15.3,' (NO DIM.)'/)
      WRITE(6,8038) FSUBPV
8038 FORMAT(T20,'PERIOD PARAMETER,'/T20'UHRMS*TBAR/DPILE ='T50,F17.5,'
     *(NO DIM.)'/)
      WRITE(6,8039) FSUBPE
8039 FORMAT(T20,'PERIOD PARAMETER,'/T20'PI*ET2RMS/DPILE ='T50,F17.5,' (
     *NO DIM.)'/)
```

```
      WRITE(6,8040) IA
8040  FORMAT(T20,'IVERSEN''S MODULUS,'/T20'AHRMS*DPILE/UHRMS**2 ='T50,F1
     *7.5,' (NO DIM.)'/)
      WRITE(6,8052) CIRMU
8052  FORMAT(T20,'RESISTANCE COEFFICIENT OF'/T20'THE IVERSEN TYPE BASED
     *ON'/T20'FBWAVE,HBWAVE AND UHRMS ='T50,F15.3,' (NO DIM.)'/)
      WRITE(6,8041) PSUBD
8041  FORMAT(T20,'DEPTH PARAMETER,'/T20'DWAT/(G*TBAR**2) ='T50,F17.5,' (
     *NO DIM.)'/)
      WRITE(6,8042) PSUBH
8042  FORMAT(T20,'HEIGHT PARAMETER,'/T20'HBWAVE/(G*TBAR**2) ='T50,F17.5,
     *' (NO DIM.)'/)
      WRITE(6,8043) PSUBF
8043  FORMAT(T20,'FORCE PARAMETER, FBWAVE/(RHO*'/T20'G*DPILE**2*HBWAVE)
     *='T50,F17.5,' (NO DIM.)'/)
      WRITE(6,8044) PSUBP
8044  FORMAT(T20,'PILE PARAMETER,HBWAVE/DPILE ='T50,F17.5,' (NO DIM.)'/)
      GO TO 1000
1003  WRITE (6,1004) NV, I
1004  FORMAT(1H0,3(/),T30, 'INSUFFICIENT DATA TO GIVE AN AVERAGE WAVE HE
     *IGHT   NV =',I2,'    I =',I2//)
      GO TO 1000
1005  WRITE (6,1006) NV,J
1006  FORMAT (1H0,3(/),T30,'INSUFFICIENT DATA TO GIVE AN AVERAGE MAX WAV
     *E FORCE   NV =',I2,'      J =',I2//)
      GO TO 1000
1001  WRITE (6,1002)
1002  FORMAT (1H1)
      STOP
      END
```

```
      FUNCTION RAD(X)
      RAD = X*PI/180.
      RETURN
      END
      FUNCTION SINH(X)
      SINH = (EXP(X)-(1./EXP(X)))/2.
      RETURN
      END
      FUNCTION COSH(X)
      COSH = (EXP(X)+(1./EXP(X)))/2.
      RETURN
      END
$DATA
```

APPENDIX 3

TABLES OF DATA

The tables in this appendix contain the data necessary for reproducing the experiments as well as a collection of the pertinent quantities obtained from the computer computations and used in evaluating the effects of surface roughness on the wave forces on a circular cylindrical pile.

Table 4 contains a summary of the water properties employed in the computations for each experiment. These water properties were interpolated from data given by Rouse [40].

Table 5 gives a summary of the wave generator settings and identifies the experiments which were made using each combination of half-stroke and percent speed setting. Also included is a statement of the ℓ_{arm}, N_{pad} and ℓ_G values which were used for all of the experiments.

Tables 6 through 17 summarize the results obtained from the computer computations of the parameters indicated. The notation in the table headings may be identified by referring to the List of Symbols.

Table 4 Summary of water properties for the experiments

Smooth Surface				Roughness No. 1 Surface			
Expt.	T_w °F	$\nu \times 10^5$ $\frac{ft^2}{sec}$	ρ $\frac{slugs}{ft^3}$	Expt.	T_w °F	$\nu \times 10^5$ $\frac{ft^2}{sec}$	ρ $\frac{slugs}{ft^3}$
1	73.4	1.009	1.937	23	85.1	0.875	1.93
2	73.4	1.009	1.937	24	84.9	0.877	1.93
3	73.4	1.009	1.937	25	84.9	0.877	1.93
4	73.4	1.009	1.937	26	84.7	0.879	1.93
5	73.4	1.009	1.937	27	84.7	0.879	1.93
6	73.4	1.009	1.937	28	84.7	0.879	1.93
7	78.8	0.944	1.931	29	84.2	0.885	1.93
8	78.6	0.947	1.931	30	84.2	0.885	1.93
9	78.8	0.944	1.931	31	84.2	0.885	1.93
10	78.8	0.944	1.931	32	84.2	0.885	1.93
11	83.3	0.895	1.93	33	84.2	0.885	1.93
12	83.3	0.895	1.93	34	84.0	0.887	1.93
13	83.3	0.895	1.93	35	83.5	0.893	1.93
14	83.3	0.895	1.93	36	83.3	0.895	1.93
15	83.3	0.895	1.93	37	83.7	0.891	1.93
16	83.3	0.895	1.93	38	83.5	0.893	1.93
17	83.3	0.895	1.93	39	83.3	0.895	1.93
18	73.4	1.009	1.937	40	83.5	0.893	1.93
19	73.4	1.009	1.937	41	83.3	0.895	1.93
20	73.4	1.009	1.937	42	83.5	0.893	1.93
21	73.4	1.009	1.937	43	83.3	0.895	1.93
22	73.4	1.009	1.937	44	83.3	0.895	1.93

Table 4 (Continued)

Roughness No. 2 Surface				Roughness No. 3 Surface			
Expt.	T_w °F	$\nu \times 10^5$ $\frac{ft^2}{sec}$	ρ $\frac{slugs}{ft^3}$	Expt.	T_w °F	$\nu \times 10^5$ $\frac{ft^2}{sec}$	ρ $\frac{slugs}{ft^3}$
45	81.5	0.914	1.93	67	79.3	0.938	1.931
46	81.5	0.914	1.93	68	79.3	0.938	1.931
47	81.5	0.914	1.93	69	79.7	0.934	1.93
48	81.1	0.918	1.93	70	79.3	0.938	1.931
49	81.1	0.918	1.93	71	79.3	0.938	1.931
50	81.1	0.918	1.93	72	79.3	0.938	1.931
51	81.1	0.918	1.93	73	79.3	0.938	1.931
52	81.1	0.918	1.93	74	79.7	0.934	1.93
53	81.1	0.918	1.93	75	79.7	0.934	1.93
54	81.5	0.914	1.93	76	79.7	0.934	1.93
55	81.5	0.914	1.93	77	79.7	0.934	1.93
56	81.5	0.914	1.93	78	79.3	0.938	1.931
57	81.5	0.914	1.93	79	79.7	0.934	1.93
58	81.5	0.914	1.93	80	79.7	0.934	1.93
59	81.5	0.914	1.93	81	79.7	0.934	1.93
60	81.5	0.914	1.93	82	80.2	0.927	1.93
61	81.5	0.914	1.93	83	80.2	0.927	1.93
62	81.5	0.914	1.93	84	80.2	0.927	1.93
63	81.5	0.914	1.93	85	80.2	0.927	1.93
64	81.5	0.914	1.93	86	80.2	0.927	1.93
65	81.5	0.914	1.93	87	80.2	0.927	1.93
66	81.5	0.914	1.93	88	80.2	0.927	1.93

Table 5 Summary of half-stroke and percent speed settings for the wave generator (ℓ_{arm} = 62 in, N_{pad} = 1, ℓ_G = 7 ft)

Generator setting		Experiments on which the generator settings were used
s_{half} (in)	N_{sp} (-)	
0.55	76.0	1, 23, 45, 67
1.05	77.0	2, 24, 46, 68
1.40	75.0	3, 25, 47, 69
0.60	63.0	4, 26, 48, 70
1.18	63.0	5, 27, 49, 71
1.75	62.0	6, 28, 50, 72
2.20	64.0	7, 29, 51, 73
0.70	52.0	8, 30, 52, 74
1.35	51.0	9, 31, 53, 75
2.00	50.0	10, 32, 54, 76
2.70	52.0	11, 33, 55, 77
3.05	54.0	12, 34, 56, 78
0.90	45.0	13, 35, 57, 79
1.75	45.0	14, 36, 58, 80
2.60	45.0	15, 37, 59, 81
2.80	45.0	16, 38, 60, 82
3.60	47.0	17, 39, 61, 83
1.00	42.0	18, 40, 62, 84
1.83	42.0	19, 41, 63, 85
2.65	39.5	20, 42, 64, 86
3.30	39.0	21, 43, 65, 87
3.90	41.0	22, 44, 66, 88

Table 6 Summary of wave characteristics, forces, drag coefficients and inertia coefficients for the smooth surface experiments (D = 3.716 in, ε = 0.0 in)

Expt.	$\overline{H}$ (in)	$\overline{L}$ (ft)	$\overline{T}$ (sec)	$\overline{F}_{h\theta_1}$ (lbs)	$\overline{F}_{h\theta_2}$ (lbs)	$\overline{F}_{hmax}$ (lbs)	C_D —	C_m —
1	1.96	3.75	0.84	0.31	-0.89	1.02	6.72	2.26
2	4.28	3.66	0.83	0.04	-1.47	1.62	0.12	1.78
3	4.45	3.99	0.86	0.57	-1.57	1.88	1.56	1.84
4	2.02	5.59	1.05	0.11	-1.00	0.93	2.35	2.55
5	4.12	5.69	1.04	0.41	-1.84	1.88	1.60	2.17
6	6.39	5.55	1.05	0.60	-2.20	2.38	0.72	1.88
7	6.37	5.20	1.01	-0.22	-2.14	2.40	-0.31	1.99
8	1.95	7.87	1.22	-0.28	-0.68	0.85	-5.59	1.71
9	3.85	8.00	1.30	-0.23	-1.33	1.54	-1.16	1.91
10	5.79	8.19	1.31	0.20	-2.00	2.51	0.38	1.91
11	7.80	7.22	1.28	-0.42	-2.59	3.17	-0.40	2.09
12	9.06	7.34	1.21	1.29	-2.58	3.27	0.70	1.59
13	2.15	10.46	1.54	-0.20	-0.68	0.70	-3.20	1.87
14	3.97	9.67	1.51	0.96	-0.04	1.47	4.44	0.06
15	7.12	9.57	1.48	0.29	-2.33	2.66	0.34	1.96
16	7.57	9.40	1.48	0.46	-2.57	2.45	0.49	2.22
17	8.43	8.86	1.35	1.49	-2.78	3.37	1.06	1.84
18	2.30	11.58	1.66	0.11	-0.75	0.66	1.48	2.02
19	4.21	11.37	1.65	-0.24	-1.26	1.35	-0.91	1.89
20	6.11	11.36	1.67	0.88	-1.86	2.08	1.41	2.10
21	7.89	11.25	1.65	1.99	-2.00	2.94	1.75	1.66
22	10.00	10.37	1.56	2.60	-0.24	3.16	1.26	0.15

Table 7 Summary of particle velocities, accelerations and displacements for the smooth surface experiments ($D = 3.716$ in, $\varepsilon = 0.0$ in)

Expt.	U_m $(\frac{ft}{sec})$	u_{rms} $(\frac{ft}{sec})$	a_{hmax} $(\frac{ft}{sec^2})$	a_{hrms} $(\frac{ft}{sec^2})$	ξ_{tmax} (in)	ξ_{trms} (in)	ζ_{tmax} (in)	ζ_{trms} (in)
1	0.71	0.30	-4.53	1.92	1.97	0.84	1.96	0.83
2	2.00	0.80	-9.74	4.11	4.29	1.81	4.28	1.79
3	1.94	0.81	-9.26	4.07	4.46	1.95	4.45	1.92
4	0.57	0.29	-3.08	1.58	2.06	1.06	2.02	0.97
5	1.33	0.65	-6.59	3.38	4.22	2.19	4.12	1.99
6	2.46	1.15	-9.28	4.78	6.53	3.34	6.39	3.06
7	2.38	1.10	-9.10	4.62	6.47	3.20	6.37	2.99
8	0.48	0.29	-2.35	1.45	2.12	1.31	1.95	1.02
9	0.96	0.57	-4.09	2.55	4.20	2.62	3.85	2.02
10	1.54	0.90	-6.07	3.84	6.35	4.01	5.79	3.04
11	2.35	1.25	-7.94	4.75	8.30	4.90	7.80	4.00
12	3.10	1.64	-10.30	6.24	9.67	5.75	9.06	4.65
13	0.46	0.32	-1.80	1.28	2.58	1.85	2.15	1.18
14	0.89	0.58	-3.32	2.29	4.60	3.17	3.97	2.14
15	1.78	1.12	-6.19	4.25	8.24	5.64	7.12	3.84
16	1.92	1.19	-6.22	4.31	8.69	5.90	7.57	4.07
17	2.42	1.43	-8.36	5.55	9.48	6.24	8.43	4.49
18	0.48	0.35	-1.73	1.30	2.90	2.17	2.30	1.27
19	0.91	0.65	-3.16	2.35	5.24	3.90	4.21	2.32
20	1.38	0.96	-4.30	3.27	7.61	5.66	6.11	3.38
21	1.89	1.27	-5.78	4.32	9.78	7.24	7.89	4.35
22	2.67	1.68	-7.87	5.67	11.94	8.51	10.00	5.46

Table 8 Summary of dimensionless parameters evaluated for the smooth surface experiments ($P_s = \epsilon/D = 0.0/3.716 = 0$)

Expt.	R_{rms} —	f_{pu} —	$f_{p\xi}$ —	I —	C_{urms} —	P_d —	P_H —	P_F —	P_P —
1	9106	0.81	0.71	6.75	18.64	0.087	0.0072	1.050	0.528
2	24670	2.15	1.53	1.97	3.83	0.091	0.0162	0.760	1.151
3	24751	2.23	1.65	1.94	4.41	0.085	0.0157	0.850	1.197
4	8772	0.96	0.90	5.99	18.23	0.057	0.0048	0.928	0.543
5	20079	2.19	1.85	2.45	6.75	0.058	0.0100	0.918	1.110
6	35332	3.91	2.82	1.12	2.64	0.056	0.0150	0.747	1.719
7	36012	3.58	2.71	1.19	2.94	0.061	0.0162	0.760	1.714
8	9544	1.15	1.11	5.27	16.13	0.042	0.0034	0.882	0.526
9	18684	2.39	2.21	2.43	7.34	0.037	0.0059	0.806	1.037
10	29663	3.82	3.39	1.45	4.58	0.036	0.0088	0.875	1.557
11	43324	5.17	4.14	0.94	2.91	0.038	0.0124	0.820	2.100
12	56608	6.38	4.86	0.72	1.72	0.043	0.0161	0.728	2.437
13	11159	1.60	1.56	3.82	10.77	0.026	0.0024	0.655	0.580
14	20214	2.84	2.68	2.08	6.67	0.027	0.0045	0.749	1.068
15	38887	5.35	4.77	1.04	3.07	0.028	0.0085	0.753	1.917
16	41131	5.68	4.99	0.94	2.51	0.028	0.0090	0.653	2.038
17	49541	6.24	5.28	0.84	2.34	0.034	0.0120	0.806	2.269
18	10722	1.87	1.83	3.29	8.64	0.022	0.0022	0.579	0.619
19	19851	3.44	3.29	1.74	4.93	0.023	0.0040	0.643	1.132
20	29431	5.16	4.78	1.10	3.35	0.022	0.0057	0.685	1.645
21	39097	6.80	6.12	0.82	2.60	0.023	0.0075	0.750	2.122
22	51555	8.46	7.19	0.62	1.55	0.026	0.0107	0.636	2.691

Table 9 Summary of wave characteristics, forces, drag coefficients and inertia coefficients for the roughness no. 1 experiments ($D = 3.772$ in, $\varepsilon = 0.028$ in)

Expt.	$\overline{H}$ (in)	$\overline{L}$ (ft)	$\overline{T}$ (sec)	$\overline{F}_{h\theta_1}$ (lbs)	$\overline{F}_{h\theta_2}$ (lbs)	$\overline{F}_{hmax}$ (lbs)	C_D —	C_m —
23	1.76	3.68	0.85	-0.32	-0.88	0.86	-9.26	2.50
24	4.06	3.77	0.83	-0.24	-1.49	1.68	-0.86	1.77
25	4.99	3.90	0.84	-0.11	-1.59	1.87	-0.21	1.58
26	2.10	5.57	1.05	0.09	-0.98	0.97	1.87	2.36
27	3.90	5.57	1.04	-0.21	-1.69	1.77	-0.97	2.24
28	6.24	5.68	1.05	0.52	-2.15	2.56	0.69	1.83
29	6.29	5.20	1.01	1.08	-1.92	2.54	1.48	1.71
30	1.68	8.29	1.30	0.04	-0.75	0.81	1.09	2.33
33	8.06	7.30	1.25	0.30	-2.72	3.16	0.25	1.99
37	6.93	9.51	1.47	0.57	-2.40	2.62	0.71	2.01
39	8.62	8.75	1.36	0.61	-2.81	3.75	0.40	1.87
40	2.25	11.84	1.67	-0.11	-0.68	0.70	-1.41	1.83

Table 10 Summary of particle velocities, accelerations and displacements for the roughness no. 1 experiments ($D = 3.772$ in, $\varepsilon = 0.028$ in)

Expt.	U_m $(\frac{ft}{sec})$	u_{rms} $(\frac{ft}{sec})$	a_{hmax} $(\frac{ft}{sec^2})$	a_{hrms} $(\frac{ft}{sec^2})$	ξ_{tmax} (in)	ξ_{trms} (in)	ζ_{tmax} (in)	ζ_{trms} (in)
23	0.62	0.26	-4.05	1.70	1.76	0.74	1.76	0.74
24	1.76	0.72	-9.43	4.01	4.07	1.74	4.06	1.71
25	2.37	0.97	-10.90	4.74	5.00	2.17	4.99	2.13
26	0.59	0.30	-3.19	1.63	2.14	1.10	2.10	1.00
27	1.24	0.60	-5.84	3.00	3.98	2.04	3.90	1.87
28	2.30	1.10	-8.94	4.69	6.39	3.31	6.24	3.00
29	2.37	1.09	-9.26	4.66	6.39	3.16	6.29	2.95
30	0.39	0.24	-1.79	1.14	1.85	1.18	1.68	0.88
33	2.51	1.34	-8.47	5.14	8.59	5.09	8.06	4.13
37	1.73	1.09	-6.08	4.14	7.99	5.46	6.93	3.73
39	2.51	1.47	-8.20	5.46	9.66	6.32	8.62	4.58
40	0.47	0.35	-1.69	1.28	2.86	2.16	2.25	1.25

Table 11 Summary of dimensionless parameters evaluated for the roughness no. 1 experiments ($P_s = \varepsilon/D = 0.028/3.772 = 0.007$)

Expt.	R_{rms} —	f_{pu} —	$f_{p\xi}$ —	I —	C_{urms} —	P_d —	P_H —	P_F —	P_p —
23	9263	0.70	0.62	8.03	20.52	0.087	0.0064	0.957	0.466
24	25746	1.90	1.45	2.44	4.94	0.090	0.0152	0.811	1.075
25	34785	2.60	1.80	1.58	2.97	0.088	0.0183	0.735	1.322
26	10572	0.99	0.91	5.85	17.57	0.056	0.0049	0.908	0.556
27	21628	2.01	1.70	2.58	7.38	0.057	0.0093	0.890	1.034
28	39212	3.65	2.75	1.23	3.11	0.057	0.0148	0.804	1.654
29	38718	3.50	2.63	1.23	3.11	0.061	0.0160	0.790	1.667
30	8639	1.01	0.98	6.05	21.67	0.037	0.0026	0.939	0.445
33	47660	5.32	4.24	0.90	2.48	0.040	0.0134	0.768	2.135
37	38408	5.10	4.54	1.10	3.18	0.029	0.0083	0.740	1.836
39	51568	6.35	5.26	0.80	2.43	0.034	0.0121	0.851	2.286
40	12178	1.84	1.80	3.35	9.16	0.022	0.0021	0.606	0.596

Table 12 Summary of wave characteristics, forces, drag coefficients and inertia coefficients for the roughness no. 2 experiments (D = 3.860 in, ε = 0.072 in)

Expt.	$\overline{H}$ (in)	$\overline{L}$ (ft)	$\overline{T}$ (sec)	$\overline{F}_{h\theta_1}$ (lbs)	$\overline{F}_{h\theta_2}$ (lbs)	$\overline{F}_{hmax}$ (lbs)	C_D —	C_m —
45	1.71	3.68	0.85	-0.15	-0.90	1.00	-4.44	2.49
46	4.24	3.66	0.83	-0.44	-1.56	1.95	-1.25	1.75
47	4.81	3.79	0.84	0.02	-1.69	2.24	0.03	1.64
48	2.03	5.55	1.04	0.04	-1.02	1.00	0.74	2.39
49	4.01	5.46	1.03	0.07	-2.04	1.90	0.31	2.55
50	5.51	5.51	1.05	-0.27	-2.54	2.86	-0.54	2.27
51	6.06	5.32	1.00	0.94	-2.13	2.58	1.36	1.82
52	2.10	7.79	1.29	0.13	-0.88	0.84	2.37	2.15
53	3.95	8.19	1.29	-0.13	-1.73	1.55	-0.55	2.20
54	5.20	7.78	1.32	0.79	-2.11	2.82	2.02	2.20
55	7.94	7.42	1.25	0.90	-3.17	3.52	0.72	2.21
56	8.96	7.39	1.21	1.40	-2.94	3.77	0.78	1.70
57	2.08	10.46	1.54	0.06	-0.74	0.84	0.97	1.95
58	3.79	9.72	1.51	-0.03	-1.48	1.53	-0.16	2.29
59	6.79	9.50	1.47	0.61	-2.62	2.94	0.78	2.16
60	7.40	9.36	1.48	1.12	-2.86	2.92	1.18	2.33
61	8.66	8.65	1.35	1.59	-2.84	4.23	1.00	1.77
62	2.28	11.76	1.65	0.01	-0.78	0.76	0.16	1.92
63	4.43	11.17	1.61	0.35	-1.54	1.74	1.09	1.98
64	6.28	11.36	1.67	0.79	-1.82	2.40	1.17	1.86
65	7.84	11.73	1.65	1.01	-2.67	3.09	0.81	1.92
66	9.34	10.78	1.56	2.52	-2.90	4.06	1.34	1.80

Table 13 Summary of particle velocities, accelerations and displacements for the roughness no. 2 experiments (D = 3.860 in, ε = 0.072 in)

Expt.	U_m $(\frac{ft}{sec})$	u_{rms} $(\frac{ft}{sec})$	a_{hmax} $(\frac{ft}{sec^2})$	a_{hrms} $(\frac{ft}{sec^2})$	ξ_{tmax} (in)	ξ_{trms} (in)	ζ_{tmax} (in)	ζ_{trms} (in)
45	0.62	0.25	-3.94	1.65	1.71	0.72	1.71	0.72
46	1.95	0.79	-9.78	4.12	4.25	1.79	4.24	1.77
47	2.23	0.91	-10.93	4.67	4.82	2.06	4.81	2.04
48	0.58	0.29	-3.15	1.60	2.07	1.06	2.03	0.97
49	1.29	0.62	-6.02	3.07	4.09	2.08	4.01	1.91
50	1.87	0.89	-8.31	4.23	5.63	2.87	5.51	2.63
51	2.25	1.05	-9.00	4.61	6.17	3.09	6.06	2.86
52	0.50	0.30	-2.28	1.40	2.27	1.39	2.10	1.09
53	1.01	0.60	-4.23	2.68	4.34	2.74	3.95	2.08
54	1.34	0.77	-5.34	3.28	5.63	3.46	5.20	2.70
55	2.48	1.34	-8.36	5.12	8.50	5.08	7.94	4.09
56	3.00	1.60	-10.14	6.16	9.57	5.71	8.96	4.61
57	0.44	0.31	-1.74	1.24	2.49	1.78	2.08	1.14
58	0.85	0.56	-3.13	2.17	4.41	3.05	3.79	2.05
59	1.69	1.06	-5.92	4.04	7.82	5.34	6.79	3.66
60	1.88	1.16	-6.11	4.22	8.49	5.75	7.40	3.98
61	2.56	1.48	-8.38	5.53	9.67	6.29	8.66	4.60
62	0.48	0.35	-1.74	1.31	2.90	2.18	2.28	1.27
63	0.99	0.69	-3.46	2.56	5.48	4.04	4.43	2.44
64	1.42	0.98	-4.41	3.35	7.83	5.82	6.28	3.47
65	1.90	1.31	-6.01	4.53	9.93	7.48	7.84	4.35
66	2.44	1.59	-7.40	5.47	11.34	8.23	9.34	5.12

Table 14 Summary of dimensionless parameters evaluated for the roughness no. 2 experiments ($P_s = \epsilon/D = 0.072/3.860 = 0.019$)

Expt.	R_{rms}	f_{pu}	$f_{p\epsilon}$	I	C_{urms}	P_d	P_H	P_F	P_P
	—	—	—	—	—	—	—	—	—
45	8944	0.67	0.59	8.23	24.07	0.087	0.0062	1.095	0.442
46	27674	2.02	1.46	2.14	4.67	0.091	0.0161	0.860	1.098
47	31899	2.37	1.68	1.83	4.00	0.088	0.0177	0.872	1.246
48	10098	0.93	0.86	6.22	18.63	0.057	0.0048	0.922	0.526
49	21794	2.00	1.69	2.56	7.29	0.058	0.0098	0.884	1.039
50	31344	2.91	2.34	1.70	5.17	0.057	0.0130	0.972	1.438
51	35752	3.26	2.51	1.35	3.36	0.062	0.0157	0.798	1.570
52	10393	1.18	1.13	5.10	14.66	0.038	0.0033	0.746	0.543
53	21210	2.43	2.23	2.35	6.29	0.037	0.0061	0.732	1.024
54	27142	3.15	2.81	1.77	6.89	0.036	0.0078	1.014	1.347
55	47057	5.19	4.14	0.92	2.72	0.040	0.0132	0.829	2.058
56	56176	6.01	4.65	0.78	2.01	0.042	0.0159	0.788	2.320
57	10934	1.49	1.45	4.12	13.49	0.026	0.0023	0.759	0.538
58	19646	2.62	2.48	2.24	7.32	0.027	0.0043	0.754	0.983
59	37401	4.86	4.35	1.15	3.68	0.029	0.0081	0.811	1.758
60	40869	5.33	4.68	1.01	3.02	0.028	0.0088	0.737	1.918
61	52088	6.22	5.12	0.81	2.64	0.034	0.0123	0.914	2.244
62	12418	1.81	1.78	3.39	9.38	0.023	0.0022	0.622	0.592
63	24400	3.46	3.29	1.71	5.34	0.024	0.0044	0.735	1.148
64	34575	5.10	4.73	1.12	3.53	0.022	0.0058	0.713	1.627
65	46006	6.70	6.09	0.85	2.50	0.023	0.0075	0.737	2.032
66	55817	7.68	6.70	0.70	2.18	0.026	0.0100	0.814	2.418

Table 15 Summary of wave characteristics, forces, drag coefficients and inertia coefficients for the roughness no. 3 experiments ($D = 4.005$ in, $\varepsilon = 0.145$ in)

Expt.	$\overline{H}$ (in)	$\overline{L}$ (ft)	$\overline{T}$ (sec)	$\overline{F}_{h\theta_1}$ (lbs)	$\overline{F}_{h\theta_2}$ (lbs)	$\overline{F}_{hmax}$ (lbs)	C_D —	C_m —
67	2.10	3.66	0.83	-0.02	-1.11	1.06	-0.35	2.24
68	4.10	3.54	0.81	0.14	-1.34	1.68	0.40	1.37
69	4.91	3.94	0.83	0.84	-1.66	2.41	1.56	1.40
70	2.10	5.31	1.02	0.18	-1.14	1.12	3.36	2.43
71	4.06	5.25	1.02	-0.14	-1.95	2.46	-0.55	2.20
72	5.74	5.36	1.03	0.22	-2.34	3.34	0.40	1.95
73	6.32	4.99	1.04	-0.01	2.26	3.02	-0.01	1.85
74	1.59	7.46	1.26	0.17	-0.95	0.94	5.37	2.88
75	3.55	7.38	1.26	1.01	-1.74	1.93	5.99	2.47
76	6.00	8.01	1.28	-0.26	-2.45	2.56	-0.40	1.95
77	9.12	7.14	1.23	1.44	-3.09	4.05	0.80	1.78
78	8.04	6.83	1.18	2.17	-2.77	3.68	1.61	1.66
79	2.20	9.08	1.49	-0.22	-0.99	1.04	-3.61	2.45
80	4.05	10.74	1.54	-0.06	-1.71	1.64	-0.22	2.10
81	7.02	9.48	1.48	-0.16	-2.82	3.16	-0.19	2.17
82	7.39	9.38	1.47	1.18	-2.71	3.63	1.22	1.91
83	8.86	8.21	1.34	1.49	-3.07	4.21	0.88	1.76
84	2.32	11.70	1.65	0.04	-0.76	0.84	0.42	1.71
85	4.19	11.07	1.65	0.17	-1.52	1.50	0.63	2.05
86	6.40	11.09	1.67	1.09	-2.03	2.65	1.56	1.93
87	8.35	11.60	1.66	1.50	-2.41	3.72	1.00	1.59
88	10.01	10.81	1.57	0.87	-3.23	4.21	0.38	1.69

Table 16 Summary of particle velocities, accelerations and displacements for the roughness no. 3 experiments (D = 4.005 in, ε = 0.145 in)

Expt.	U_m $(\frac{ft}{sec})$	u_{rms} $(\frac{ft}{sec})$	a_{hmax} $(\frac{ft}{sec^2})$	a_{hrms} $(\frac{ft}{sec^2})$	ξ_{tmax} (in)	ξ_{trms} (in)	ζ_{tmax} (in)	ζ_{trms} (in)
67	0.80	0.33	-5.03	2.11	2.11	0.89	2.10	0.88
68	1.96	0.78	-10.29	4.26	4.11	1.71	4.10	1.69
69	2.30	0.95	-11.29	4.90	4.92	2.14	4.91	2.10
70	0.61	0.30	-3.35	1.67	2.14	1.07	2.10	0.99
71	1.36	0.64	-6.40	3.18	4.12	2.05	4.06	1.91
72	1.96	0.93	-8.51	4.31	5.84	2.94	5.74	2.72
73	2.29	1.04	-9.26	4.52	6.41	3.10	6.32	2.93
74	0.38	0.22	-1.76	1.06	1.70	1.02	1.59	0.82
75	0.89	0.51	-3.81	2.29	3.79	2.26	3.55	1.82
76	1.69	0.97	-6.39	4.02	6.54	4.08	6.00	3.14
77	3.00	1.57	-9.71	5.85	9.68	5.67	9.12	4.66
78	2.66	1.38	-9.56	5.54	8.45	4.83	8.04	4.06
79	0.47	0.30	-1.87	1.24	2.49	1.66	2.20	1.18
80	0.91	0.63	-3.42	2.47	4.92	3.56	4.05	2.22
81	1.73	1.09	-5.93	4.07	8.08	5.51	7.02	3.78
82	1.86	1.16	-6.46	4.38	8.48	5.75	7.39	3.98
83	2.68	1.50	-8.69	5.55	9.73	6.16	8.86	4.66
84	0.48	0.36	-1.78	1.33	2.93	2.21	2.32	1.28
85	0.89	0.63	-3.08	2.27	5.16	3.79	4.19	2.31
86	1.44	0.98	-4.44	3.33	7.89	5.80	6.40	3.53
87	2.06	1.40	-6.19	4.68	10.51	7.88	8.35	4.62
88	2.64	1.70	-8.60	5.87	12.18	8.85	10.01	5.49

Table 17 Summary of dimensionless parameters evaluated for the roughness no. 3 experiments ($P_s = \varepsilon/D = 0.145/4.005 = 0.036$)

Expt.	R_{rms}	f_{pu}	$f_{p\varepsilon}$	I	C_{urms}	P_d	P_H	P_F	P_P
	—	—	—	—	—	—	—	—	—
67	11654	0.81	0.70	6.57	14.64	0.091	0.0079	0.873	0.525
68	27659	1.88	1.34	2.35	3.96	0.095	0.0162	0.709	1.023
69	33832	2.36	1.68	1.83	3.80	0.089	0.0183	0.854	1.225
70	10535	0.91	0.84	6.36	18.95	0.060	0.0052	0.922	0.525
71	22747	1.95	1.61	2.60	8.63	0.060	0.0101	1.054	1.013
72	32964	2.87	2.30	1.68	5.39	0.058	0.0140	1.011	1.432
73	36955	3.23	2.44	1.40	3.84	0.058	0.0152	0.829	1.579
74	7899	0.83	0.80	7.24	28.84	0.039	0.0026	1.023	0.397
75	18198	1.92	1.77	2.95	10.76	0.039	0.0058	0.945	0.885
76	34706	3.73	3.20	1.42	3.75	0.038	0.0095	0.742	1.497
77	56164	5.78	4.45	0.79	2.14	0.041	0.0157	0.772	2.277
78	49047	4.86	3.79	0.97	2.58	0.045	0.0150	0.796	2.007
79	10833	1.35	1.30	4.51	16.82	0.028	0.0026	0.822	0.549
80	22620	2.92	2.80	2.06	5.85	0.026	0.0044	0.701	1.012
81	38890	4.84	4.32	1.15	3.61	0.028	0.0083	0.782	1.752
82	41616	5.09	4.51	1.09	3.65	0.029	0.0089	0.853	1.846
83	54118	6.03	4.83	0.82	2.44	0.035	0.0128	0.825	2.212
84	12833	1.77	1.73	3.50	9.79	0.023	0.0022	0.630	0.578
85	22600	3.11	2.97	1.92	5.43	0.023	0.0040	0.621	1.046
86	35356	4.93	4.55	1.15	3.76	0.022	0.0059	0.719	1.599
87	50196	6.92	6.18	0.80	2.52	0.023	0.0079	0.773	2.084
88	61348	8.02	6.94	0.67	1.86	0.025	0.0105	0.731	2.499